AD NUMBER

AD456965

NEW LIMITATION CHANGE

TO

Approved for public release, distribution unlimited

FROM

Distribution: No Foreign

AUTHORITY

USAEC LTR 4 FEB 66

RESEARCH ON MICROWAVE WINDOW MULTIPACTOR AND ITS INHIBITION

FINAL REPORT

CONTRACT NUMBER DA 36-039 SC-90818
DEPARTMENT OF THE ARMY
TASK NUMBER 1G6-22001-A-055-04

FINAL REPORT COVERING PERIOD

1 JULY 1962 THROUGH 30 JUNE 1964

U. S. ARMY ELECTRONICS LABORATORIES
FORT MONMOUTH, NEW JERSEY

EITEL-McCULLOUGH, INC.
301 INDUSTRIAL WAY
SAN CARLOS, CALIFORNIA

RESEARCH ON MICROWAVE WINDOW MULTIPACTOR AND ITS INHIBITION

FINAL REPORT
CONTRACT NUMBER DA 36-039 SC-90818
DEPARTMENT OF THE ARMY
TASK NUMBER 1G6-22001-A-055-04

FINAL REPORT COVERING PERIOD
1 JULY 1962 THROUGH 30 JUNE 1964

Object of Research: (1) Attain a more complete theoretical understanding of microwave tube window multipactor, its inhibition and sustainment, and the tube performance limitations it imposes; (2) Investigate techniques to inhibit multipactor without degrading tube performance.

Prepared by: R. Hayes
Raymond Hayes

Approved by: D. Preist
Donald H. Preist

This research is a part of Project Defender, sponsored by the Advanced Research Projects Agency, Department of Defense, under ARPA Order Number 318-62, Project Code Number 7300, and is conducted under the technical guidance of the U. S. Army Electronics Laboratories, Fort Monmouth, New Jersey.

TABLE OF CONTENTS

Table of Contents (cont'd)

Table Of Contents (cont'd)

SECTION

1. PURPOSE

The purpose of the study was to provide a deeper understanding of multipactor effects, which occur at waveguide windows used with high-power microwave tubes and to determine practical methods of preventing or eliminating multipactor, thereby raising the power handling capacity of windows. Throughout the investigation emphasis was placed on an understanding of the basic phenomena involved so that general solutions would be obtained which would be applicable over a wide range of conditions.

Prior to the inception of this contract certain types of multipactor which are liable to occur at waveguide windows had been recognized as the result of company-sponsored research at Eitel-McCullough. A method of eliminating multipactor had been devised and partially developed. This consisted of the application of an evaporated film of titanium in order to reduce the secondary emission coefficient of the window and adjacent surfaces. This work was carried out on cylindrical ceramic windows at a frequency of 650 megacycles per second and the results have been summarized in two published articles [1, 2].

There was a need for further investigation of multipactor effects which could occur at other window geometries and at different frequencies. It was desirable to evaluate further the evaporated titanium coating method and to investigate other window coatings such as films of sputtered titanium monoxide.

As an alternative approach, other possible methods of eliminating multipactor were to be investigated such as phase or space defocusing of the electron cloud near the window. It seemed possible that if the electric fields in the window region were properly shaped or if the window configuration were suitably designed, secondary electrons produced would be driven from the window surface. This method would not, in principle, require a reduced secondary emission coefficient at the window surface.

To ensure adequate attention to both of the above approaches, the first year's work carried out between July 1962 and June 1963, was divided into two tasks with the following objectives:

Task A: An Experimental Study of Electron Bombardment Phenomena at the Output RF Windows of High Power Microwave Tubes.

Phase 1. Experimental and analytical study of multipactor effects at waveguide windows under high power conditions.

Phase 2. Development and application of evaporation coatings and techniques applied to the window and surrounding metal parts in order to reduce secondary emission coefficient to less than unity.

Task B: Study of the Inner-Window Surface and Configurations Affecting Power-Handling Capabilities of High Power Microwave Tubes.

Phase 1. Analysis of various means of obtaining space and phase defocusing of electrons by shaping the fields and window surfaces.

Phase 2. Study of materials and coatings in conjunction with shaped fields to develop windows capable of handling higher powers without multipactor.

There was a reorientation of the program for the second year, which will be referred to as Task C. This was carried out between July 1963 and June 1964 and the objectives were to obtain more detailed knowledge of the behavior of the above methods, especially the coatings, and to arrive at numerical values for the important properties involved. These included the useful range of thickness of the coatings, the conditions of application, the temperatures and other factors involved in the processing and the constitution of the coating material itself.

Another major purpose was to test these windows at much higher average power levels than formerly, to reveal any weaknesses in the techniques used for multipactor suppression, and approximate more closely than before the conditions existing in a super power microwave tube. An investigation of gas evolution from windows under multipactor conditions was to be made to throw more light on the nature of the multipactor problem. Other phenomena such as window puncture and arcing, which may cause power limitations, were to be investigated as the need arose. In addition, a reevaluation of other window geometries, such as cones or domes, coated to prevent multipactor, was to be made, as these offer significant potential advantages compared with discs.

2. ABSTRACT

The problem of multipactor at microwave windows is discussed and the results of theoretical and experimental studies on multipactor at a single dielectric surface are presented, with information on the power levels at which such discharges may be expected to occur. Methods of eliminating multipactor at windows are described and include surface coatings, applied by evaporating titanium in vacuum or sputtering titanium monoxide in argon or mercury, and grooves cut in the window surface perpendicular to the electric field. Factors affecting the nature of the surface coatings during application and in subsequent tube processing are described. A wide variety of coatings have been evaluated at S-band on alumina, beryllia, and quartz windows at power levels up to 100 Mw peak equivalent transmitted power and average dissipations equivalent to over 300kw of average power. The maximum peak power supported by multipactor resistant windows was limited by arcing at the metal-dielectric seal. Various methods of increasing the threshold power for arcing have been tried. The most successful arrangement employed a window ceramic of "H" shaped cross section in which the metal-dielectric seal was located in a region of weak electric intensity.

3. PUBLICATIONS, LECTURES, REPORTS AND CONFERENCES

3.1 Publications

"The Effects of Titanium Films on Secondary Emission Phenomena in Resonant Cavities and at Dielectric Surfaces", by Ruth Carlson Talcott, Trans. IRE, PGED, Vol. ED-9, September 1962.

3.2 Lectures

"Multipactor Motions in Microwave Tubes", by D. H. Preist, paper read at the International Congress on Microwave Tubes, The Hague, Holland, September 1962.

At an ARPA-USAEL-sponsored symposium on windows held at Varian Associates in February, 1963, the following lectures were given:

1. "Development of a general theory of multipactor electron motion at windows", by Donald H. Preist.

2. "Multipactor suppression by surface forming and surface coating of alumina and silica windows", by Oskar Heil.

3. "An account of unpublished experiments on window multipactor at Eitel-McCullough, leading to coating techniques in current use", by Ruth C. Talcott.

3.3 Conferences Held

During the period of the contract conferences were held with various other workers in the field from time to time. These are summarized below:

At Stanford University, August 30, 1962. Those present: Don Preist, Ruth C. Talcott, John Soderstrum, from Eimac, and John Jasburg and Dr. Pedro Szenti of Stanford.

At the Hague, Holland between Preist of Eimac and Dr. G. Schaffer of the Hamburg Linear Accelerator Project (DESY), September 7, 1962.

At EMI, Hayes, Middlesex, England between Preist of Eimac and Dr. Kreuchen, Mr. Dixon and Mr. Barnes of EMI, September 12, 1962.

At Stanford Linear Accelerator Center, Stanford University, Stanford, California, on January 23, 1964, with J. Jasberg, R. W. Bierce, and W. R. Fowkes, Stanford University, and D. Preist, R. Talcott and R. Hayes, Eitel-McCullough.

The following conferences were held with representatives of ARPA and the U. S. Army Electronics Laboratories, Fort Monmouth, New Jersey, during which plans and progress were reviewed.

At Eitel-McCullough, San Carlos, California, with Lt. Col. W. B. Lindsay of ARPA, August 23, 1962.

At Eitel-McCullough, with Mr. Louis Heynick of the U. S. Army Electronics Laboratories, Fort Monmouth, New Jersey, July 12, July 19, October 5 and October 8, 1962.

At Eitel-McCullough, with Lt. Col. W. B. Lindsay of ARPA and Mr. Louis Heynick of the U. S. Army Electronics Laboratories, Fort Monmouth, New Jersey, November 29, 1962.

At Eitel-McCullough, with Mr. Louis Heynick of the U. S. Army Electronics Laboratories on January 15, February 5 and March 8, 1963.

At Eitel-McCullough, with Mr. Louis Heynick, Mr. Gunther Wurthmann and Miss Barbara Malley all of the U. S. Army Electronics Laboratories, Fort Monmouth, New Jersey, May 16, 1963.

At Eitel-McCullough, with Mr. Gunther Wurthmann, of the U. S. Army Electronics Laboratories, Fort Monmouth, New Jersey, on August 21, 1963, February 12, 1964 and July 9, 1964. At the first meeting Mr. Bernard Smith of USAEL was also present.

4. FACTUAL DATA

4.1 Introduction

This is a final report covering 2 years of study on multipactor and its suppression at waveguide windows. Multipactor at alumina, beryllia and quartz windows has been investigated in the S-band region. Power levels at which multipactor commences have been established and the effects of magnetic fields on the discharge determined. Various methods of eliminating multipactor have been evaluated. These include evaporated titanium coatings, sputtered titanium monoxide coatings and grooves cut in surface of windows perpendicular to the electric field. In preparing this report the work of the three tasks described in the previous section has been reviewed and the various results combined to enable a complete and unified picture to be presented.

4.2 The Multipactor Problem

4.2.1 Types of Multipactor

Secondary electron resonance or multipactor has been known for a number of years. It may exist in a variety of forms;[3] the double surface or single surface variety, on conducting or insulating surfaces with or without magnetic field. The phenomenon is liable to occur in any device supporting high intensity rf electric fields in vacuum or gases at low pressure.

Multipactor was first recognized in the two-surface form[4], and this type has been

fully analyzed in the literature[5,6]. It occurs between two parallel plates in vacuum or low pressure gas, where an rf field exists perpendicular to the plates. If the distance between the plates is such that an electron emitted from one surface when the field is zero and accelerated across the gap arrives at the second surface when the field is again zero, then any secondary electrons emitted will be returned to the first plate as the field reverses. If the surfaces have a maximum secondary emission coefficient greater than one and the arrival energy of the electrons is favorable for the release of secondaries the number of oscillating electrons will increase rapidly. Oscillating electrons gain kinetic energy from the rf field which is dissipated at the surfaces in the form of heat. The net result is the creation of a relatively low impedance discharge which can cause severe loading of the rf field and intense heat dissipation at the surfaces. The phenomenon is dependent on the magnitude of the field, the frequency, the gap length, the phase angle of the field at which an electron is emitted, and the secondary emission characteristics of the surface involved in the discharge.

The form of multipactor which is the most troublesome at the microwave windows is the gliding single surface type first described by Preist and Talcott[1]. This can occur at the dielectric surface in vacuum in the presence of an rf electric field parallel to the dielectric, a situation which is inherent in many microwave window designs. The process is initiated by stray electrons bombarding the surface and liberating secondaries.

These are initially carried away from the surface by the emission velocity, but are then returned by a restoring force, due to either a positive surface charge or the presence of a magnetic field. During the period that the electrons are free they are accelerated by the rf electric field and may return to the surface with considerable kinetic energy, depending on the phase of the rf field at emission and the duration of the period that the electrons are free. This kinetic energy is dissipated on impact, releasing further secondary electrons and causing local heating. Typical motions are shown in Fig. 1. The conditions under which single surface multipactor may occur are much less critical than for the two-surface type, since no fixed distances are involved. The effect is possible over a wide range of field strengths and phase angles, the major requirement being that electrons are returned to the surface with kinetic energies in the range for which the secondary emission coefficient is greater than one.

Multipactor is dependent on the dc motions of the electrons in addition to the oscillating motion due to the rf field. The following processes create dc velocities:

1. The phase at which the electron is liberated or emitted into the h.f field.

2. The acceleration of electrons in an inhomogeneous electric field where the field strength varies:

   a) in the direction of the lines of force of the electric field (diverging lines of force)

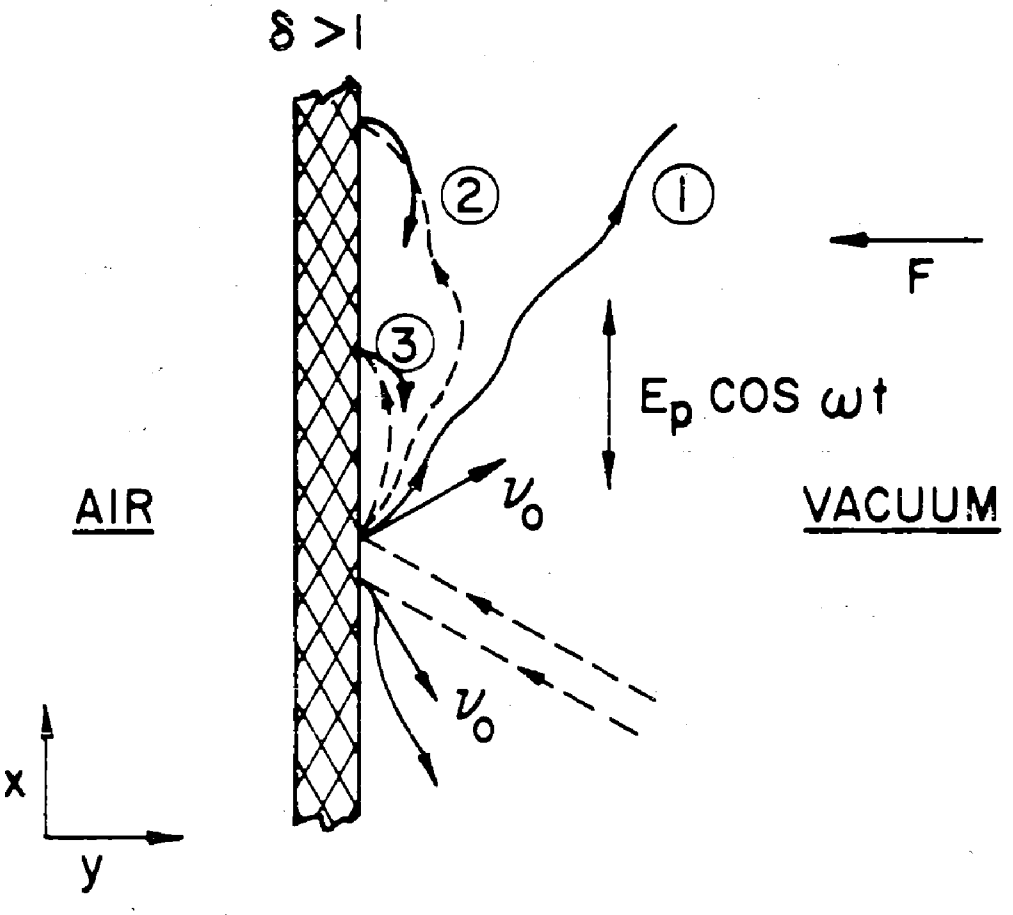

ELECTRON MOTIONS WITH ZERO MAGNETIC FIELD

① F = 0
② $F_1 > 0$
③ $F > F_1$

FIG. 1

b) perpendicular to the lines of force (curved lines of force)

c) perpendicular to the lines of force (parallel lines of force in standing waves; dynamic inhomogeneity)

3. Electron velocity obtained from impulse transfer from the propagating wave (radiation pressure).

The electron velocities in 2c) and 3 are obtained by deflection of the moving electrons in the high frequency magnetic field of standing or propagating waves. Whereas in 2c) the electrons are strongly accelerated, they obtain in 3 only a small constant dc velocity superimposed on a second harmonic oscillation. The average forward energy of the electron is proportional to the fourth power of the high frequency electric field. See Appendix III. The effect therefore becomes noticeable at windows only at very high powers producing different conditions on the input and output side of a window due to the different direction of energy flux.

Process 1) explains the positive dc potential of the window surface as a result of the net loss of electrons from the window to the surrounding waveguide.

It will also be shown how all three field inhomogeneity effects can be utilized to drive electrons away from the window surface.

4.2.2 Electron Motion During Multipactor At A Dielectric Surface

An analysis of the motion of an electron near a single dielectric surface due to an rf electric field parallel to the surface and a static electric field normal to the surface is given in Appendix I.

The maximum velocity will be gained by electrons which leave the surface at the most favorable phase of the rf electric field and, neglecting initial velocities, is given by,

$$v_{max} = \frac{2\ e\ E}{m\ \omega} \qquad (1)$$

where E is the peak rf electric field, ω is the angular velocity and e/m is the charge to mass ratio of an electron.

The corresponding electron energy in terms of a maximum voltage V_{max} is given by

$$V_{max} = 2\ \frac{e\ E^2}{m\ \omega^2} \qquad (2)$$

For multipactor to occur at a window surface electrons must gain sufficient energy from the electric field to liberate secondaries on impact. The minimum energy necessary is dependent on the nature of the surface and will normally correspond to the lower cross over potential of the secondary emission characteristic curve (See Fig. 2).

From the results of experiments described in Sec. 4.4 multipactor at alumina and beryllia surfaces commences at a maximum tangential field strength of about 2.1 kv/cm at a frequency of 2700 Mc. Substituting in equation (2) and neglecting the initial electron velocity the corresponding energy is 54 eV. which may be considered as the minimum energy required to start a multipactor discharge on alumina or beryllia. (See also Appendix IV.)

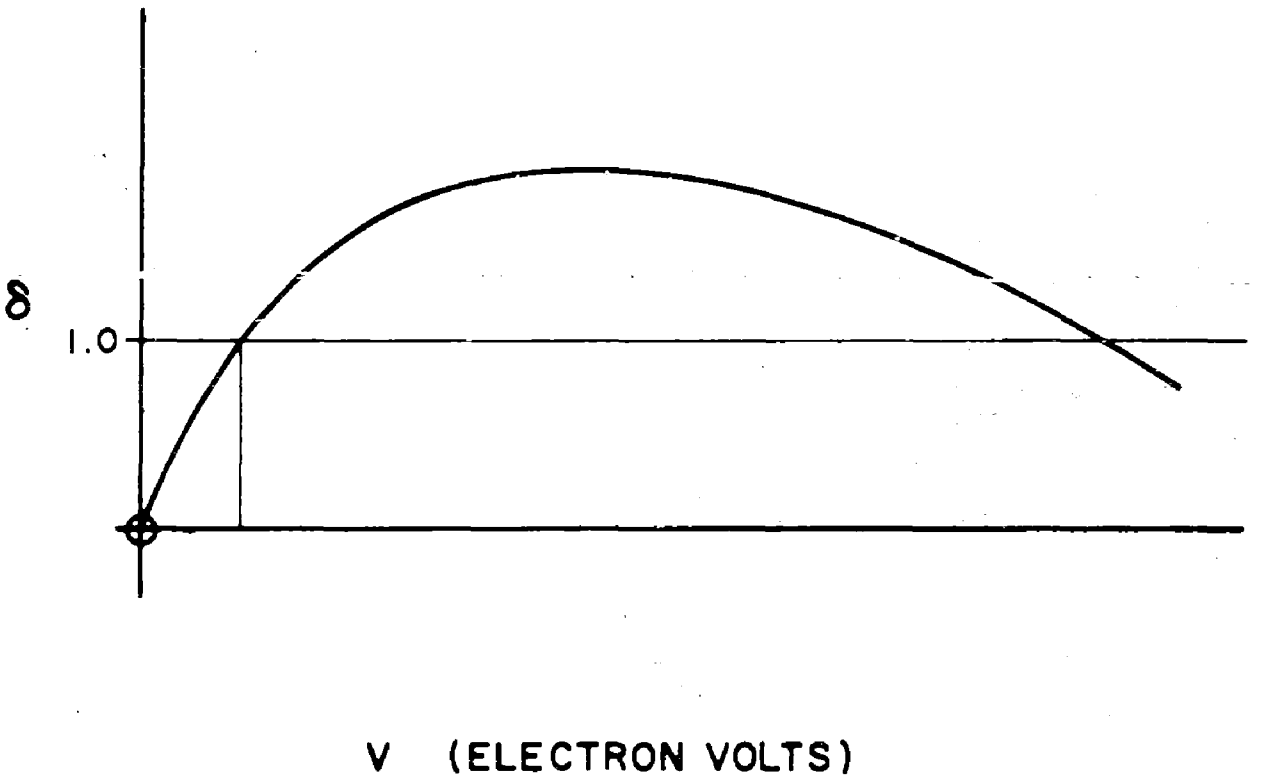

FIG. 2. Secondary emission coefficient δ as a function of velocity of bombarding electrons expressed in electron volts.

In a practical case it is usually desired to determine the power level at which multipactor is liable to occur in a given window. This is easily calculated as illustrated in the following example,

Example 1

Alumina disc window in a circular waveguide 3.7 inches in diameter operating at 2700 Mc in TE_{11} mode.

The relationship between power flow and maximum peak field strength for the TE_{11} mode in a circular waveguide is given by,

$$P = 1.99 \times 10^{-3} \sqrt{1 - \left[\frac{\lambda}{3.41a}\right]^2} a^2 E^2 \qquad (3)$$

where P = power flow in watts

E = peak electric field strength in volts/cm

a = guide radius in cm

Taking the critical electron energy as 54v the corresponding field strength from equation (3) is 2.1 kv/cm (neglecting initial velocities) and the equivalent transmitted power is 140kw.

Example 2

Rectangular block beryllia window in WR 112 waveguide operating in the TE_{10} mode at 9000 Mc.

The critical field strength is again obtained from (2). Using a minimum voltage of 54 volts for beryllia, the value 7.02 kv/cm is obtained. For a rectangular waveguide operating in the TE_{10} mode the relationship between power flow and peak electric field strength is given by

$$P = \sqrt{\frac{\varepsilon}{\mu}\left[1 - \frac{\lambda}{2a}\right]^2} \quad \frac{ab}{2} \quad E^2 \qquad (4)$$

$$P = 0.663 \times 10^{-3} \sqrt{1 - \left[\frac{\lambda}{2a}\right]^2}\, abE^2$$

where a and b are the width and depth of the waveguide respectively in cm. Substituting for E gives a power of 196kw. In both of the above examples the windows were located in straight waveguide sections. Many window designs contain waveguide discontinuities near the window or irises for broadbanding. In such cases equations (3) and (4) do not apply and it is necessary to estimate the relationship between power flow and electric field strength at the window surface.

It is interesting to note that for a given window material or surface condition the power necessary for multipactor is largely independent of frequency. Equation (2) may be written:

$$E^2 = \frac{2\, m\, (\tau c)^2\, V}{e} \cdot \frac{1}{\lambda^2} \qquad (5)$$

Assuming that in the case of the circular waveguide the radius is proportional to wavelength, $a/\lambda = k$, and combining (3) and (5)

$$P = 1.99 \times 10^{-3} \sqrt{1 - \left[\frac{1}{3.41k}\right]^2} k^2 \lambda^2 \cdot 2 \frac{m}{e} (\pi c)^2 \frac{V}{\lambda^2} \qquad (6)$$

P = constant x V, and is independent of λ

4.2.3 The Elimination of Multipactor

In order to prevent multipactor from occurring in a device it is necessary to ensure that the conditions are unfavorable for the discharge. One method of achieving this is to employ surfaces which have a low secondary emission yield. Multipactor is dependent on a copious supply of secondary electrons and if this supply is restricted the multiplication of free electrons in the vicinity of the window is prevented thus inhibiting the buildup of a multipactor discharge.

Since all useable dielectric materials have high secondary electron emission coefficients it is necessary to employ surface coatings with low secondary yields when applying the method to microwave windows. It is also necessary to ensure that the coatings do not introduce appreciable RF loss.

An alternative approach is to prevent electrons from returning to the window by shaping the electric fields or the window surface to cause space or phase defocusing of the electrons. The form that this approach actually took in this program was grooving of the window surface.

A combination of the two approaches was also thought to be worth investigating.

The material used to form the low secondary emitting coatings was basically titanium. This element was chosen in the earlier work at Eitel-McCullough, Inc., prior to the inception of the present study [2] because the published secondary emission data for the element titanium indicated a maximum value of δ of 0.9 (page 39 of Ref. 9). The other metals having coefficients of unity or less (same reference) are Aluminum, Barium, Beryllium, Carbon, Caesium, Potassium, Lithium, Magnesium, and Rubidium. Most of these were ruled out because of chemical instability, toxicity and poor availability. A mandatory requirement was that the coating should be able to withstand a typical electron tube exhaust and bake-out process at 500°-600°C.

It was suspected that during this process all the elements listed, with the exceptions of titanium and carbon would oxidize, resulting in the high secondary emission characteristic of most oxides (page 53 of Ref. 9). Titanium was known to be able to dissolve surface oxide layers by gaseous diffusion [2] so that some hope of obtaining a final surface of titanium metal with its low value of δ existed. Experiments [1] had confirmed this. Some attention had been given to carbon as it was known that the oxides would be in the form of volatile CO or CO_2, enabling a pure carbon surface to exist after a bake-out process. However, the difficulty of obtaining and maintaining the thin films necessary to keep the RF losses down to an acceptable level, together with the possibility that such thin films would be hard to control in an oxidizing atmosphere, militated against the use of carbon.

The early work referred to was restricted to titanium, evaporated in a bell jar, for these reasons. In the present study this approach was pursued further.

In addition, in the present study another approach previously suggested by O. Heil was pursued also. This was to use titanium oxide (TiO) as the basic material. Data in Ref. 14 seemed to indicate that this material being in many respects like a metal, and having a positive temperature coefficient of resistance, might well be expected to have a low secondary emission coefficient. Sputtering was chosen as the method of application, rather than evaporation, for the reasons given later (See Section 4.6).

4.3 Equipment and Experimental Procedure

4.3.1 Methods Used

All three tasks of the program used different equipment and procedures. In Tasks A and C, windows were tested using a resonant cavity method while in Task B, a traveling wave ring resonator was employed. A description of the facilities and test methods used with each task is given in the following sections.

4.3.2 Task A

Windows tested in Task A were 3.7 inch diameter discs which formed part of a cylindrical resonant cavity operating in the TE_{111} mode. The discs were metalized and brazed into demountable vacuum tight test units. Each unit contained a getter ion pump and was baked out at 400°C during evacuation on a diffusion pump station.

The first test unit design (Model 1) is shown in Fig. 3. This was modified (Model 2) to include an optical window for viewing the test ceramic through perforations in one of the cavity end walls. These units were used during the initial experiments but were not completely satisfactory. Inadequate RF contact was sometimes obtained at the compression seal between the copper cylinder and the end flanges resulting in low Q and arcing at the contact. Accordingly, a third design was evolved (Model 3, shown in Figs. 4, 5, and 6 in which the Rf and vacuum seals were made with expendable copper gaskets of the type described by Goertz.[7] This design was satisfactory and used for the remainder of the program.

After assembly, window test units were checked at low power for resonant frequency, and input vswr.

For evaluation at high power, window test units were connected to a waveguide run fed by a high power klystron. Experiments were carried out under CW and pulsed conditions at frequencies near 2850 Mc. Instrumentation was similar to that used in Task C which is described in detail in Sec. 4.3.4.

4.3.3 Task B

All work connected with the high frequency matching and testing of the windows evaluated in Task B of the program was carried out at the facilities of the Stanford Linear Accelerator Center, Stanford University.

The windows tested were all 3 inch diameter discs. They were not metalized but shrunk into copper cylinders in which they

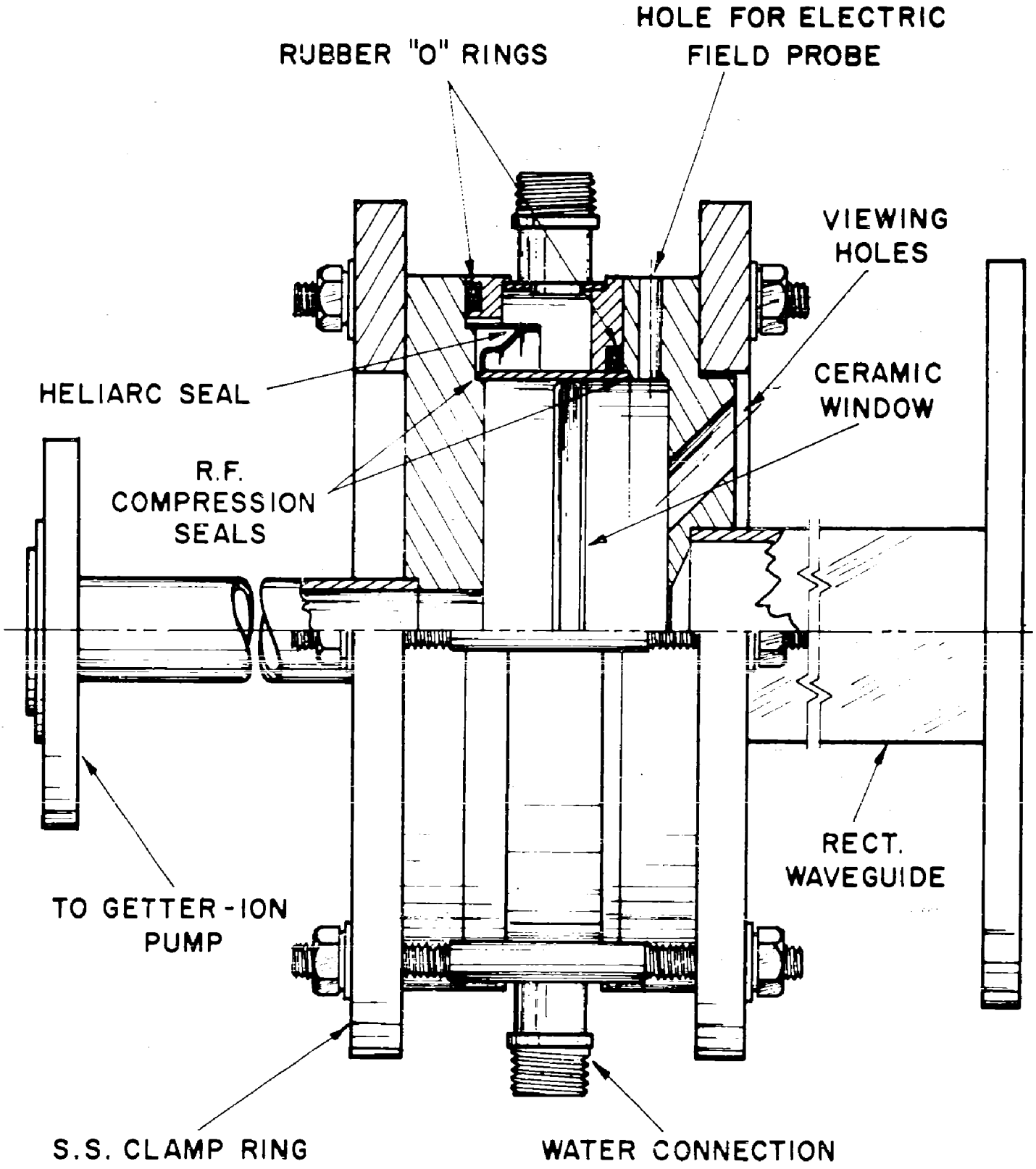

"WINDOW BOX" ASSEMBLY

Fig. 3

were held in good thermal contact. For testing at high power, window assemblies were mounted in a ring resonator operating at 2850 Mc. The ring resonator employed a fixed pulse width of 3 microseconds. During testing the pulse repetition rate was normally 60 pulses per second but was increased to 240 and 360 pulses per second in order to increase the average power in the window. The highest powers obtainable in the Stanford ring resonator at the time these experiments were carried out were approximately 85 Mw peak and 15kW average at 60 pulses per second and 40 Mw peak, 43 kW average at 360 pulses per second. The ring resonator was evacuated to pressures of about 10^{-6} Torr prior to the high power testing but no window bakeout was employed.

4.3.4 Task C

The procedure for testing windows in the 2nd year of the program was similar to that used in Task A. A resonant cavity method was employed, windows being built into sealed off assemblies which were processed in the same way as an electron tube prior to testing at high power.

Two types of test units were used, Model 3 (Figs. 4, 5 and 6) in which only one side of the window is under vacuum, and Model 4 (Figs. 7, 8 and 9) in which both sides of the unit are evacuated. Prior to metalizing, window ceramics are heated in a diabasic acid solution on an ultrasonic cleaner, then rinsed several times in deionized water followed by an acetone rinse. Ceramics are then clean-fired at 800°C in a hydrogen furnace. Brazed window assemblies are coated without further cleaning and built into test units.

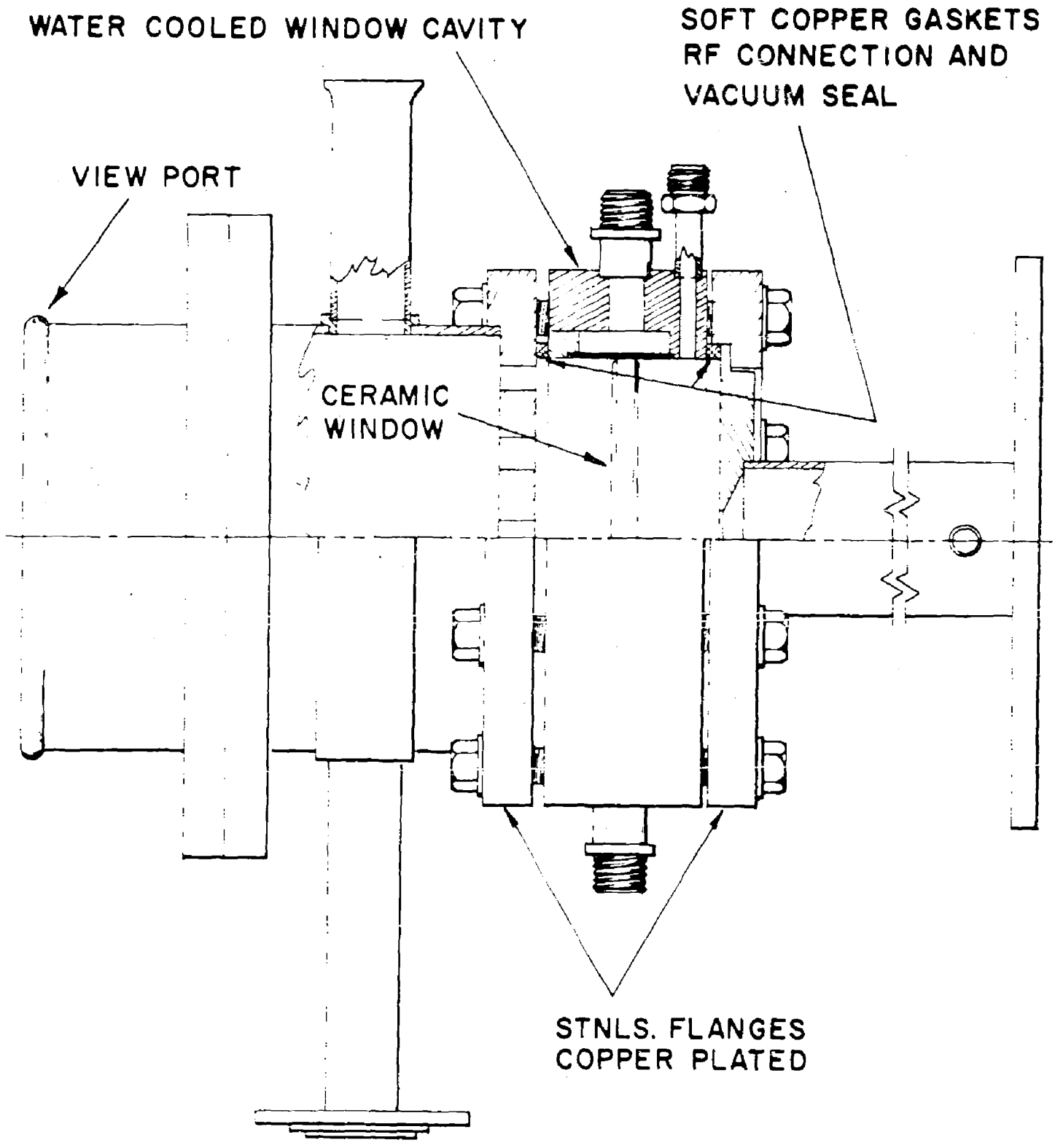

TEST UNIT ASSEMBLY - MODEL 3

Fig. 4

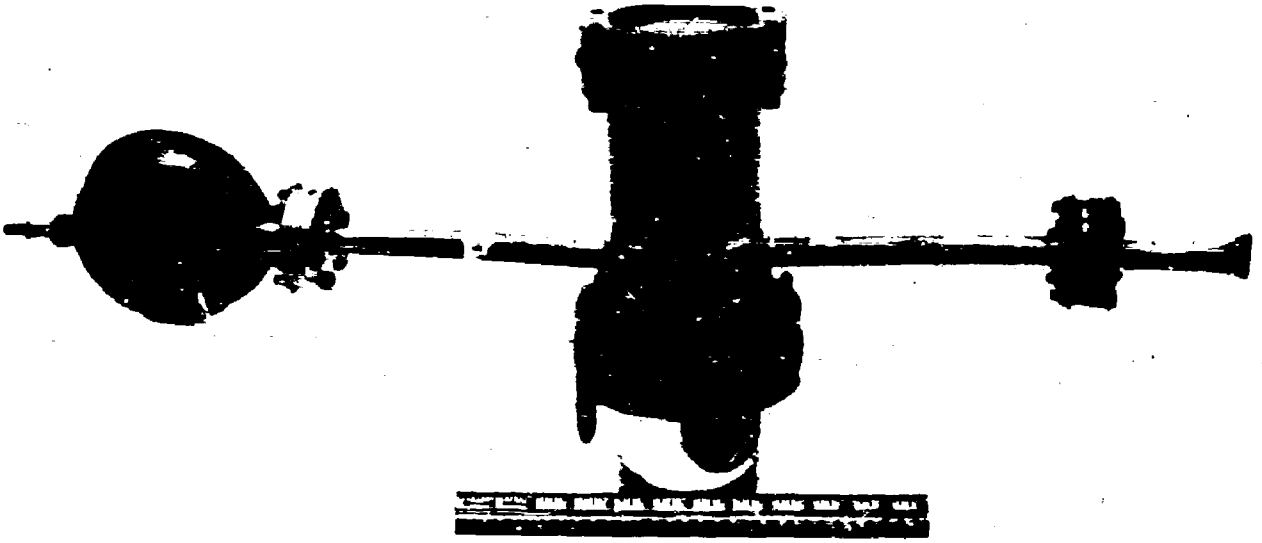

Fig. 5 Single Vacuum Test Unit Components

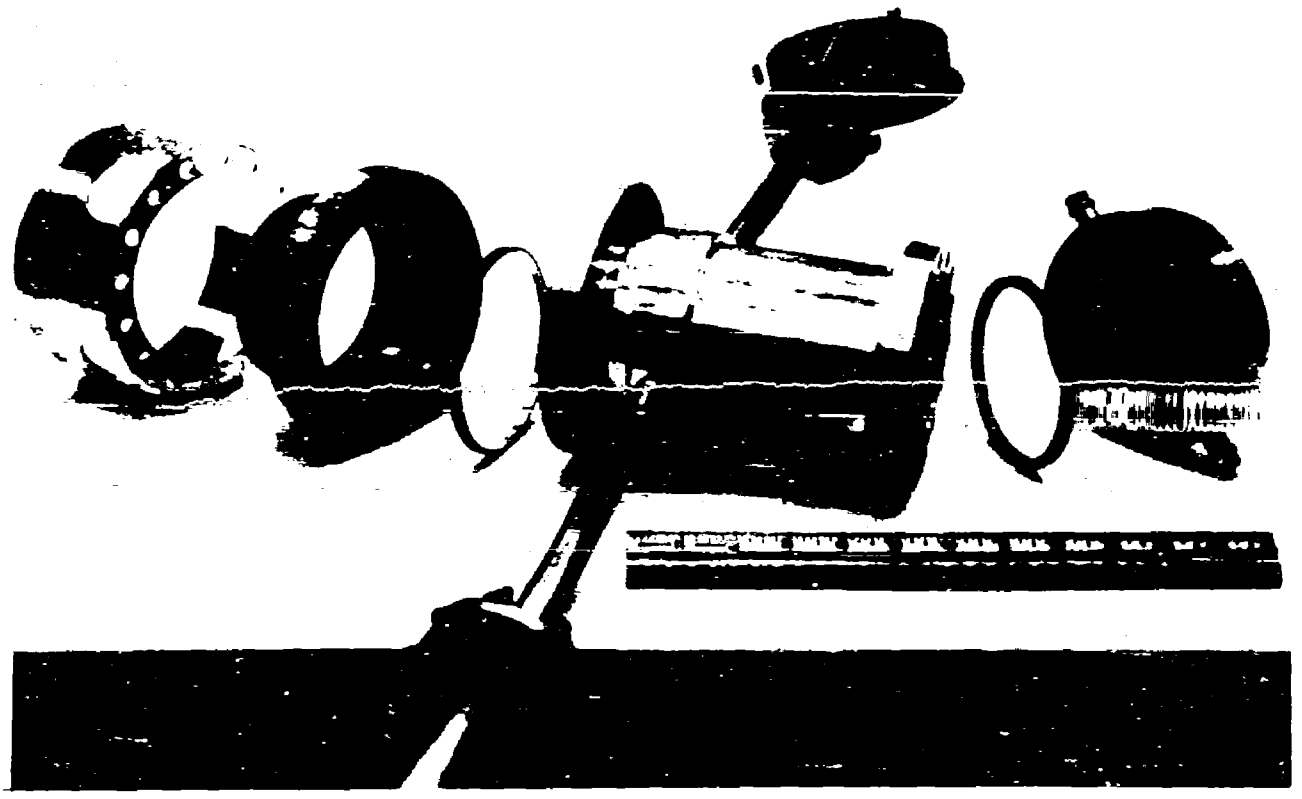

Fig. 6 Single Vacuum Test Unit Assembly

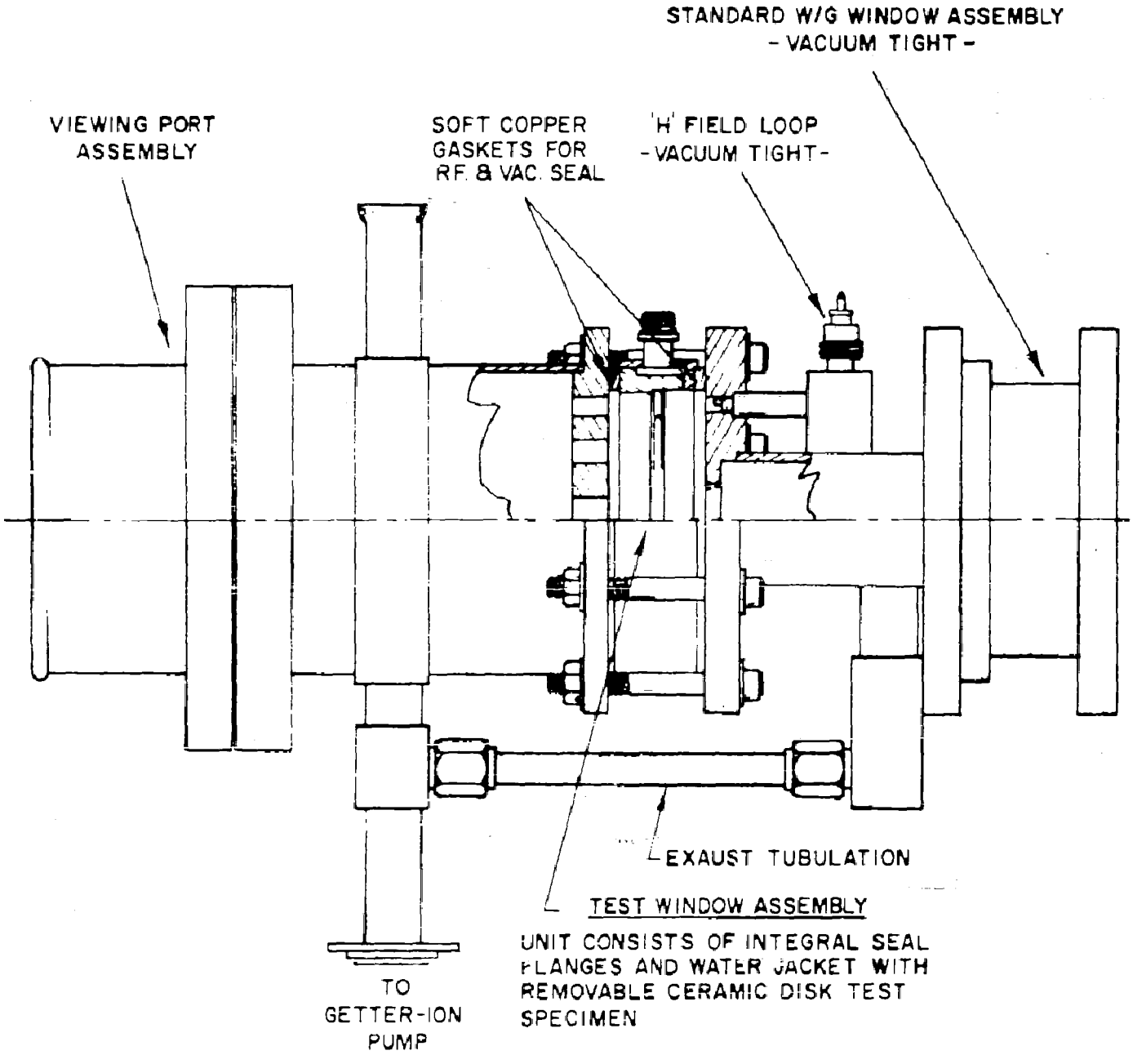

TEST UNIT WITH VACUUM ON BOTH SIDES OF WINDOW

Fig. 7

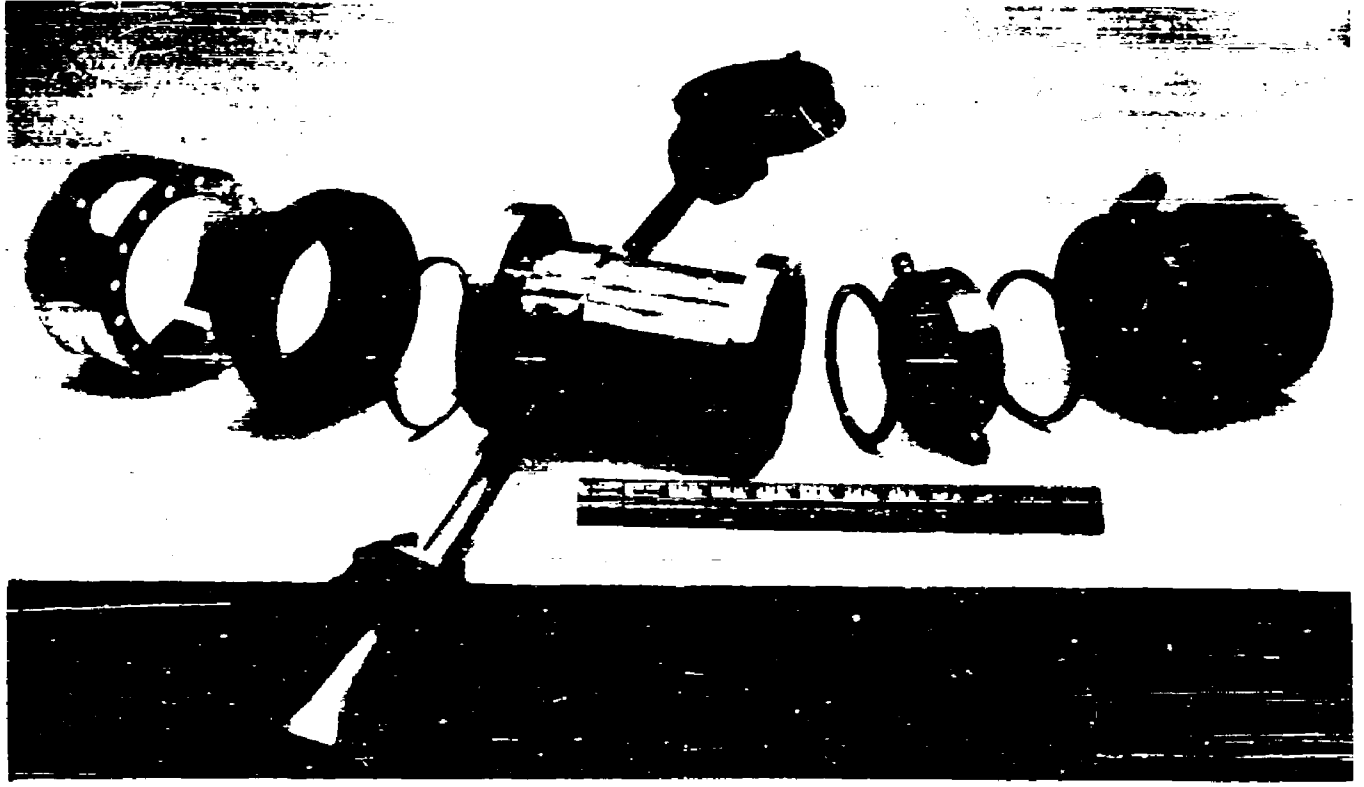

Fig. 8 Double Vacuum Test Unit Components

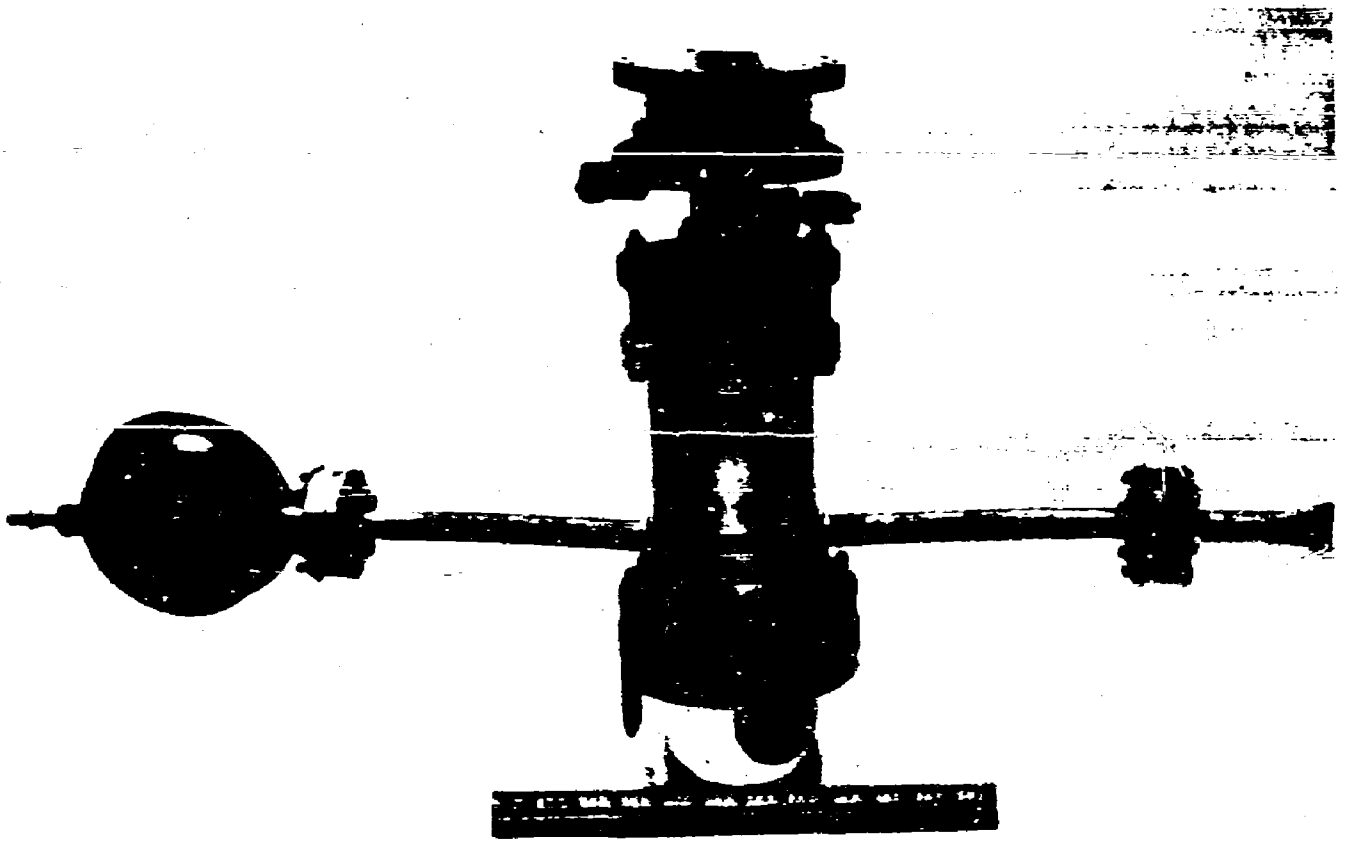

Fig. 9 Double Vacuum Test Unit Assembly

Prior to high power testing, the units are tested at low power to test the resonant frequency, the input vswr at resonance, and the loaded Q of the unit. The Q is used to determine the ratio of the power dissipated in the cavity to the equivalent transmitted power.

On completion of the test on a coated window, the coating is removed from the window assembly which can then be used again. The ceramic is etched with a nitric hydrofluoric acid solution to remove titanium or titanium monoxide coatings, treated with an ammonium hydroxide solution and finally rinsed several times in deionized water.

The High Power Test Facility used in Task C was constructed for the exclusive use of the window program. It consists of a pulsed klystron amplifier with associated modulator, trigger circuits and rf oscillator. The equipment is capable of delivering rf power up to several hundred kilowatts peak and 4 kilowatts average, in the frequency range 2625 to 2675 megacycles per second. A fixed pulse width of 20 microseconds is used with a duty cycle variable up to 2% maximum. The Eimac X-3040 klystron amplifier is a specially designed tube which will operate at a high efficiency over a wide range of power output, allowing operation at high average power without exceeding the modulator rating.

As will be shown in detail in Appendix IV, the resonant cavity produces an electric field strength at the window which is much greater than that in the output waveguide of the klystron. If the window, instead of being in a resonant cavity, were in a waveguide transmitting power in one direction to a

matched load, as in normal klystron operation, this large field strength would correspond to a transmitted power approximately equal to $\frac{Q_2}{Q_1}$ x power dissipated in the cavity

where Q^2 is the Q of the cavity without external connections, and Q_1 is its Q when "matched" to a load as in the normal operation referred to above.

Since, for the windows tested in this program, $\frac{Q_2}{Q_1}$ was 300 to 500, the 4kw average power available from the klystron would give an "equivalent average transmitted power" of about 4 x 300 to 500 kw, or 1.2 MW to 2 MW, assuming all the 4 kw were dissipated in the cavity. Likewise, a peak power of 200 kw, dissipated in the cavity, would correspond to an "equivalent peak transmitted power" of about 200 x 300 to 500 kw or 60-100 MW peak power.

A block diagram of the test facility and the arrangement used for window experiments is given in Fig. 10. The waveform generator allows the modulator to be triggered at a selected pulse recurrence frequency. RF drive is provided by a signal from a variable frequency oscillator amplified by a TWT amplifier. Power from the klystron is transferred to the window test unit by a directional coupler which facilitates monitoring of the forward and backward power. The electric intensity within the cavity is measured by a probe connected to a calorimeter. Power dissipation in the window may be measured by a water calorimeter and the pressure within the test unit is monitored by the attached getter ion pump.

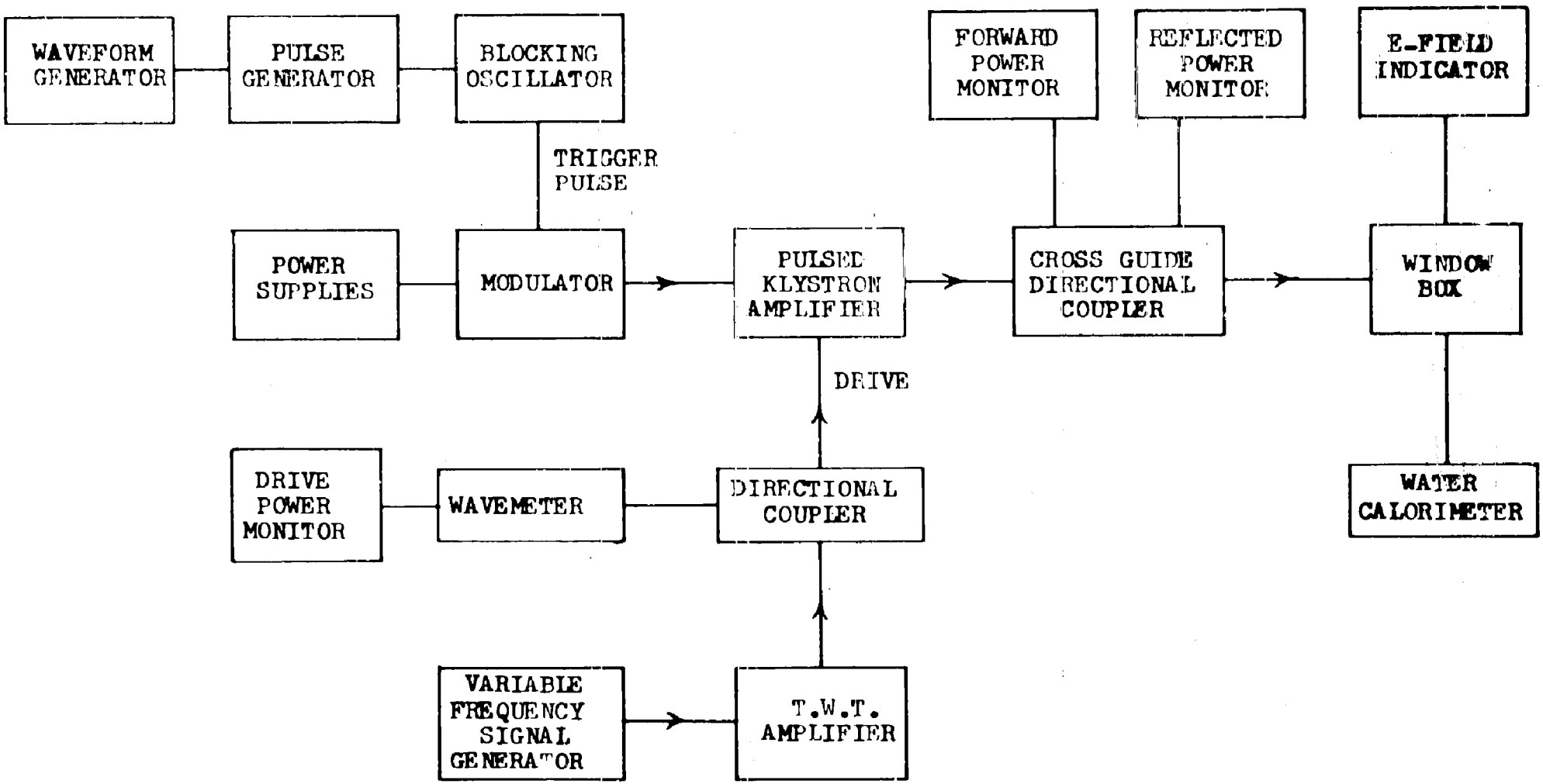

Fig 10 BLOCK DIAGRAM OF HIGH POWER TEST FACILITY

For most of the tests, the electric field probe consisted of a short-piece of small diameter coaxial line, open at one end, the other end being connected to either a crystal or a bolometer. This unit was pushed into the hole in the cylindrical wall of the resonant cavity shown in Figs. 3 and 4, the depth being adjusted to give a convenient signal level.

For other tests, a loop was used in the cavity end wall (Figs. 7, 8, and 9). This measures the magnetic field which is proportional to the electric field.

For pulse tests the crystal detector was found convenient, in that an oscilloscope presentation of the electric field pulse is provided. To obtain reasonable linearity between RF electric field and rectified voltage displayed on the oscilloscope, a high load impedance is required (10 kΩ is typical). To minimize distortion of the waveform the product of this load resistance and the load RF by-pass capacitance must be small. This necessitates the use of a special capacitor having a few micro-microfarads capacitance rather than the standard capacitors in crystal mounts which sometimes have several hundreds of micro-microfarads.

The disadvantage of the crystal is that it has to be calibrated (most crystals are nonlinear) and the calibration has to be checked regularly. For this reason the bolometer was preferred for the CW tests. When using the crystal, which gives a signal voltage proportional (after correction) to RF field, this signal squared was plotted as the abscissa of graphs such as Fig. 12. When the bolometer was used, the output power (indicated on the

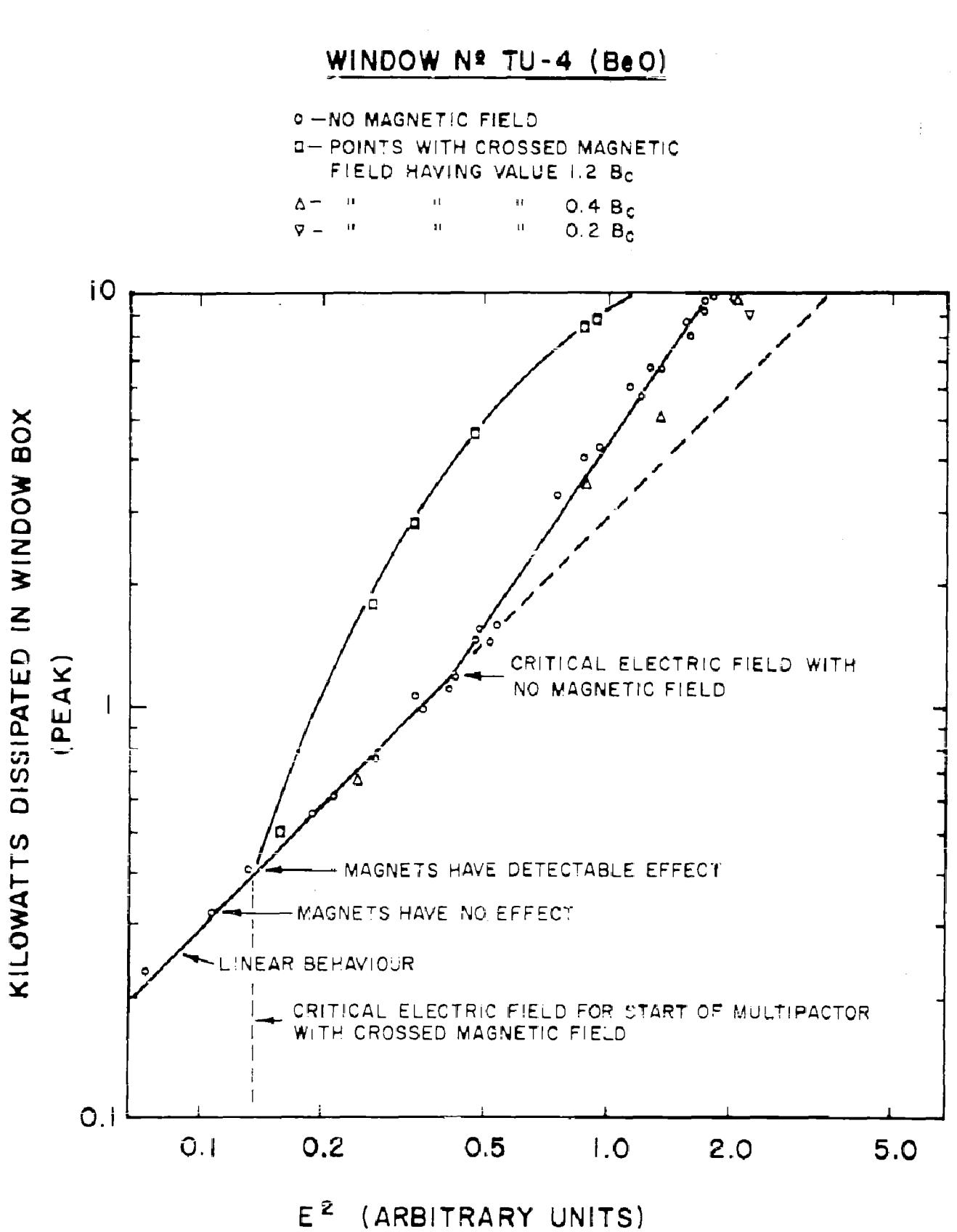
WINDOW Nº TU-4 (BeO)
o —NO MAGNETIC FIELD
□— POINTS WITH CROSSED MAGNETIC FIELD HAVING VALUE 1.2 Bc
Δ— " " " 0.4 Bc
▽ — " " " 0.2 Bc
10
1
0.1
KILOWATTS DISSIPATED IN WINDOW BOX (PEAK)
CRITICAL ELECTRIC FIELD WITH NO MAGNETIC FIELD
MAGNETS HAVE DETECTABLE EFFECT
MAGNETS HAVE NO EFFECT
LINEAR BEHAVIOUR
CRITICAL ELECTRIC FIELD FOR START OF MULTIPACTOR WITH CROSSED MAGNETIC FIELD
0.1
0.2
0.5
1.0
2.0
5.0
E² (ARBITRARY UNITS)
EQUIVALENT MEGAWATTS TRANSMITTED (APPROXIMATE)

Fig. 12

Hewlett-Packard Model 430C Microwave Power Meter) was plotted as the abscissa.

If the cavity is "linear", as it will be when only ohmic losses are present (i^2R losses in metal walls and dielectric losses in window) the power dissipated (measured in the cooling water, or by the directional coupler) varies as the electric field squared:

$$W_{diss} = KE^2$$

If multipactor exists, this is no longer the case, as can be seen from Fig. 12 and others.

To detect the existence of multipactor it is necessary only to measure W_{diss} for various values of E^2, regardless of K, and to plot the results as shown. In this investigation, however, it was desirable to measure the absolute value of electric field, so that the minimum or threshold field at which multipactor began could be checked against the theory.

Two methods of calibrating the field probe to obtain absolute values of field were used. In one method the approximate relationship described on page 19 and in Appendix IV between power dissipated and equivalent power transmitted was used. For a measured dissipation an equivalent transmitted power was calculated. Then, by using the equation relating power to field strength in a matched unperturbed circular waveguide (page 11, eq. (3)) a corresponding electric field strength was calculated, and used for calibrating the probe. This is only approximate.

The other method was to calculate the relationship between field strength and total loss in the cavity, and to calibrate the probe on this basis, for a given measured loss. The calculation is given in Appendix II.

4.3.5. Analysis Of The Window Cavity

A field analysis of the window cavity was carried out to obtain a better understanding of the field distribution in the cavity and to determine the relationship between field strength and power input. The analysis applies to a cylindrical cavity with a dielectric disc at the center, having the parameters shown in Fig. 11.

The cavity was designed to operate in the TE_{111} mode. Similar field patterns exist in both the vacuum and dielectric sections but the value of the propagation constant β will be different in each section. The field equations for the TE_{111} mode, in terms of cylindrical coordinates z (y in the dielectric) r and ϕ, are given in Appendix II. By applying the appropriate boundary conditions at the walls and at the vacuum-dielectric interface the following equation is obtained which gives the condition for resonance:

$$\beta_2 \tan \beta_1 p = -\beta_1 \cot \beta_2 q \qquad (7)$$

where β_1 and β_2 are the propagation constants in the air and dielectric sections respectively, q is 1/2 the dielectric thickness and p the space each side of the disc. (see Fig. 11)

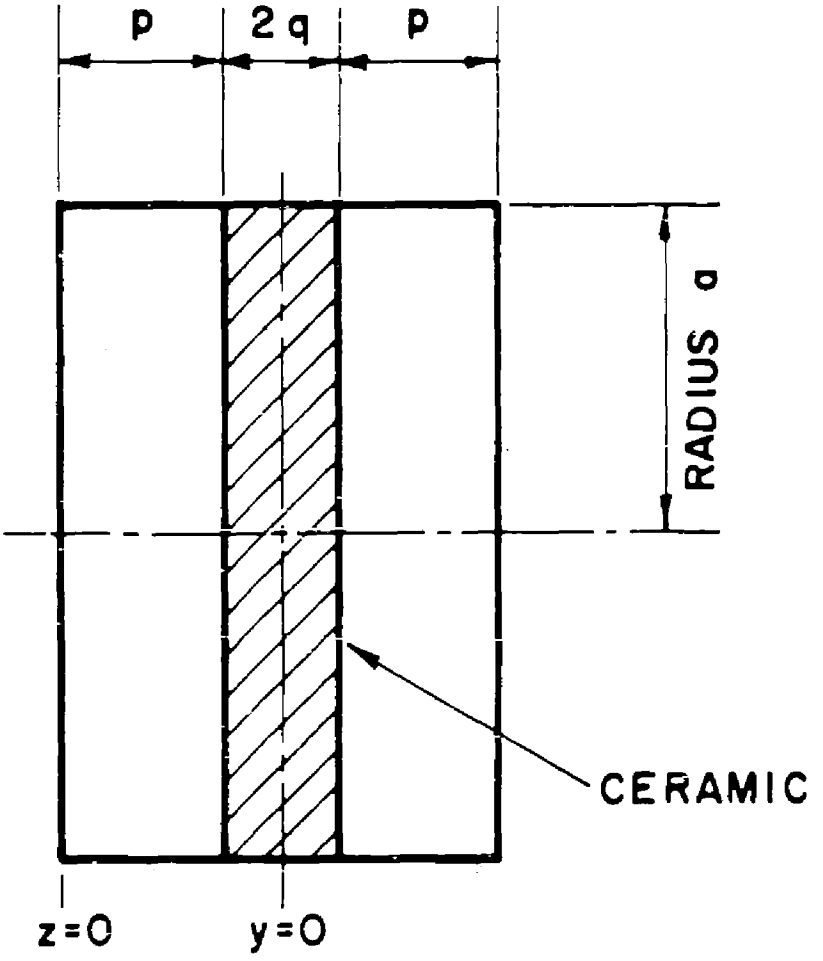

DIELECTRIC LOADED CAVITY

Fig. 11

The equation was used to calculate values of p for a cavity resonance at 2700 Mc when loaded with an alumina and a beryllia disc, and compared with the value required in practice.

The values are given below together with the relevant cavity parameters.

Resonant frequency	2700 Mc	2700 Mc
Cavity radius	4.7 cm	4.7 cm
Dielectric thickness(2q)	.325cm	.508cm
Relative permittivity of dielectric (E_r)	9.0	6.65
Calculated p	1.79 cm	1.62 cm
Actual value of p	1.64 cm	1.57 cm

The discrepancy in the values of p is due to the fact that the calculated value does not take into account perturbations due to the coupling hole or the viewing window.

Calculation of the Cavity Q

The unloaded Q of a cavity is given by the following expression:

$$Q_o = \frac{\omega_o \text{ stored energy}}{\text{mean power loss}} \qquad (8)$$

where ω_o is the resonant frequency. Since the mean energies stored in the magnetic and electric fields are equal,

the total stored energy (U) may be calculated by considering the electric field components only.

$$U = \int_{\text{volume}} \frac{\varepsilon |E|^2}{2} \, dv \qquad (9)$$

Details of the calculation are given in Appendix II. The power dissipated in the cavity is due to losses in the walls and the dielectric. The wall losses are estimated by considering the wall currents, due to the field pattern of the loss-free case (as given by equations 1 to 10 in Appendix II) flowing in a surface of resistivity R_s. For copper at 2700 Mc the value of R_s is 14.3×10^{-3} ohms/square. The dielectric loss is obtained from the field equations and a knowledge of the loss tangent.

A numerical calculation for the loaded Q of the cavity gave a value of 1800 for the alumina-loaded cavity and 1100 for the beryllia-loaded cavity. In practice Q values of this order were obtained. (See Tables 2 and 3) There was considerable variation in the measured value of Q which depended on the condition of the surfaces, seals and the brazed joint at the metal-dielectric junction.

4.4. Observations On Multipactor At Microwave Windows

4.4.1 Experiments With Untreated Windows

In order to study multipactor effects at microwave windows, several plain untreated ceramics were tested using the

TABLE 2

EVAPORATED TITANIUM COATINGS ON BERYLLIA
SUMMARY OF HIGH POWER TEST RESULTS

Test Unit	Coating Resistivity (ohms/sq.)	Cavity Q_L	Peak Power Equiv. Dissipated (kw)	Peak Power Equiv. Trans. mitted (Mw)	Average Power Equiv. Dissipated (watts)	Average Power Equiv. Transmitted	Remarks
14	$>10^{10}$		40				Some clean up but multipactor not eliminated completely
17	$2.5\ 10^{9}$	1270	8	3.4			Initial multipactor cleared up.
18	$2.5\ 10^{7}$	1300	40	17	520	225	" " "
20	$> 10^{7}$	1030	64	27	350	120	" " "
29	10^{6}	1300	55	24	750	325	No multipactor.
31	10^{6}	1300	90	39	650	280	No multipactor. Peak power achieved with short pulse.
36	2.10^{6}	1000	19	6.3	400	133	Initial multipactor cleared up.
39	10^{5}	1300	141	61	950	410	No multipactor. Peak power achieved with 3μsec. pulse.
49	10^{10}	1200	45	18	600	240	Initial multipactor cleared up.
51	10^{5}	1300	22	-	-		Slight multipactor.

TABLE 3

EVAPORATED TITANIUM COATINGS ON ALUMINA
SUMMARY OF HIGH POWER TEST RESULTS

Test Unit	Coating Resistivity (ohms/sq.)	Cavity Q_L	Peak Power		Average Power		Remarks
			Dissipated (kw)	Equiv. Transmitted (Mw)	Dissipated (watts)	Transmitted	
19	$2.5\ 10^7$	1400	46	22	220	100	Initial multipactor cleared up. Later window cracked due to excessive average power
22	$> 10^7$	1500	45	22	230	115	Initial multipactor cleared up.
32	10^7	1500	46	23	200	100	Slight multipactor initially
37	3.10^5	1350	75	34	150	68	Initial multipactor cleared up.
48	10^7	1500	70	35	70	35	Initial multipactor cleared up.

resonant cavity method. The test procedure was to increase the peak power gradually at low duty cycle until a multipactor discharge commenced. This would be indicated by an increased pressure, as monitored by the getter ion pump, a change in forward to backward power ratio due to the mismatch created by the discharge and a reduction in the reading of the electric field probe in the cavity. Values of forward and backward power were recorded, together with the readings of the electric field probe (proportional to the square of the field), the pressure, and notes on visual observations. A plot of the peak power dissipated versus the probe reading would be non-linear in the multipactor region. A typical result is shown in Fig. 12, which shows non-linear behavior starting at a peak power dissipation of 1.3 kilowatt or an equivalent transmitted power of 0.4 megawatts. A sample calculation showing how these numbers were arrived at is given in Appendix IV.

The discharge could be observed visually through perforations in one of the cavity end walls and would consist of a blue or purple glow covering the surface. Usually, the intensity of the glow corresponded to the field pattern of the TE_{11} mode, i.e., brightest in the center, but sometimes this pattern was distorted, particularly when a magnetic field was applied to the window. A typical glow pattern is shown in Fig. 13.

The effect of immersing the window in a static magnetic field directed parallel or perpendicular to the electric component of the electro-magnetic field in the resonant cavity, was generally to cause the multipactor to start at lower values of peak power dissipation. Magnetic field strengths up

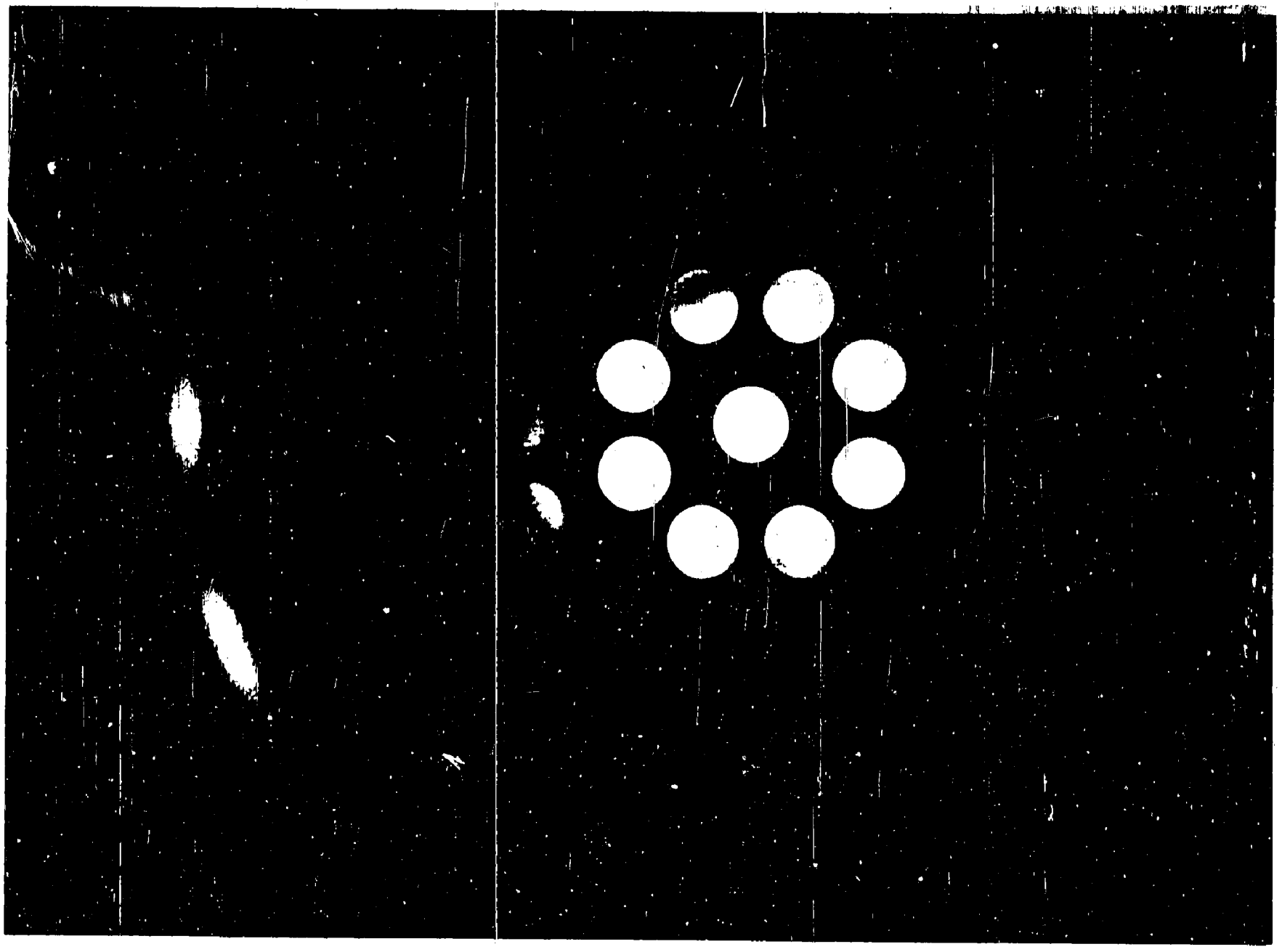

FIG. 13 Multipactor Discharge At A Plain Alumina Window

to 1.5 times the cyclotron resonance value were applied. In general, the higher field strengths caused a more intense discharge, but certain values of magnetic field would stop the discharge completely. The values of magnetic field strength which would increase or decrease the intensity of a multipactor varied from window to window and no correlation between the magnetic and electric field strength for starting or stopping a multipactor could be determined. Typical results obtained with a beryllia window are shown in Fig. 14. The threshold power levels for window multipactor with and without a static magnetic field are indicated. A plot of power dissipation versus electric field strengths squared, for various values of magnetic field are shown in Fig. 15.

The threshold power levels for multipactor at all the plain windows tested during the program are shown in Table 1. There is no marked difference between the field strengths for starting multipactor at beryllia, alumina or quartz windows. Values of equivalent transmitted power at which multipactor started with or without a magnetic field, were in the range 0.1 to 0.6 megawatts. This is the power range in which multipactor effects may be expected with circular disc windows operating at S-band, or at other frequencies if the window dimensions are scaled linearly with wavelength. See Section 4.2.2.

Some window conditioning was observed. In a typical case multipactor would commence at a certain power level when the windows were first exposed to high power microwave fields. In order to extinguish the multipactor the power level would have to be reduced below the starting level. After a period of operation with a multipactor

WINDOW Nº TU-1 (BeO)

THRESHOLD POWER LEVELS FOR WINDOW MULTIPACTOR WITH AND WITHOUT STATIC MAGNETIC FIELD. F = 2860 MC

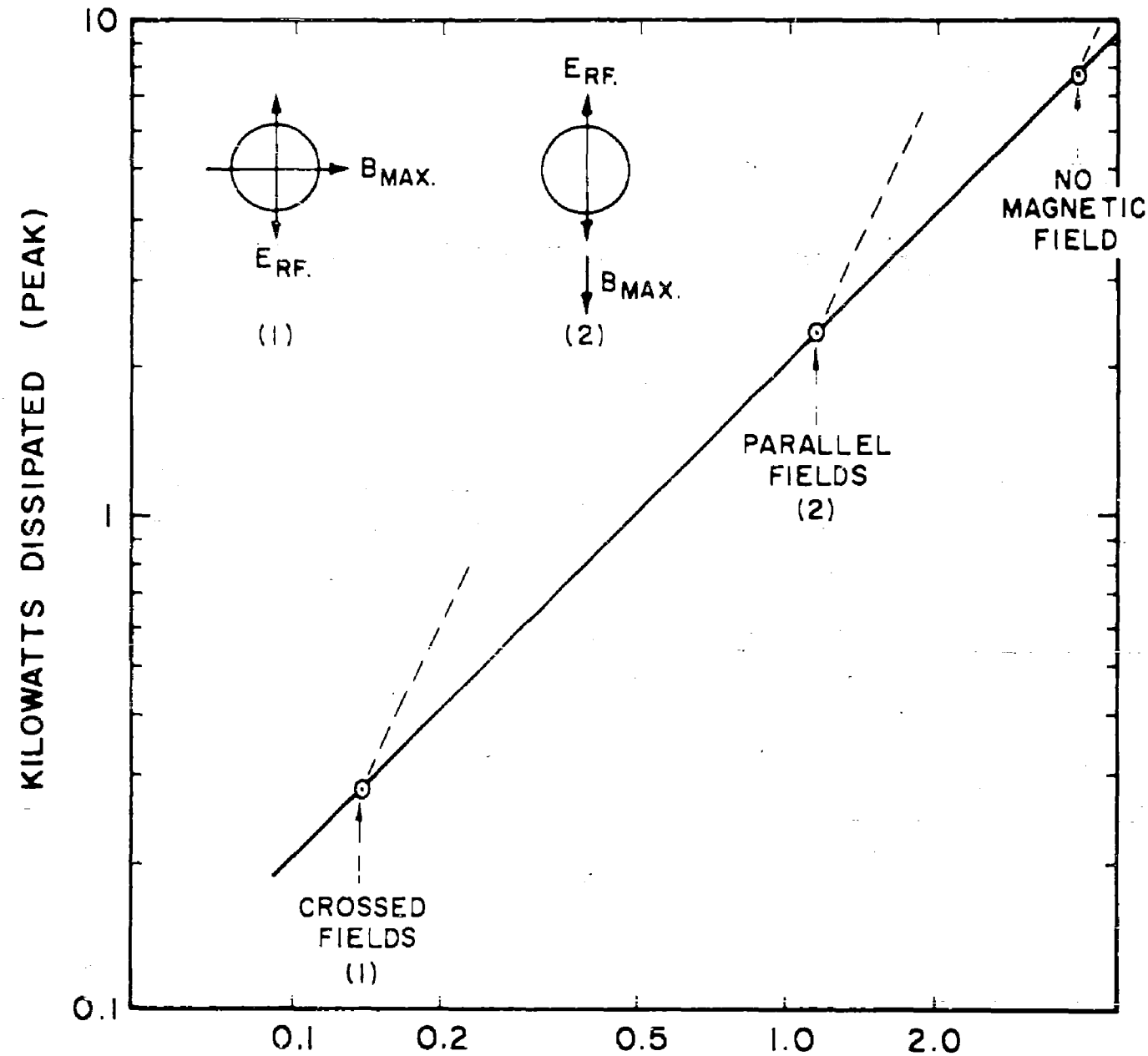

Fig. 14

WINDOW Nº TU-1 (BeO)

WINDOW MULTIPACTOR WITH CROSSED FIELDS OF DIFFERENT VALUES
F = 2860 MC

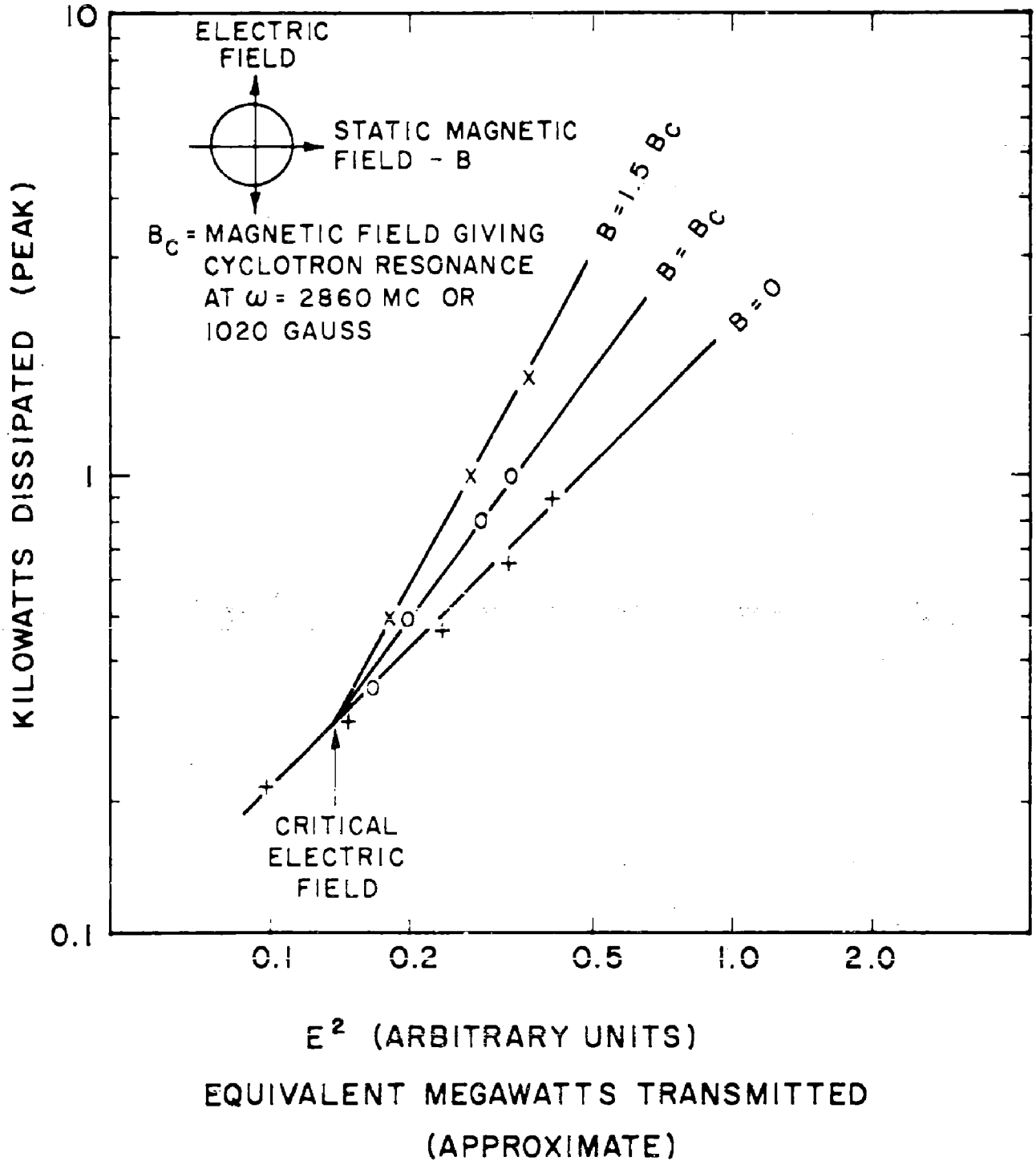

Fig. 15

discharge, the threshold power would increase sometimes by a factor of 2 or 3 until a fixed threshold power level was obtained. No further conditioning would then occur.

4.4.2 Gases Evolved During A Multipactor Discharge

A multipactor discharge at a ceramic surface is invariably accompanied by an increase in pressure within the test unit. The pressure remains at a high value while the discharge lasts, returning to a low pressure immediately after the multipactor stops.

Various explanations for this effect had been suggested as follows:

1. A continuous disassociation of window material under the influence of electron bombardment.

2. The amount of adsorbed gas on the window and other surfaces is much larger than is commonly supposed.

3. Ionized gases which are not pumped by the appendage pump, such as argon, may be continuously recirculated within the system.

4. There is a gas transport mechanism not presently understood.

To investigate the nature of this pressure rise, a study was made of gases evolved during a multipactor discharge at an alumina surface. A standard window assembly containing a plain uncoated alumina disc was used for the study. The window was assembled in a test unit to which a Diatron mass spectrometer had been attached and processed in

the normal way (i.e., baked at 400°C for 24 hours during evacuation at an oil diffusion pump station). The partial pressure of residual gases in the test unit was measured with the unit on the diffusion pump system prior to nip-off, just after nip-off with the getter ion pump on and again 24 hours later.

After checking the resonant frequency, loaded Q and input vswr of the unit at low power, the assembly was mounted on the high power waveguide run. A photograph of the unit mounted for testing is shown in Fig. 16.

When operated at high microwave power, multipactor first started when dissipating 1.5 kw peak and 30 watts average power in the window cavity, and was therefore typical as can be seen from Table 1. A bright discharge glow appeared at the window and the pressure indicated by the getter ion pump increased from $<10^{-8}$ Torr to 10^{-6} Torr. A mass spectrometer run indicated an increase in the partial pressure of hydrogen from 10^{-8} to 6×10^{-5} Torr, the partial pressures of $CO + N_2$ and CH_4 increased from $< 5 \times 10^{-9}$ to 1×10^{-6} Torr and 3×10^{-6} respectively.

After this first set of measurements the window was operated for 2 hours at 37 kw peak 150 watts average dissipation with the multipactor discharge present; the getter ion pump was operating continuously during this period.

A further mass spectrometer run indicated a decrease in the partial pressures of H_2, $CO + N_2$ and CH_4 to 1×10^{-5}, 5×10^{-7} and 3×10^{-7} Torr respectively. Changes in the

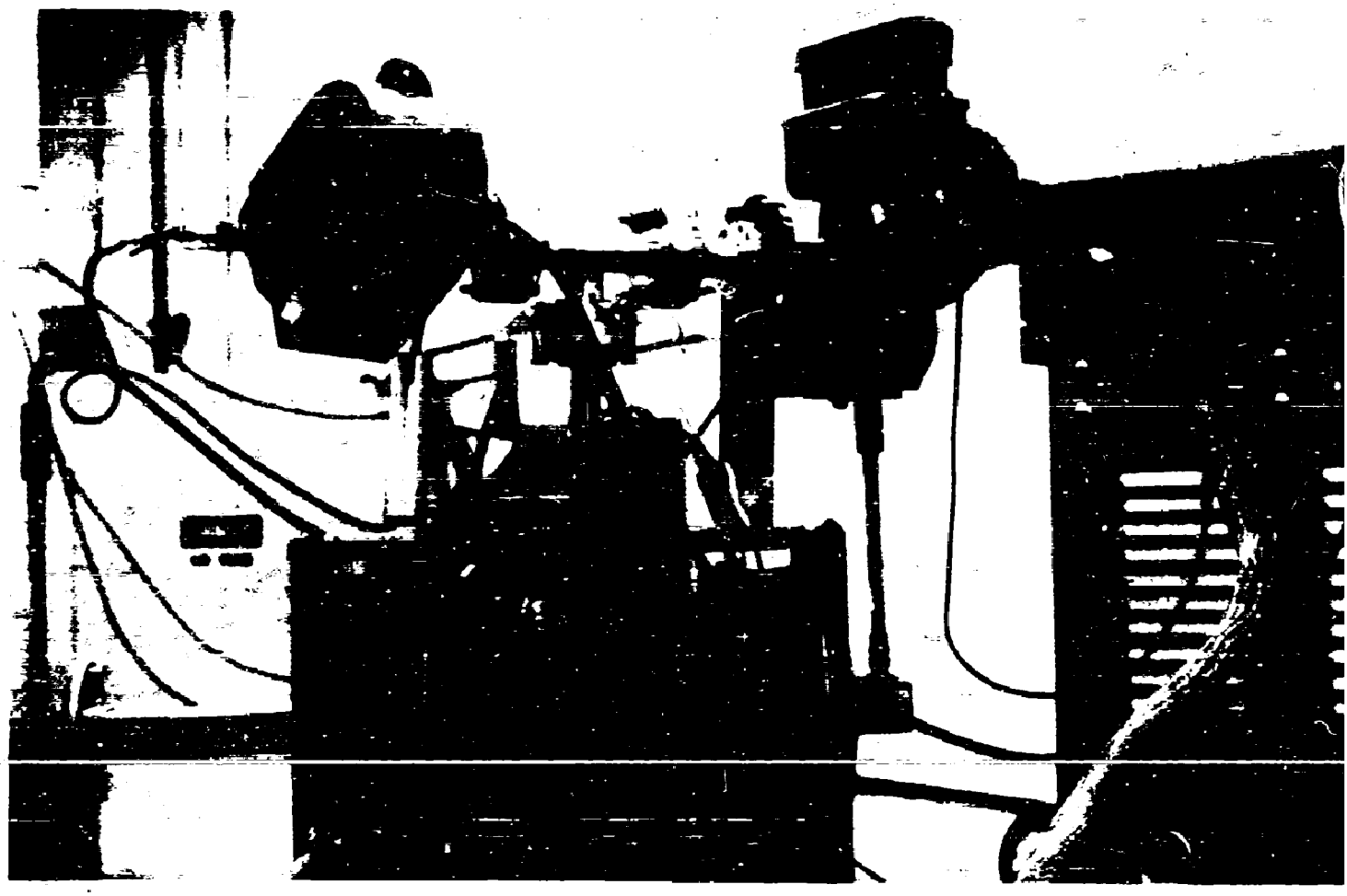

Fig. 16 Equipment For Gas Analysis Experiment

TABLE 1

MULTIPACTOR AT PLAIN WINDOWS
(All Quantities are Peak Values)

Multipactor Starts

Window		Material	No Magnetic Field			With Magnetic Field			Remarks
			Power Dissipated (kw)	Field Strength (kv/cm)	Approx Trans. (Mw)	Power Dissipated (kw)	Field Strength (kv/cm)	Approx Trans. (Mw)	
A	1	Beryllia	8.0	9.2	2.7	.28	2.1	.14	
A	4	"	1.3	3.6	0.4	0.4	2.0	.13	
C	16	"	2.2	5.0	0.8	-	-	-	Higher power necessary after period of operation.
A	12	Alumina	0.3	2.5	0.2	0.3	2.5	0.2	
C	15	"	1.6	4.3	0.6	-	-	-	
C	41	"	1.4	4.9	0.75	-	-	-	Multipactor may have started at a lower power.
C	59	Quartz	0.2	2.1	0.14	-	-	-	

partial pressures of the principal gases are shown in Fig. 17.

It is clear that the dominant gas in the system was hydrogen, which comprised 90% of the gas evolved during multipactor. To determine the effect of multipactor intensity on the evolution of gas the Diatron was held steady at the hydrogen mass level. Switching on the multipactor caused an immediate increase in the hydrogen partial pressure, a steady value being reached within a few seconds. On extinguishing the multipactor the partial pressure immediately fell to the pre-discharge value. Varying the intensity of the multipactor, by adjusting the input power to the cavity, caused a corresponding variation in hydrogen partial pressure. Applying a crossed magnetic field to the cavity of sufficient strength to extinguish the multipactor over approximately the bottom half of the disc caused the partial pressure to decrease by one half. This indicates that the volume of gas evolved is proportional to the intensity of the multipactor and to the area over which the discharge occurs.

Several conclusions may be drawn from the results of this experiment. It is clear that the pressure increase observed with multipactor is not due to disassociation of the window material, since in this case a much larger proportion of oxygen would have been present in the evolved gases. Since 90% of the gas evolved was hydrogen, the pressure increase cannot be attributed to argon or other gases not pumped by the getter-ion pump.

The most plausible explanation is that the pressure increase during multipactor is due to outgassing of the ceramic surface under the influence of electron bombardment.

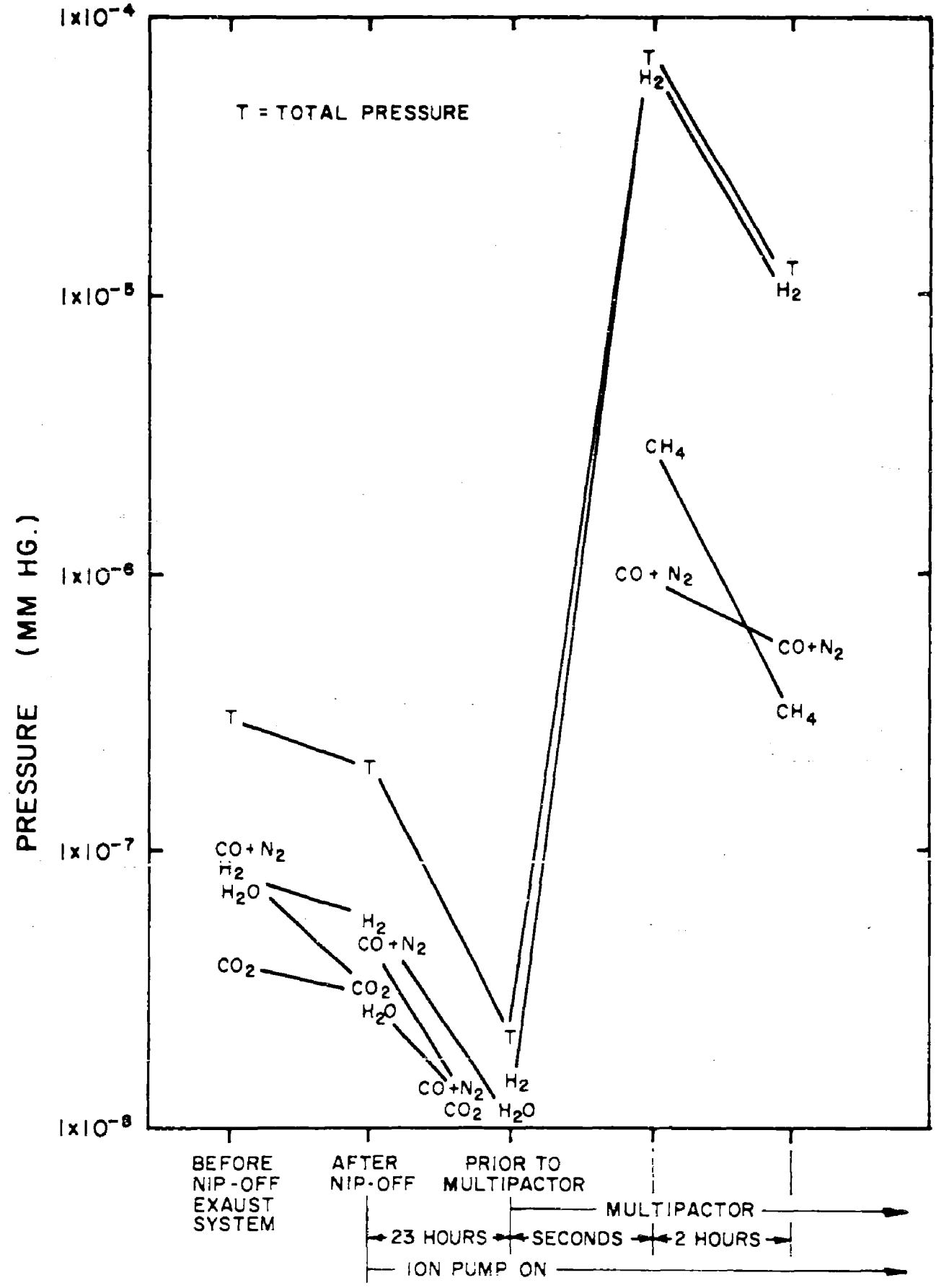

PARTIAL PRESSURES OF GASES DURING STUDY OF MULTIPACTORING ON CERAMIC WINDOW

FIG. 17

The gas evolution observed resembles that occurring at the internal surfaces of electron tubes when bombarded with electrons. Similar types of gases are evolved in about the same relative quantities. The rate of gas evolution decreases with the time a multipactor is maintained but it is probable that many hours of operation would be required to outgas the ceramic completely. Gas molecules released from the surface of the window by multipactor will strike the walls of the test vehicle many times before they reach the getter ion pump and are removed from the system. Interaction with the walls may cause further gas evolution in which case the pressures measured by the Diatron are not due to gases released by the ceramic alone. It can be concluded that gas evolution is a by-product of multipactor and not an integral part of the discharge. Large quantities of gas released by multipactor, even after a prolonged bakeout during evacuation could cause considerable deterioration in the vacuum of sealed off tubes. This is another harmful effect of multipactor discharge.

4. 5 Evaporated Titanium Coatings

4.5.1 Film Thickness Required

The film thickness necessary for the suppression of multipactor is dependent on the penetration depth of electrons involved in the discharge. At microwave frequencies the penetration will be small since maximum energy gained by an electron accelerated in an RF field is limited to that gained in one-half cycle. For transmission in a circular waveguide 3.7 inches in diameter

at a frequency of 2700 Mc the maximum energy is about 300 electron volts at 1 Mw and 3 kv at 10 Mw. Films of gold 130 Angstroms thick are reported opaque to electrons of less than one kev energy[8] and only a small fraction of 20 kv electrons can be transmitted through aluminum foil, 3.5 microns thick.[9] Thus films of a few hundred Angstroms should be thick enough to suppress secondaries at the power levels of interest, even for bombardment normal to the surface. In the gliding single surface multipactor the bombardment is at grazing incidence.

4.5.2 Method of Application

Evaporated titanium window coatings were prepared in a commercial vacuum evaporating unit. This consisted of an 18-inch vacuum bell jar equipped with an oil diffusion pump and liquid nitrogen trap together with vacuum gauges and power supplies.

Titanium metal was evaporated from a filament made of alternate turns of .010 inch molybdenum and titanium wire wound on a .030 inch diameter molybdenum core. To evaporate titanium the filament was heated to about 1200°C by current from a low voltage 60 cycle AC transformer.

Control of the film thickness during evaporation was achieved by monitoring the resistance of a small sample located next to the window. At the beginning of the program a long thick sapphire bar, metalized on two faces, was used as the monitor. This provided a short resistance path with a large surface area, so that when the unmetalized face was coated the bar resistance was about 100 times less than the resistance per square

of the coating. This allowed high values of resistivity to be easily monitored. In practice this monitor was not satisfactory, particularly for the heavier coatings used, since the short resistance path was easily contaminated and the resistivity values of films deposited on sapphire are different from the values of similar films deposited on alumina or beryllia. An alumina bar 2 inches long x 1/4 inch wide having a longer resistance path (1/4") was then employed and proved satisfactory.

The resistivity of thin evaporated films of the order of 100 Angstroms is much higher than that which would be expected from calculations based on the resistivity of the metal. This is due, in part, to the tendency of thin films to form discontinuous coatings during the initial stages of the film formation. This is fortunate from the window coating point of view since it allows films of sufficient thickness to be used without high surface conductances which would be detrimental to window performance.

A typical window coating process would proceed as follows:

a. Assemble the filament and resistance monitor on the bell jar plate and place the window to be coated about 6 inches from the filament.

b. Close the bell jar and pump down to a pressure below 1×10^{-5} Torr.

c. Supply current to the filament and allow the vacuum to recover to below 1×10^{-5} Torr while the filament is under 1000°C. This is to outgas the filament.

d. Raise the filament temperature gradually until the desired coating resistance is obtained.

e. Turn off the filament, allow to cool, open the bell jar and remove the window.

Even though the filament is outgassed below the evaporating temperature, further outgassing will occur as the filament temperature is increased. This causes an increase in pressure which will result in some contamination of the deposited film. It is necessary to shield the substrate from the filament with a shutter during the outgassing process if pure films are to be obtained as will be described below. However, films deposited without a shutter form satisfactory window coatings and have the advantage of possessing a higher surface resistivity.

A photograph of the bell jar system is Fig. 18. A detailed specification for evaporative coating of windows is given in Appendix V.

4.5.3 The Effect of Vacuum Conditions On Evaporated Films

The properties of deposited films may vary considerably with the evaporation procedure and under certain conditions the residual gases can cause severe contamination of deposited films. The number of gas molecules striking the substrate per unit time is dependent on the pressure, temperature and molecular weight of the gas. At a pressure of 10^{-5} Torr and normal temperatures the arrival rate of oxygen is of the order of 1 mono molecular layer every two seconds. For a deposition rate of 100 Angstroms per

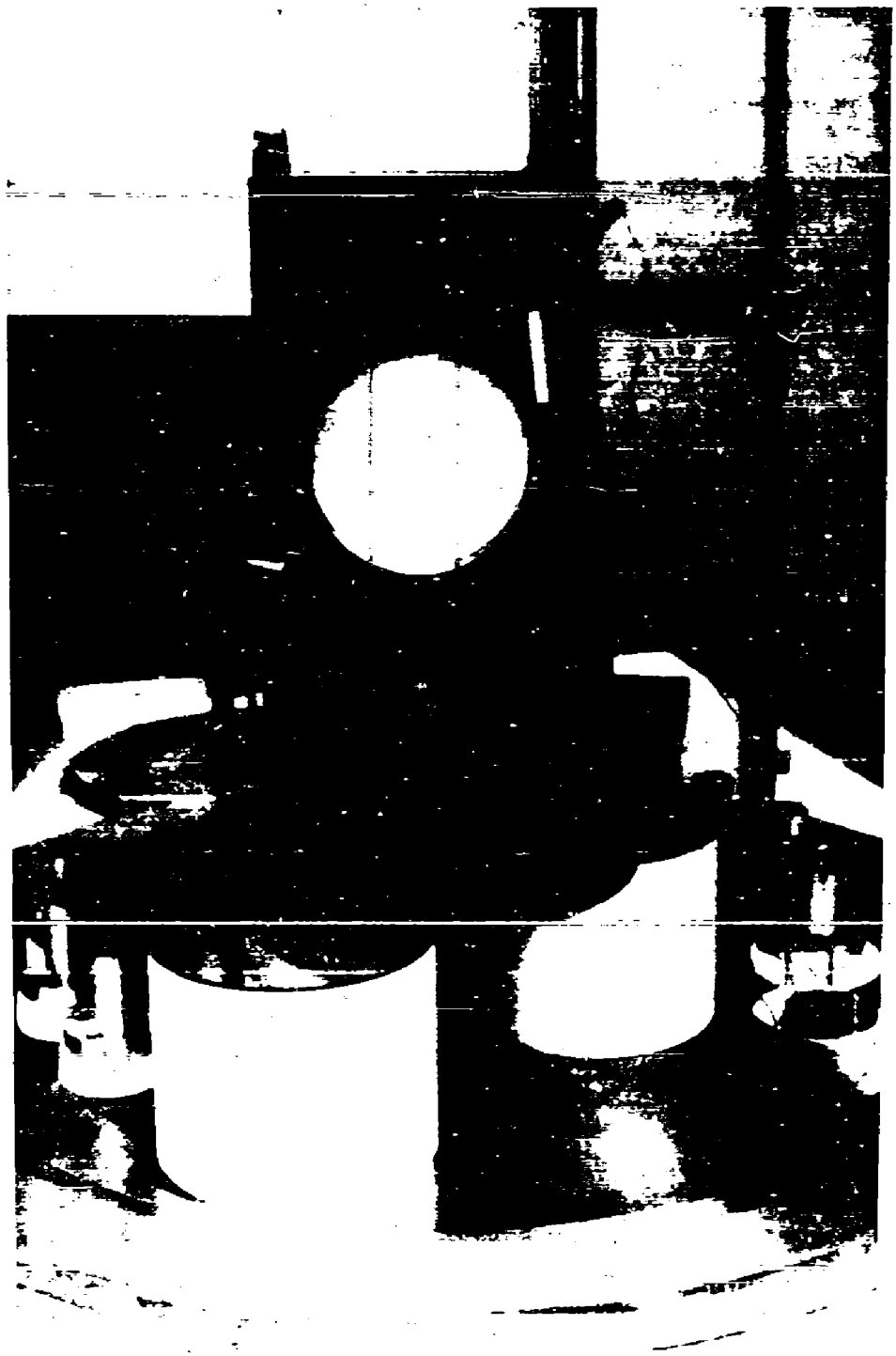

Fig. 18 Vacuum Evaporation Equipment

minute the arrival rate of the film material is about the same. Since titanium is an active metal most of the gas molecules can be expected to react to the deposited film. If the pressure is reduced to 10^{-7} Torr, the arrival rate of gas molecules is reduced by a factor of 100.

The effect of pressure on the resistance of deposited titanium films on glass substrates is illustrated by the results of experiments carried out using equipment of the University of California. The electrical resistance of the films was measured during deposition and the film thickness was determined by an optical interferometer at the conclusion of the deposition. A shutter prevented deposition on the substrate until the filament temperature and the vacuum level stabilized. Often a vacuum could be improved an order of magnitude during this stabilization and depositions at pressures lower than 4×10^{-7} Torr were possible.

The results are shown in Figs. 19 and 20. Fig. 19 is a plot of resistance versus time for depositions at 2 different pressures, and Fig. 20 shows film resistance versus thickness assuming a linear relationship based on the thickness values measured at the end of the coating period. The results are in fair agreement with the behavior of thin films as discussed in the literature. Data from Bond [10] is shown in Fig. 20 for comparison.

4.5.4 Effect Of Exposing Films To Air

One of the phenomena experienced with thin titanium films is their tendency to oxidize on exposure to air at atmospheric pressure. This is particularly the case with films deposited at the higher pressures which show increases in resistivity of several orders

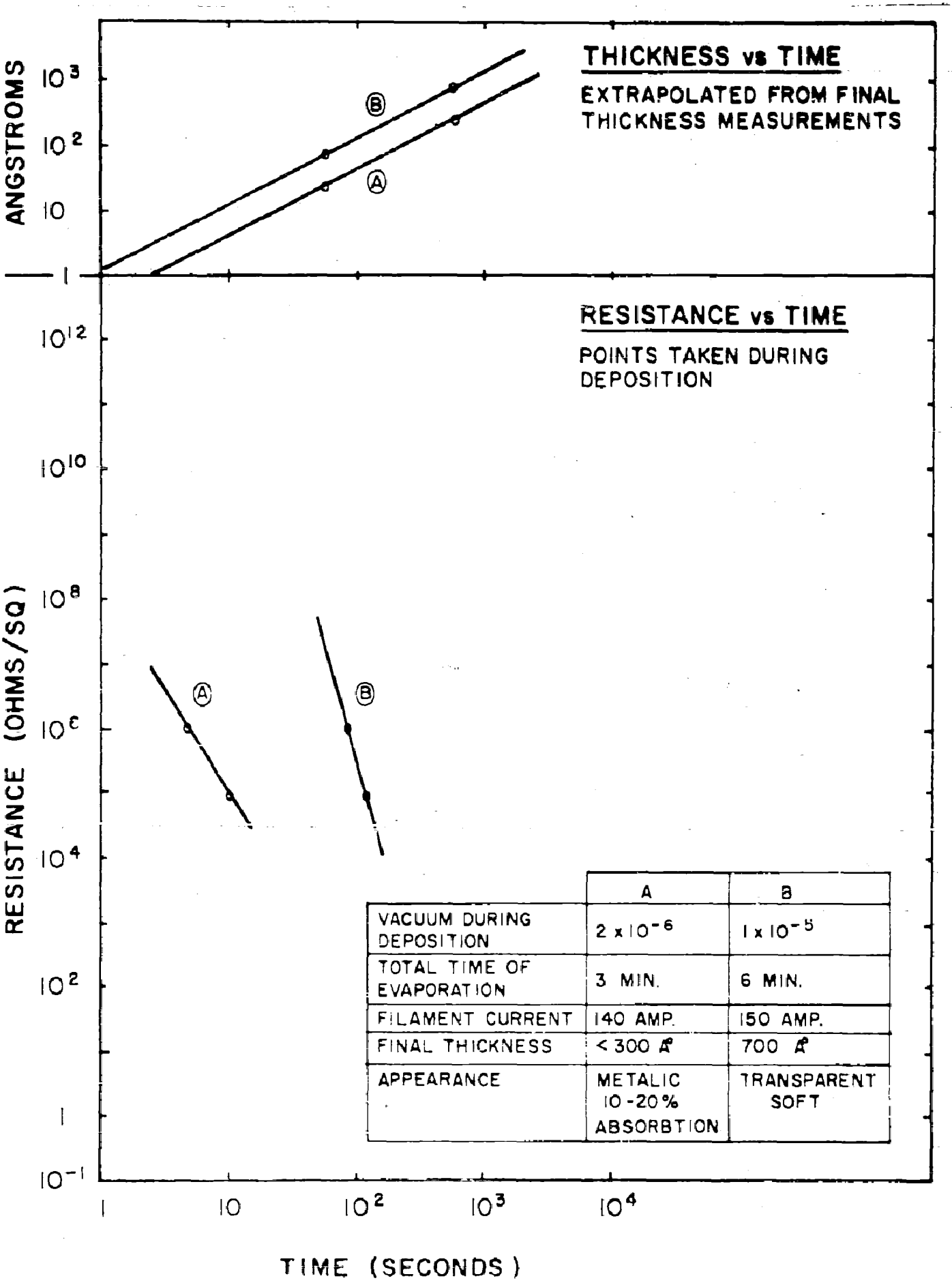

	A	B
VACUUM DURING DEPOSITION	2×10^{-6}	1×10^{-5}
TOTAL TIME OF EVAPORATION	3 MIN.	6 MIN.
FILAMENT CURRENT	140 AMP.	150 AMP.
FINAL THICKNESS	< 300 Å	700 Å
APPEARANCE	METALIC 10-20% ABSORBTION	TRANSPARENT SOFT

Fig. 19

RESISTANCE vs THICKNESS
FOR DEPOSITION AT TWO
DIFFERENT PRESSURES

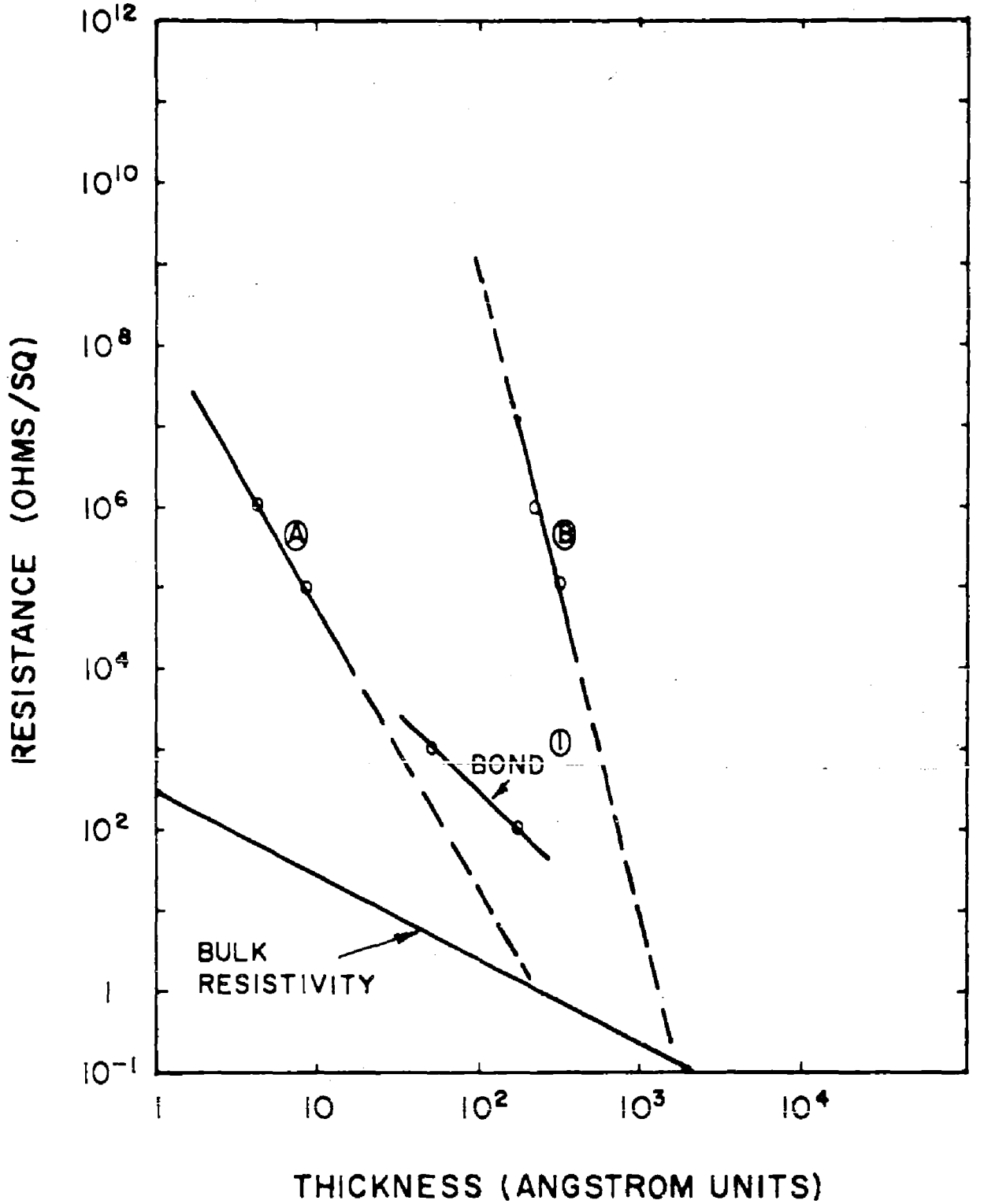

Fig. 20

of magnitude on admitting air into the bell jar. This oxidation causes an increase in the secondary yield. The results of Holland and Laurenson [11] show that maximum secondary emission coefficient of thin titanium films increases from .9 to 1.45 on exposure to dry air.

Since coated microwave windows used in test units or in an actual tube must inevitably be subjected to different atmospheres during processing, the final coating resistivity will be quite different from the original value measured during deposition. When using coated windows therefore it is important to consider all the processes to which the window is subjected in addition to the actual deposition. However, tube windows are subject to bakeout under vacuum, a process which tends to reduce any oxides which have been formed. This, and possibly additional reduction due to electron bombardment, probably accounts for the fact that most of the coatings tested in this program successfully suppressed multipactor after vacuum processing.

4.5.5 Evaluation Of Titanium Coatings At High Power

To evaluate the effectiveness of evaporated titanium coatings in eliminating multipactor at waveguide windows, a series of experiments were carried out on coatings of various thickness applied to beryllia, alumina and quartz windows. Coated windows were tested using the resonant cavity method described in Section 4.3.

For the main series of coating tests, the evaporation process was standardized as far as possible. A typical coating would take two to three minutes to deposit at a pressure

of 5×10^{-6} Torr. Although the filament was outgassed below the evaporating temperature, no attempt was made to shield the window from the filament during the outgassing process. The behavior of coatings deposited at lower pressures with the aid of a shutter is described in Section 4.5.7.

Coated windows were assembled into test units and processed as described in Section 4.3. Low power measurements were made on the units before and after evacuation and bakeout. Normally no changes would occur except in the case of thick coatings where changes in Q were sometimes observed after bakeout.

Most of the coatings tested suppressed multipactor but some required an initial period of conditioning. In such cases multipactor discharge would occur on first exposing the window to high intensity microwave fields, but after a period of operation the discharge would disappear. The window would then be completely free of multipactor, a linear plot of power dissipated versus field strength squared would be obtained and the pressure within the test unit would remain steady in the region of 10^{-8} Torr. The initial multipactor would usually be weak in intensity and would not show a nonlinearity in the power dissipation versus field strength plot, although the discharge would cause visible glow and a pressure increase in the test unit. The length of the conditioning period varied from zero to about 1 hour. In general, thicker films required little or no conditioning, the thinner the film the longer was the conditioning period.

In most of the tests, the maximum peak electric fields that could be sustained at the window surfaces were limited by arcing at the metal dielectric seal. Arcing occurred at the top or bottom of the window corresponding to the region of maximum electric intensity in the TE_{111} mode. The threshold field strength for arcing varied somewhat from window to window, but for pulse widths of 20 microseconds, generally occurred when the maximum electric field strength at the window surface was in the region of 25 to 31 kv per centimeter corresponding to a transmitted power of 20 to 30 megawatts peak. A typical plot is shown in Fig. 20a.

Windows were tested at the highest average powers possible. With alumina windows the average power was limited by dielectric losses within the material which caused the windows to crack when average powers of about 200 watts* were dissipated. Beryllia windows were capable of handling much higher average powers. An average power dissipation in the window cavity of about 900 watts* was necessary to cause cracking of the window. However, considerable instability occurred when operating at average power above about 700 watts* because of the excessive heat dissipation in the cavity which caused a rapid drift in the resonance frequency in spite of water cooling on both side and end walls of the cavity.

The results of high power tests on coated beryllia and alumina windows are given in Tables 2 and 3, respectively. A total of 10 coatings were tested on beryllia windows. Of these, 3 did not multipactor at all, and 6 showed some multipactor initially which cleared up after a period of conditioning. On one window, multipactor was not

---

* Actual dissipation not equivalent average transmitted power.

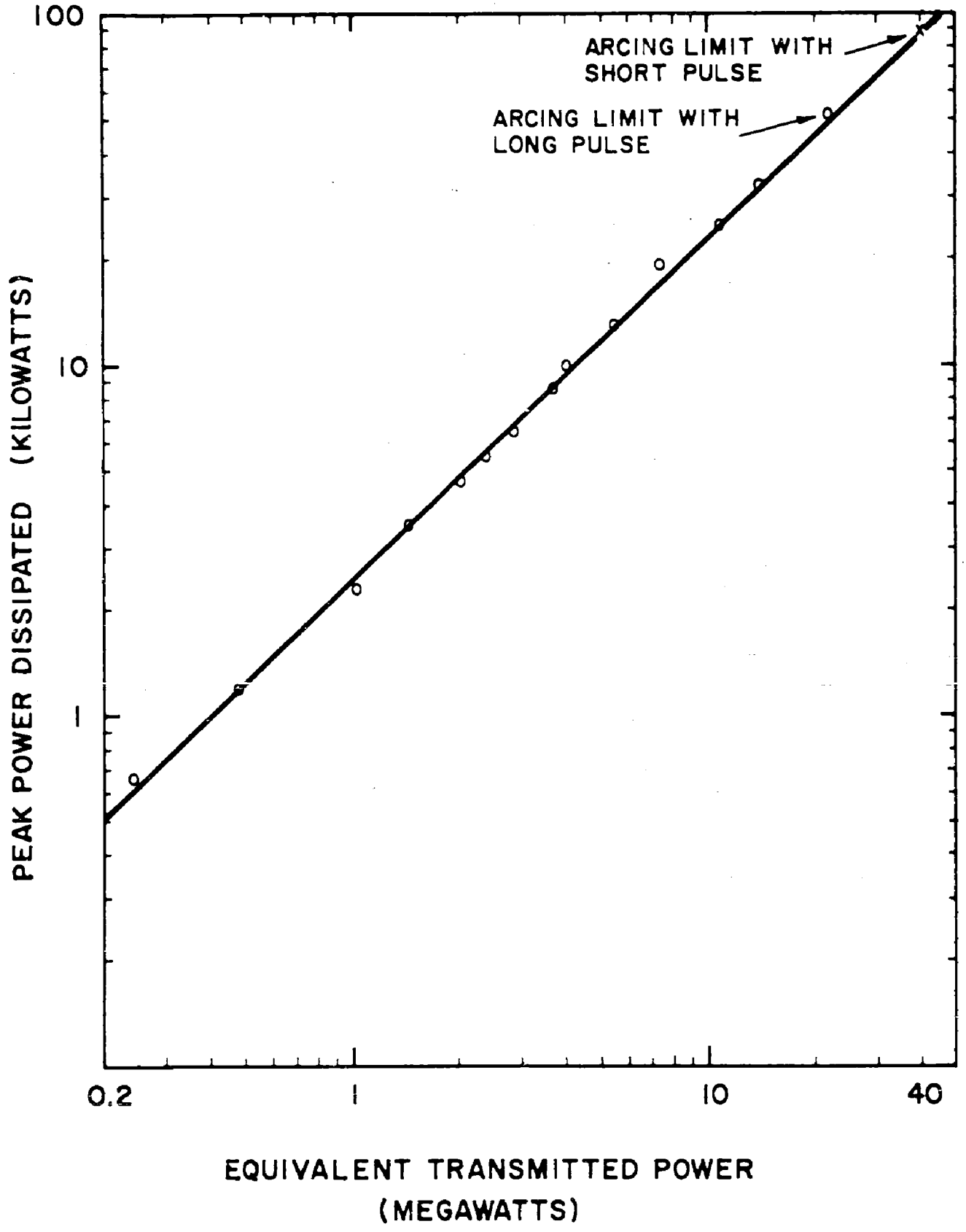
WINDOW Nº TU-31
COORS BD 96 BERYLLIA
EVAPORATED TITANIUM COATING
100
10
1
PEAK POWER DISSIPATED (KILOWATTS)
ARCING LIMIT WITH SHORT PULSE
ARCING LIMIT WITH LONG PULSE
0.2
1
10
40
EQUIVALENT TRANSMITTED POWER (MEGAWATTS)

Fig. 20a

eliminated but this had a very thin coating (resistivity 10^{10} ohms/square). Of 8 coatings tested on alumina windows, 7 suppressed multipactor after various periods of conditioning. Only 1 coating failed but this had been applied to the window prior to brazing ceramic into its assembly.

Evaporated titanium coatings with resistivities greater than 10^{6} ohms/square did not affect the Q of alumina or beryllia cavities. Thicker films tended to reduce the Q and are considered unsuitable for use on windows. A plot of cavity Q versus film resistivity is shown in Fig. 21, the range of film resistivity considered suitable for multipactor is indicated.

During the conditioning period the surface coating undergoes some change but it is not clear exactly what processes occur. Several possibilities have been considered as follows:

a. Outgassing of the window surface.

b. Reduction of the surface coating.

c. Removal of contaminants from the window surface.

Adsorbed gas in the surface of any material will alter the surface characteristics considerably. This is particularly the case with the secondary emission coefficient. It is not unlikely, therefore, that outgassing of the window will change the surface properties in such a way as to be unfavorable for multipactor.

EFFECT OF EVAPORATED TITANIUM COATINGS ON CAVITY Q

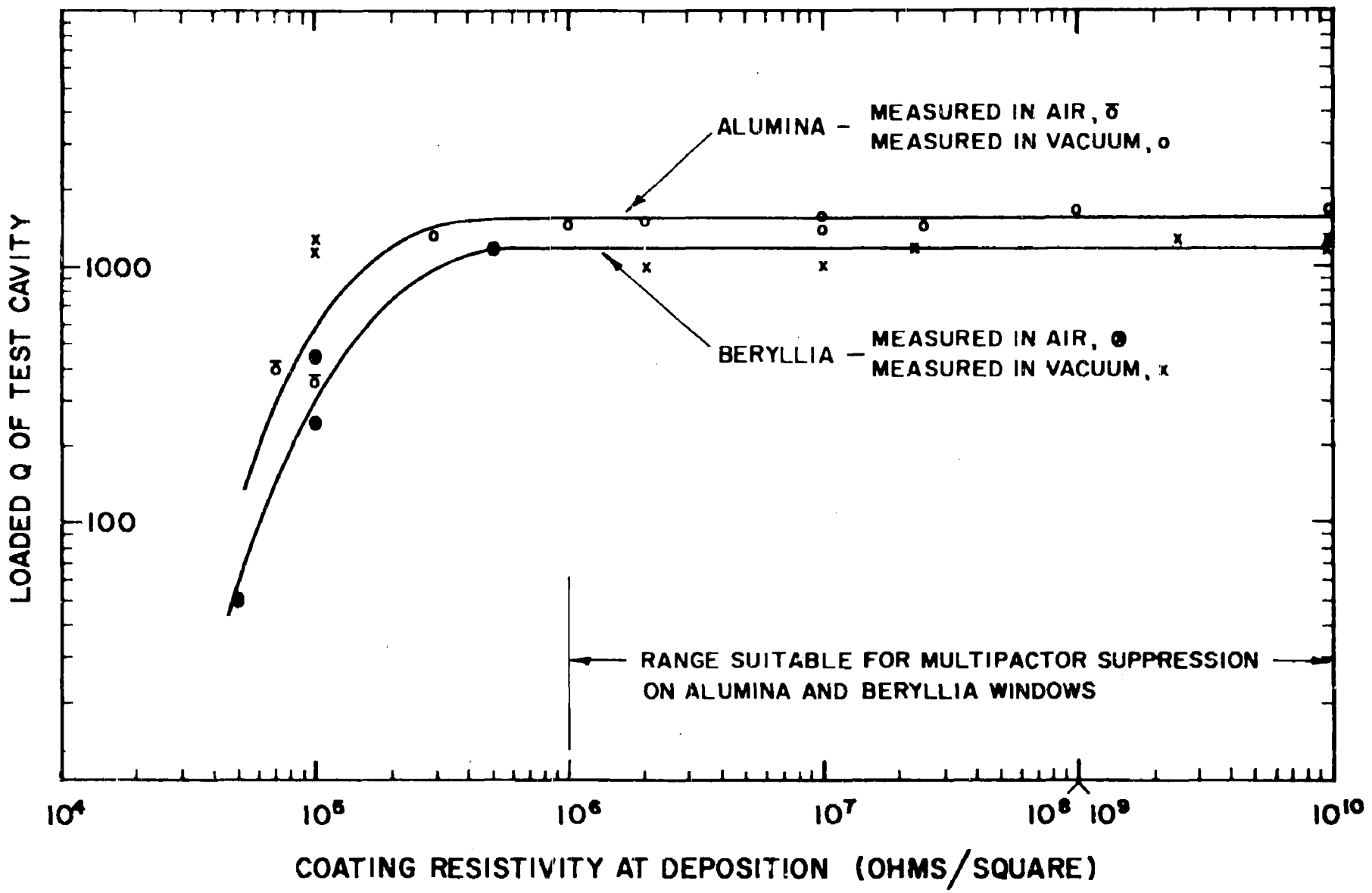

Fig. 21

It is known that thin films of titanium oxidize on exposure to air, resulting in an increase in secondary emission coefficient. The evacuation and bakeout processes to which the windows are subjected tends to reduce the oxides but this process is not always complete. Electron bombardment of the coated window will cause further reduction of the oxidized titanium films and this may occur during the cleanup period.

It is thought that contamination of the window surface during processing may be contributing to the need for window cleanup. For example, thin films of copper are commonly found in window surfaces immediately after exhaust. These can be attributed to the deposition and subsequent reduction of one of the compounds of copper such as the chloride or oxide. These films can be thicker than the penetration depth of secondary electrons and will thus determine secondary yield of the surface. Steps were taken to avoid such contamination. On some of the units tested the side walls of the cavity were coated with titanium in addition to the window surface and a heliarc weld in the exhaust tubulation (a possible source of copper oxide) was eliminated. However, even with these precautions conditioning was still necessary.

Some conditioning has been observed on uncoated windows. The threshold level of multipactor will sometimes rise as time progresses. However, cleanup is generally more pronounced with coated windows. This suggests that several of the above-mentioned processes may be involved.

4.5.6 Evaporated Titanium Coatings On Quartz

Evaporated titanium films showed higher losses when applied to quartz. The Q of a quartz-loaded cavity decreased from 2200 to 700 when the quartz was coated with titanium to a resistivity at deposition of 10^7 ohms/square (measured on a standard ceramic control piece). It appeared that the smooth glossy surface of the quartz produced a more continuous film than the ground surfaces of alumina or beryllia. To confirm this the surface of a quartz disc was roughened by sandblasting prior to coating with titanium to a resistivity of 10^7 ohms/square. A cavity-loaded Q of 1700 was then measured indicating a considerable reduction in the losses. A high power test carried out on this window showed that the treatment was effective in suppressing multipactor on quartz.

The results of high power tests on plain quartz windows are summarized in Table 4. The first test was carried out on an uncoated window to determine the behavior of quartz when subjected to high intensity microwave fields and to provide a comparison for the results of coated windows. Severe multipactor was obtained commencing at an equivalent transmitted power in the region 100-200 kw peak. The behavior of the window is shown in Fig. 22.

The next window tested had a very thin coating (resistivity 10^{10} ohms/square measured on an alumina control) which did not increase the window losses. With this window, multipactor started at about 2 Mw equivalent transmitted power. The discharge was less intense than that observed on the uncoated window and some conditioning occurred, but multipactor was not completely eliminated.

TABLE 4

EVAPORATED TITANIUM COATINGS ON QUARTZ
SUMMARY OF TEST RESULTS

Window	Coating Resistivity (ohms/sq.)	Q_L	Peak Power Dissipated (kw)	Peak Power Transmitted (Mw)	Average Power Dissipated (watts)	Remarks
C 59	None	2100	42	-	50	Severe multipactor
C 61	10^{10}	2000	30	-	50	Some conditioning but multipactor not eliminated.
C 63	10^{7}	1500	200	100	60	Surface sandblasted prior to coating. Multipactor eliminated.

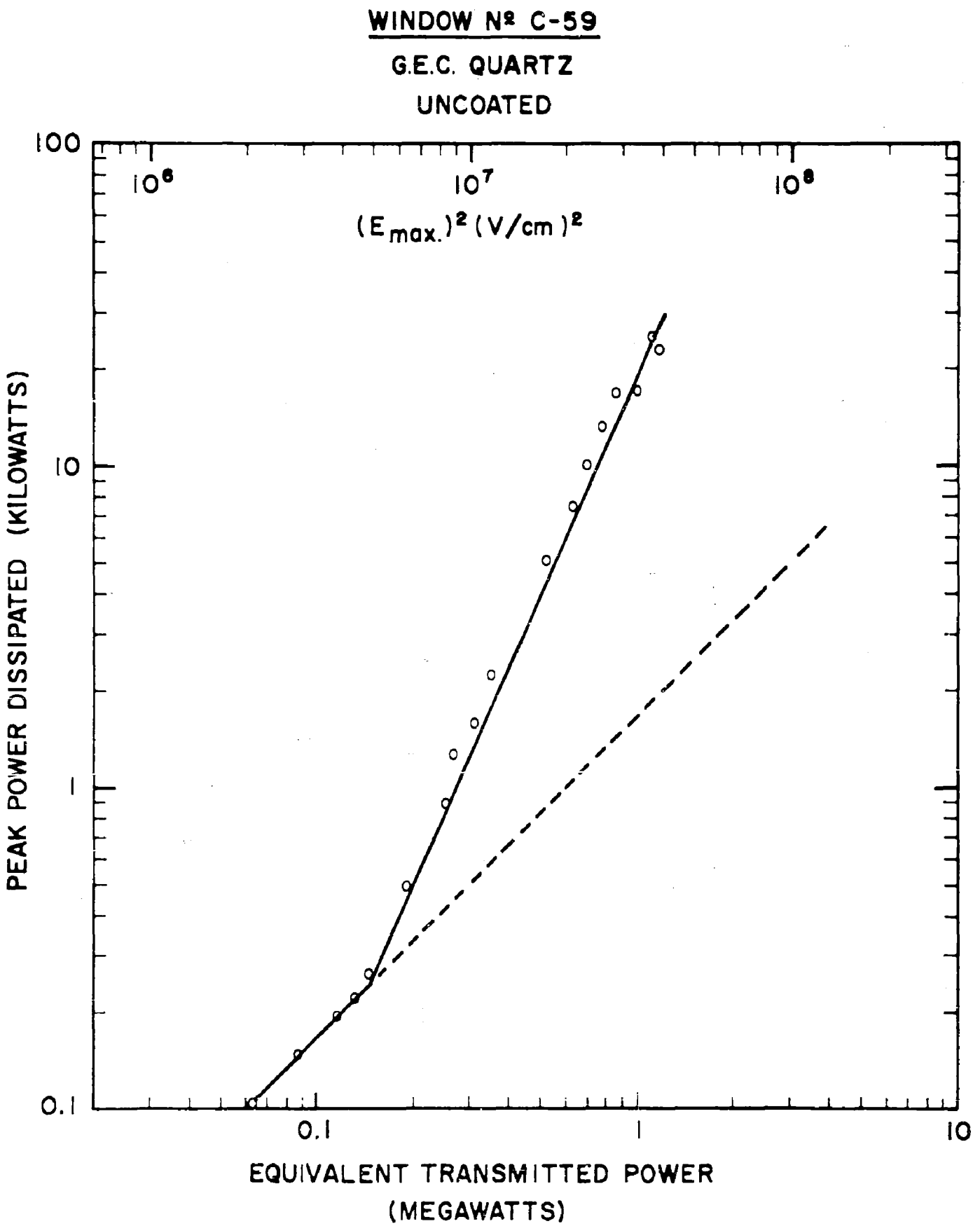
WINDOW Nº C-59
G.E.C. QUARTZ
UNCOATED
100
10
1
0.1
10^6
10^7
10^8
$(E_{max.})^2$ (V/cm)^2
PEAK POWER DISSIPATED (KILOWATTS)
0.1
1
10
EQUIVALENT TRANSMITTED POWER
(MEGAWATTS)

Fig. 22

A window which was coated (to a resistivity of 10^7 ohms/square on the control) after the surfaces had been roughened by sandblasting gave a satisfactory performance. The coating was thick enough to suppress multipactor completely (apart from some intermittent discharges during the initial operation) but did not increase the window losses unduly. The results for this window are plotted in Fig. 23.

Quartz windows were tested at average powers up to 60 watts dissipation. On attempting to increase the average power beyond this value changes in the resonant frequency and the coupling of the cavity would occur, due to the temperature rise in the quartz, preventing further increase in average power. Operating at the maximum average power of about 60 watts dissipation sometimes resulted in a crazing at the center of the quartz indicating excessive heating of the material in that region.

4.5.7 Rapid Evaporations At Low Pressure

A number of experiments were carried out on coatings evaporated rapidly at low pressures, to determine if this process gives better coating control. A shutter was used to shield the window to be coated from the evaporating filament while the latter was outgassed and the system pressure was reduced to about 5×10^{-7} Torr. The shutter was then removed and the window coated in a few seconds.

This procedure produces a stable metallic film which is largely free from contamination. The film resistivity remains steady when the system is let down to air, in contrast to films deposited at higher pressures which

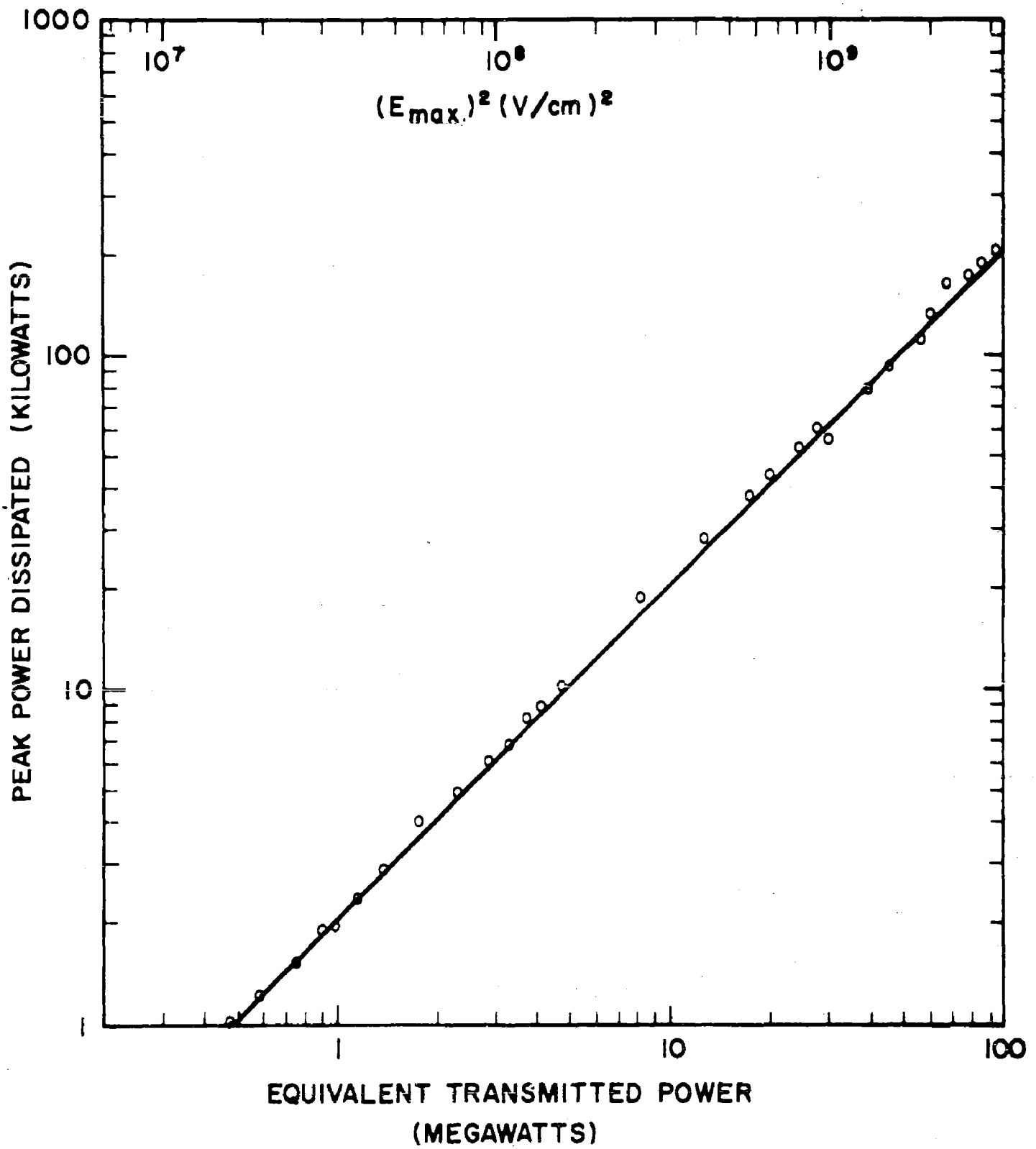
WINDOW Nº C-63
G.E.C. QUARTZ
SANDBLASTED AND Ti COATED
1000
100
10
1
10^7
10^8
10^9
$(E_{max.})^2$ (V/cm)²
PEAK POWER DISSIPATED (KILOWATTS)
1
10
100
EQUIVALENT TRANSMITTED POWER
(MEGAWATTS)

Fig. 23

show large changes in resistivity. For a given film thickness the resistivity is much lower for films deposited at low pressure, which means that they have higher RF losses. Two ways of avoiding the high RF losses were tried: (a) partially oxidizing the film after deposition and (b) using very thin films.

The first coating tested was applied to an alumina disc to a resistivity of 10^4 ohms/square. This was then partially oxidized by heating in wet hydrogen. The window was then assembled in a test unit (C53) and tested at high power. Considerable multipactor was obtained which cleaned up at low power levels after a period of operation but was not completely eliminated at the highest powers used (30-40 Mw equivalent transmitted power).

A window coated to 10^7 ohms/square (C56) and tested without subsequent oxidation also supported multipactor. Some conditioning was observed but the discharge was not completely eliminated, although a graph of peak power dissipated versus electric field strengthsquared was linear indicating that the discharge was rather weak. A somewhat thicker coating (resistivity 6×10^5 ohms/square) was tried on window C57 which slightly lowered the window Q. This effectively suppressed multipactor after a short conditioning period. The results of these tests are summarized in Table 5.

The results indicate that the range of coating resistivity satisfactory for use on windows is very limited due to the increased conductivity. It is possible though that control of final film thickness is easier because of the reduced effect of processing subsequent to the coating. An attempt to reduce the conductivity by partially oxidizing a film was not successful.

TABLE 5

EVAPORATED TITANIUM COATINGS APPLIED AT LOW PRESSURE TO ALUMINA
SUMMARY OF TEST RESULTS

Window	Coating Resistivity (ohms/sq.)	Q_L	Peak Power Dissipated (kw)	Peak Power Transmitted (Mw)	Average Power Dissipated (watts)	Remarks
C 53	10^4	900	160	–	100	Coating oxidized by heating. Considerable multipactor.
C 56	10^7	1500	70	35	100	Some conditioning. Multipactor not eliminated.
C 57	6.10^5	1500	20	10	150	No multipactor after conditioning.

4.6 Sputtered Titanium Monoxide Coatings

4.6.1 Preparation Of Coatings

In contrast to vapor deposition, coatings deposited by sputtering are not dependent on temperature effects. In a sputtering process the coating material is removed by high energy bombarding ions. The sputtered molecules have energies of several electron volts, which is well above any thermal energy and results in higher impact velocities.

The initial work on sputtered titanium monoxide coatings was carried out during Task B of the program. Coatings were prepared in a glass bell jar pumped by a mercury diffusion pump. The mercury ions for this sputtering process were obtained from the diffusion pump; mercury pressure in the bell jar was kept constant at about 1 micron by a cold trap held at 15°C located in the pump and bell jar. At this pressure the mean free path was greater than the cathode-substrate distance. Dispersion of the sputtered molecules by collision with gas molecules was thus avoided, resulting in maximum sputtering efficiency and a good substrate bond. The gas density was not high enough to maintain an adequate discharge with a dc voltage alone and an rf field was necessary to confine the plasma. This was generated by an HF coil wound around the outside of bell jar which was energized by a 27-megacycle per second oscillator of several hundred watts output power. The ion bombarding energy was 1300 ev.

A photograph of the bell jar arrangement is given in Fig. 23a. To coat a window the sample is placed on the stand and the system evacuated. The dc and rf voltages are then

Fig. 23a Sputtering Equipment

applied, the rf coupling being adjusted to achieve the desired ion current. The amount of material sputtered is dependent on the current time product. However, it is preferable to sputter at high ion currents for short periods since film contamination by background gases is then minimized. Sputtering currents used during the program varied from 4 to 10 milliamps.

During Task C some windows were coated in an argon sputtering system. The sputtering process was basically the same as that used with the mercury system, the difference being in the use of argon in place of mercury sputtering ions. In the argon system an oil diffusion pump and cold trap were used to evacuate the bell jar to 10^{-6} Torr prior to the introduction of argon gas. The argon pressure was maintained below 5 microns and an RF oscillator was required to produce a plasma as in the case of mercury sputtering. The same bell jar was used on both systems.

4.6.2 Coating Control

During the early work on sputtering some experiments were carried out to determine the nature of the coatings produced. Relatively thick coatings were applied to samples of alumina and silica. The temperature coefficient of the resistivity was taken as an indication of the chemical composition of the coating. This varies continuously with the degree of oxidation in a known manner [12]. In a series of experiments the distance between the titanium momoxide cathode and the substrate was varied and the sputtering rate kept constant. Targets at a greater distance showed

a high degree of oxidation. Because the coverage rate becomes smaller with distance more oxygen or other impurities are built in the coating and the observations indicate the quality of the vacuum was not sufficient for reproducible coatings. However, coatings in an actual tube have to go through a bakeout process. Several samples of coatings, varying greatly in resistance value and also in temperature coefficient, were sealed in a glass vacuum envelope and submitted to one hour bakeout at about 350°C. The resistance values changed but the temperature coefficient resistivity was practically the same for all samples and corresponded to that of Ti_2O_3. This indicates that the initial composition of the coating is of no great importance.

During the initial sputtering experiments, coatings were classified by the sputtering time and current. However, the current is sensitive to the cathode substrate geometry and small changes in the cathode area were found to alter the conditions appreciably. In later work (Task C) coating resistivity was measured also. Some experiments were carried out in the argon system to determine the relationship between the sputtering conditions and the coating resistivity. A typical plot of resistivity versus time for a sputtering current of 4 milliamps is shown in Fig. 24. The slope of this curve varied with the sputtering current in a reproducible manner. Sample coatings were applied to glass substrates and the thickness later measured by an optical interferometer. The results are shown in Fig. 25 which is a semi-log plot of resistivity versus thickness. Most of the data falls on a straight line indicating an exponential dependence.

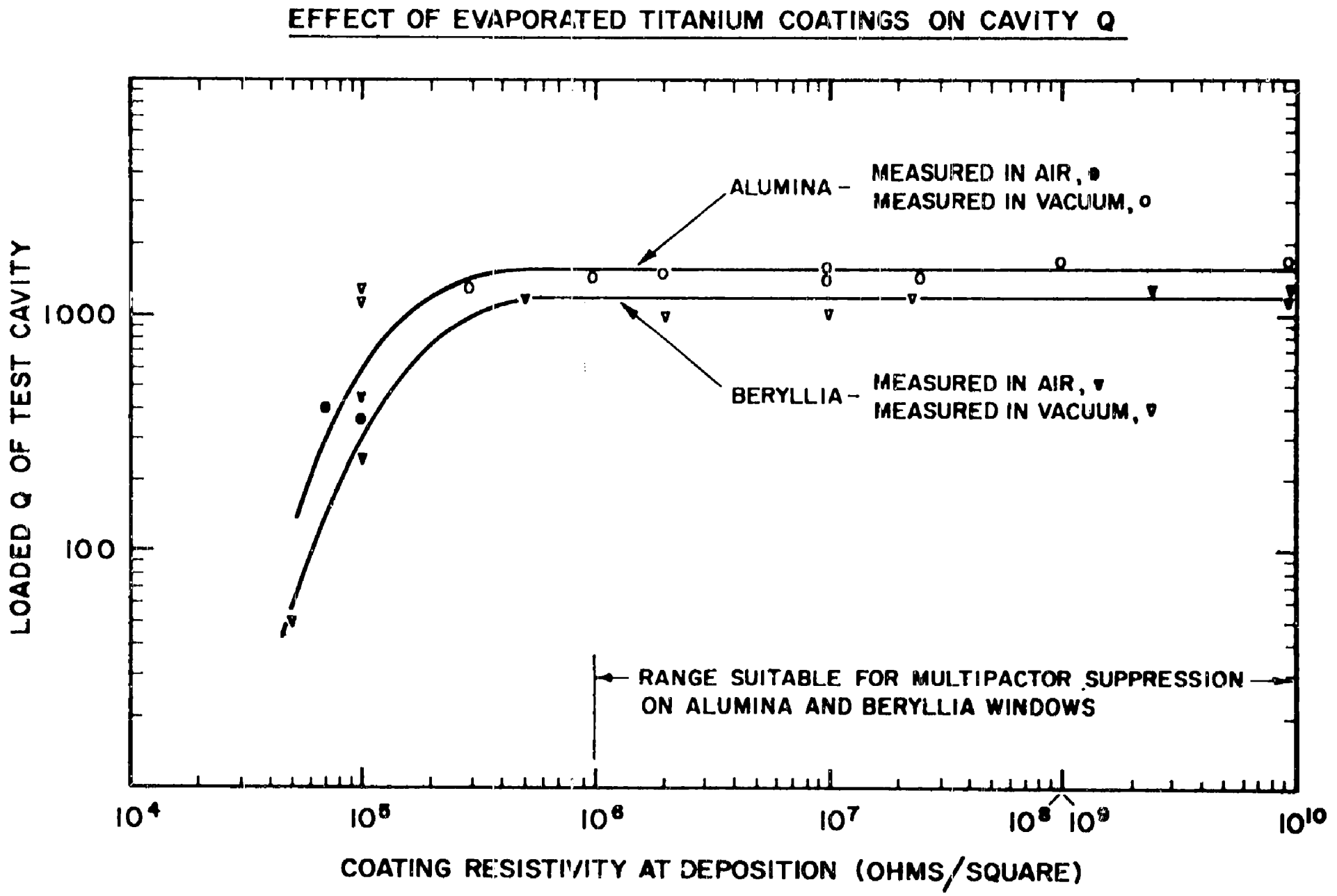
EFFECT OF EVAPORATED TITANIUM COATINGS ON CAVITY Q
LOADED Q OF TEST CAVITY
1000
100
ALUMINA – MEASURED IN AIR, ●
MEASURED IN VACUUM, o
BERYLLIA – MEASURED IN AIR, ▼
MEASURED IN VACUUM, ▽
RANGE SUITABLE FOR MULTIPACTOR SUPPRESSION
ON ALUMINA AND BERYLLIA WINDOWS
10⁴
10⁵
10⁶
10⁷
10⁸
10⁹
10¹⁰
COATING RESISTIVITY AT DEPOSITION (OHMS/SQUARE)

Fig. 24

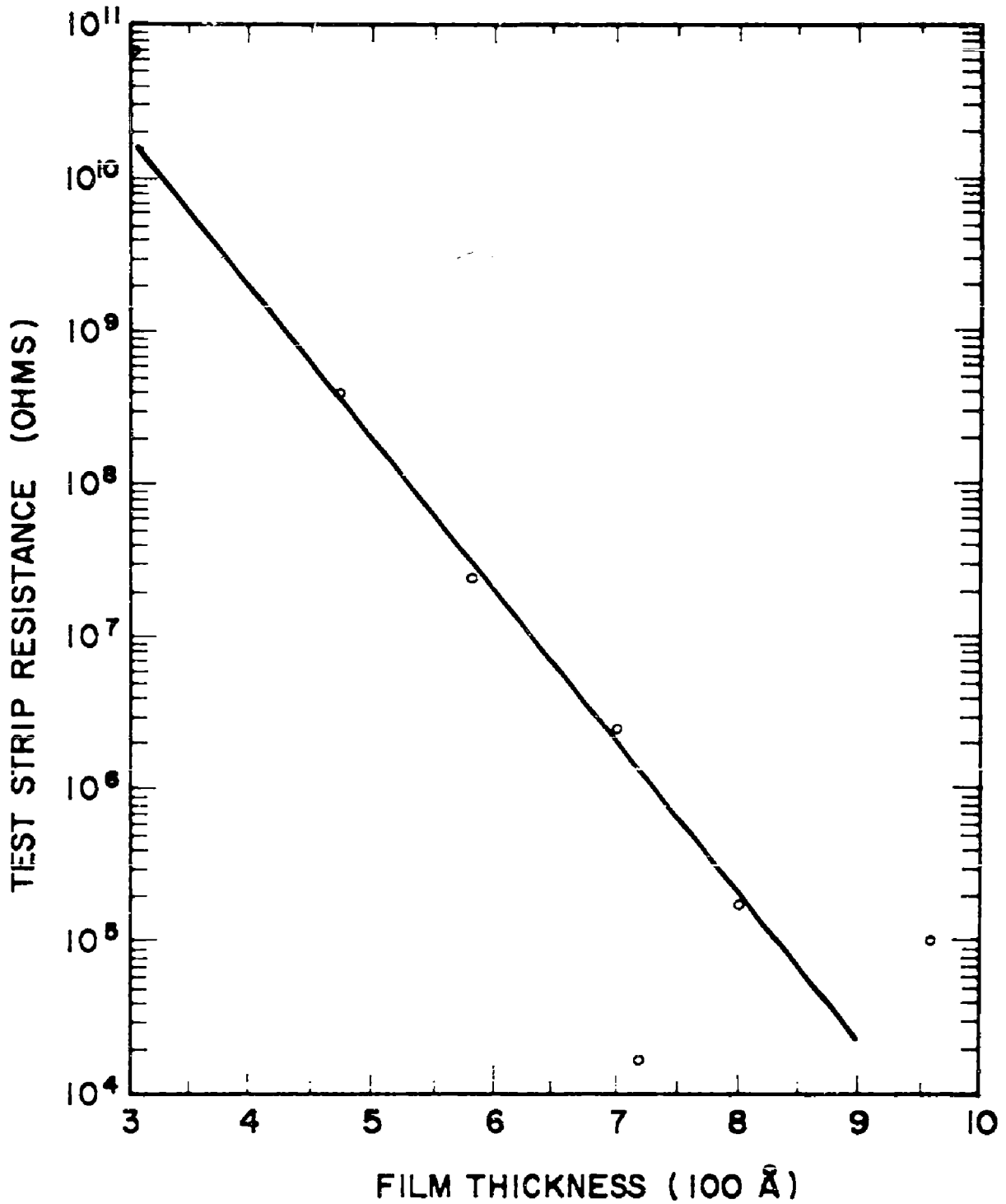

VARIATION OF RESISTANCE
WITH FILM THICKNESS
(TiO SPUTTERED IN ARGON)

FIG. 25

4.6.3 Evaluation Of Sputtered Titanium Monoxide Coatings At High Power

Experiments with titanium monoxide coatings were carried out in Tasks B and C. During the early work both mercury and argon sputtered coatings were tested. However, after it had been demonstrated that similar results could be obtained with both mercury and argon sputtering, further efforts were confined to the argon method, because of difficulties in using the mercury equipment due to instability. The results obtained from coating tests on alumina and beryllia windows are given in Tables 6 and 7 respectively. Conditioning was again observed at some windows; multipactor would occur on first exposure to high intensity microwave fields but would disappear after a period of operation. Once a window had been conditioned no further discharges would occur during operation at high peak or average power. Multipactor could sometimes be induced by the application of a crossed magnetic field but such discharges would clear up after a further period of conditioning. Coated windows were tested up to peak powers equivalent to 42 megawatts of transmitted power and at average power dissipations in the cavity up to 570 watts. Peak powers were again limited by arcing at the metal dielectric seal.

Of 5 coatings applied to alumina in an argon atmosphere, 2 suppressed multipactor completely, 2 required some conditioning, and 1 failed due to insufficient thickness. Two of the coatings decreased the loaded Q of the test cavity and are considered to be

TABLE 6

SPUTTERED TITANIUM MONOXIDE COATINGS ON ALUMINA
SUMMARY OF HIGH POWER TEST RESULTS

Window	Sputtering Current-Time (mA-min.)	Coating resistivity (ohms/sq.)	Cavity Q_L	Peak Power Dissipated (kw)	Peak Power Equiv. Transmitted (Mw)	Average Power Dissipated (watts)	Remarks
Coatings sputtered in Argon							
C 40	150	2.10^7	1800	61	36	150	Initial multipactor cleared up. Peak power obtained with 3μ sec. pulse.
C 44	245	5.10^6	300	37	3.7	150	No multipactor. Low Q due to heavy coating.
C 46	70	2.10^9	1800	33	9	100	Little multipactor, which cleared up.
C 47	45	3.10^{10}	1800	20	12	150	Intermittent multipactor throughout test.
C 26	240	5.10^6	500	67	11	134	No multipactor. Low Q_L due to heavy coating.
Coatings Sputtered in Mercury							
C 33	300	-	1350	94	42	150	Initial multipactor cleared up.

TABLE 7

SPUTTERED TITANIUM MONOXIDE COATINGS ON BERYLLIA
SUMMARY OF HIGH POWER TEST RESULTS

Window	Sputtering Atmosphere	Sputtering current-time mA-min.	Cavity Q_L	Peak Power Dissipated (kw)	Peak Power Equiv. Transmitted (Mw)	Average Power Dissipated (watts)	Remarks
C 23	Mercury	135	1200	42	17	510	No multipactor.
C 25	Mercury	280	1200	50	22	535	No multipactor.
C 21	Argon	450	1200	50	22	570	No multipactor.
C 24	Argon	240	1000	100	-	70	Severe multipactor.

too thick for use on windows. A graph of loaded Q versus coating resistivity is given in Fig. 26. The range of resistivity suitable for multipactor suppression is 10^7 to 10^{10} ohms/square, corresponding film thickness being approximately 300 to 550 Angstroms. These results are tentative since they are based on limited data.

Two Argon sputtered coatings were applied to beryllia; one suppressed multipactor but the other was considerably thinner and failed.

A total of 3 coatings were deposited in a mercury atmosphere. Two were applied to beryllia and suppressed multipactor completely, the other was applied to alumina and suppressed multipactor after a period of conditioning.

Sputtered coatings tested in Task B were applied in the form of dots. This was achieved by masking the window with a nickel wire mesh flattened in a press, which produced a network of dots 0.75 millimeters apart covering 20% of the area. The dotted coating was used to demonstrate the migration effect of surface coatings, the multipactor suppressing properties gradually extending over the complete window surface during operation at a high power. In addition, coating losses were reduced by the use of dots and consequently the coating thickness could be increased.

A coated alumina and a coated quartz window were tested in the ring resonator. Both suppressed multipactor after a period of conditioning. The alumina window was tested after 84 megawatts peak at 15 kilowatts average and 39 megawatts peak at 42 kilowatts average. The silica window would not perform

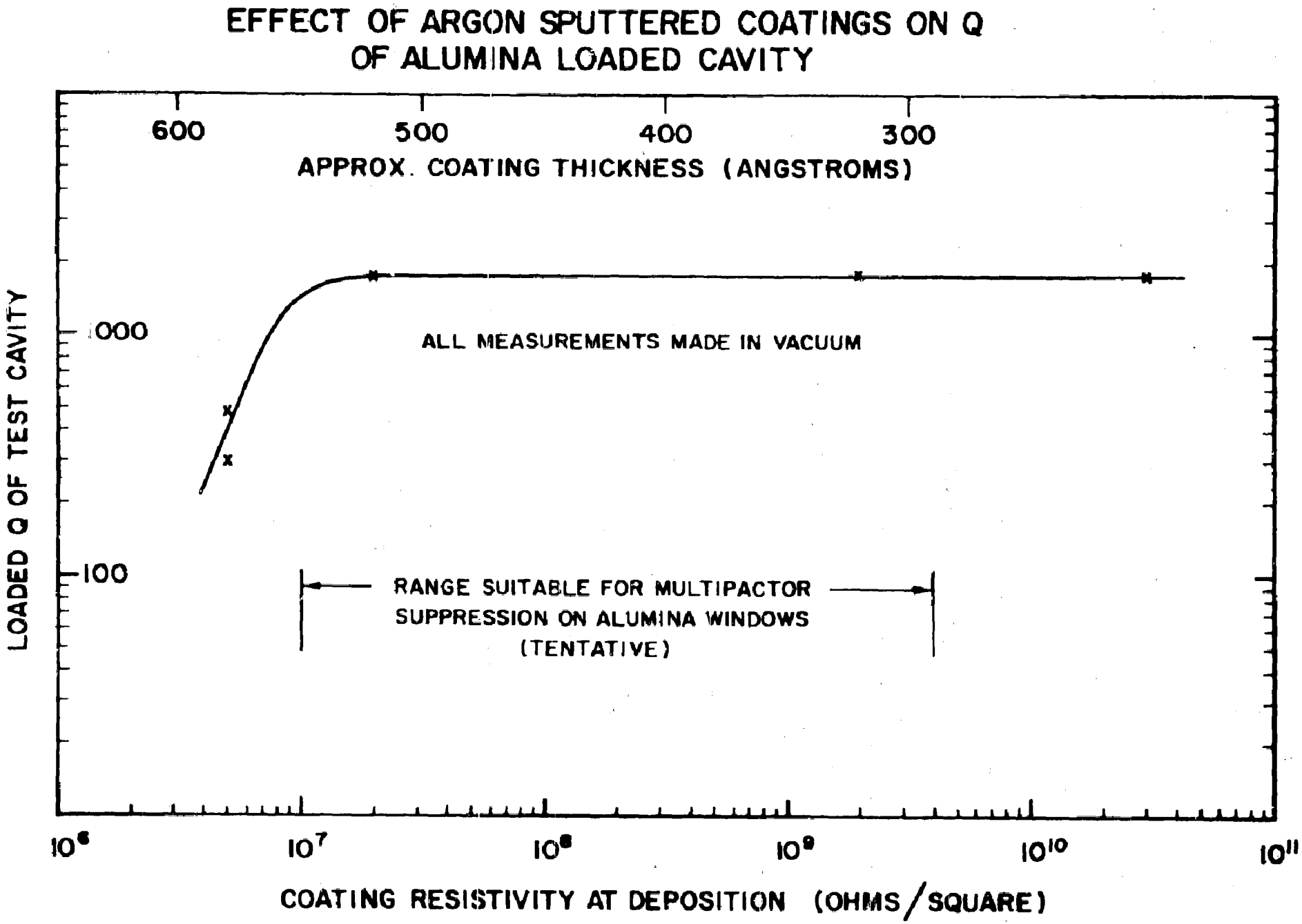
EFFECT OF ARGON SPUTTERED COATINGS ON Q
OF ALUMINA LOADED CAVITY
600
500
400
300
APPROX. COATING THICKNESS (ANGSTROMS)
LOADED Q OF TEST CAVITY
000
100
ALL MEASUREMENTS MADE IN VACUUM
RANGE SUITABLE FOR MULTIPACTOR
SUPPRESSION ON ALUMINA WINDOWS
(TENTATIVE)
10^6
10^7
10^8
10^9
10^{10}
10^{11}
COATING RESISTIVITY AT DEPOSITION (OHMS/SQUARE)

Fig. 26

properly because the dots were sputtered on too thick. The electric conductivity was so great that at a power level of only 10 megawatts surface sparks developed between the dots, which made high power testing impossible. The experiment was not repeated with the proper coating thickness.

4.7 Grooved Windows

4.7.1 The "Venetian Blind" Idea

If a metal "venetian blind" is arranged in a waveguide with the blades in the direction of the electric equipotential surfaces, the passing of electromagnetic wave is not greatly disturbed. Electrons, however, cannot pass the screen in the presence of the electromagnetic wave if the amplitude of oscillation is considerably bigger than the distance between blades. Such a screen put in direct contact with the window surface would prevent any multipactor.

A practical method of approximating a "venetian blind" at a window surface is to prepare V-shaped parallel grooves in the surface running approximately perpendicular to the electric field. To determine the effect of the grooves on the field configuration at a window surface, field plots were made using a resistance network for a dielectric constant of 8 and 4 and for groove angles of 60° and 120°. A dielectric constant of 8 is close to that of alumina and 4 is close to that of silica. The resulting fields are illustrated by equipotential surfaces in Fig. 27 for alumina and Fig. 28 for silica. The field variation across the top and bottom of the grooves is

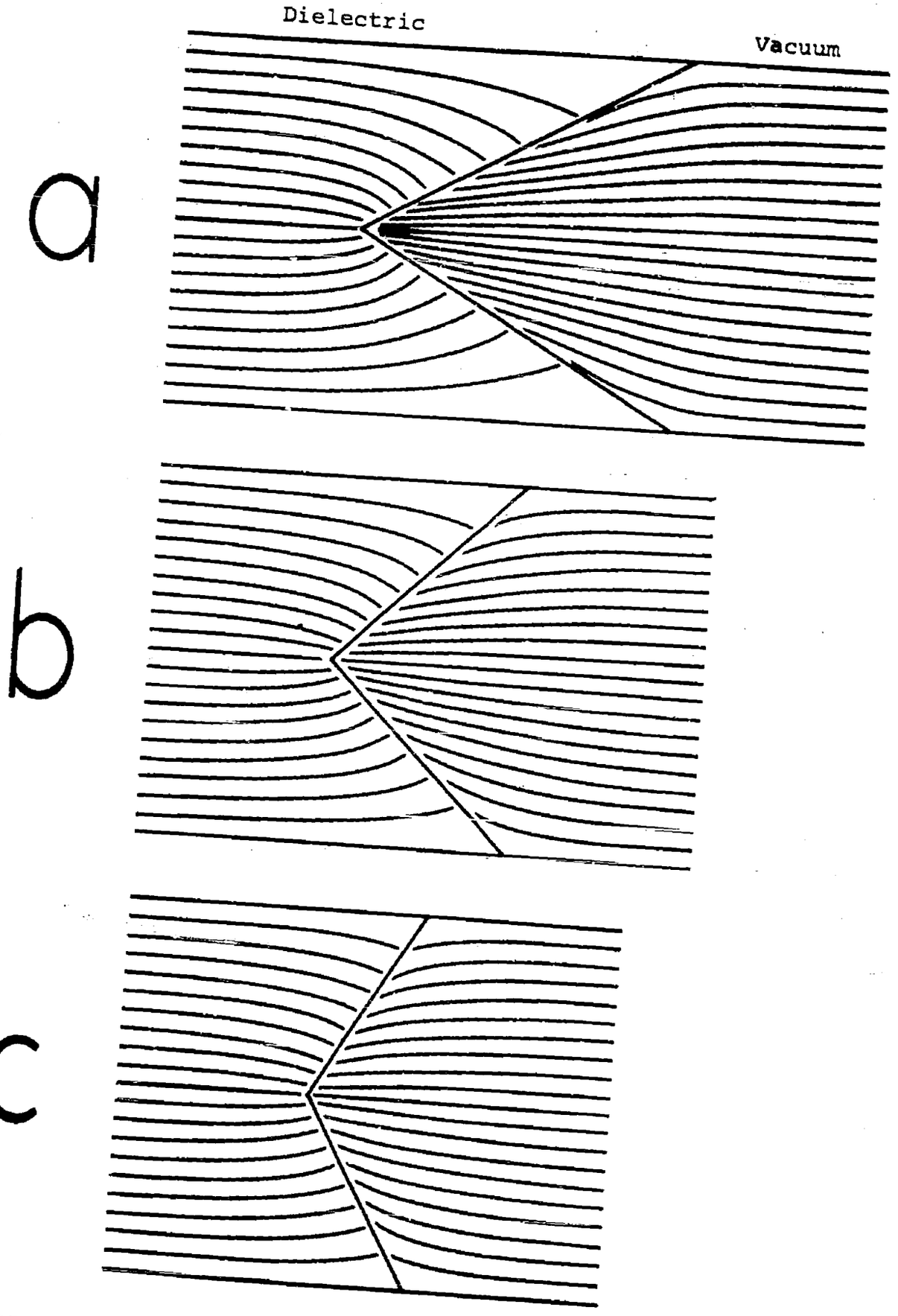

Fig. 27 Field Inhomogeneity Around Grooves (Alumina)
a (60°); b (90°); (c 120°)

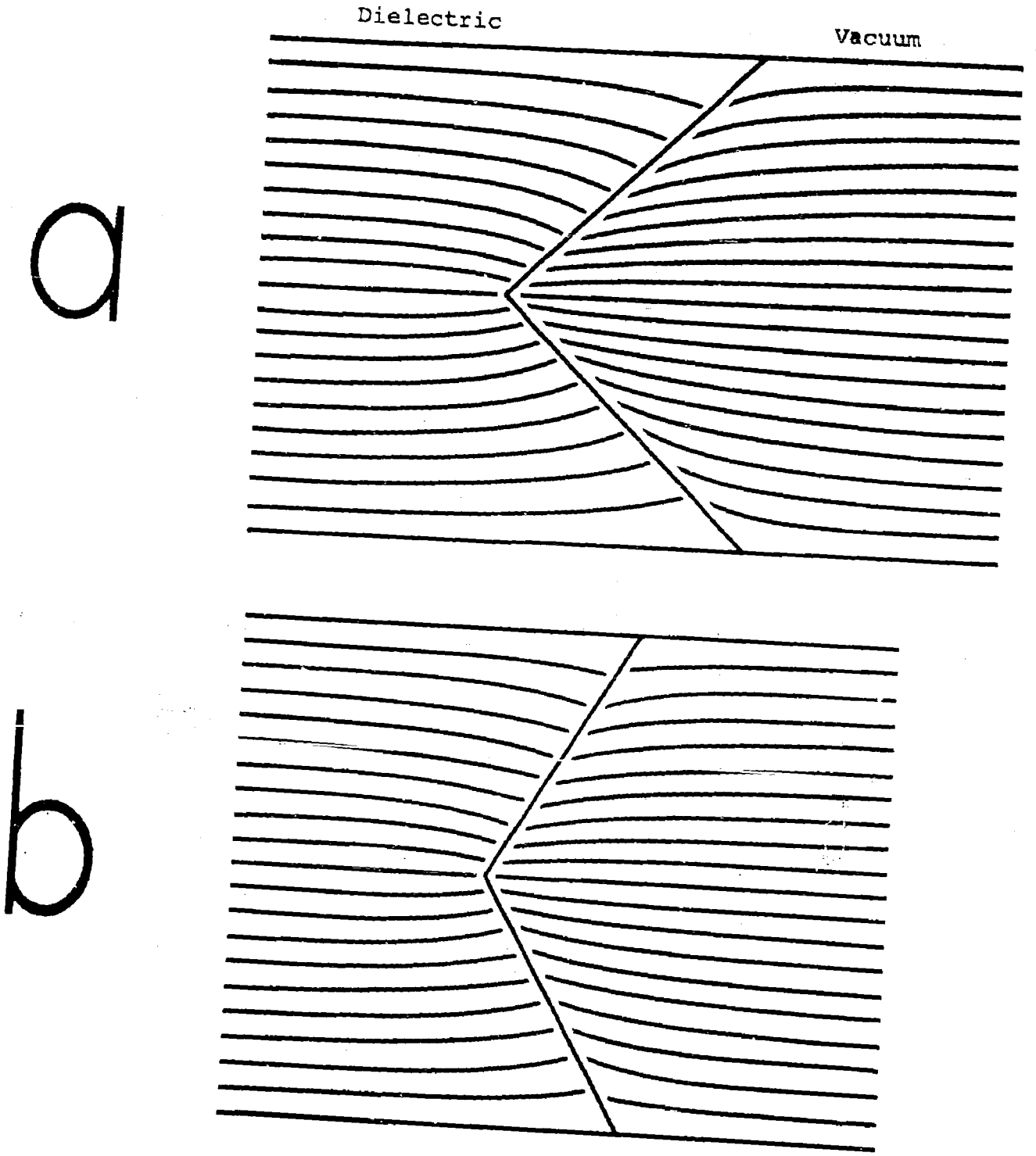

Fig. 28 Field Inhomogeneity Around Grooves (Silica)
a (90°); b (120°)

shown in Fig. 29 for a 90° groove angle and a dielectric constant of 8. For electron amplitudes smaller than the groove width the field inhomogeneity effect will drive electrons away from the window thereby tending to destroy the multipactor. In the case of large electron amplitudes the periodic field distortion produced by the grooves will repel electrons away from the surface. For an electron oscillating across the crests of the ridges, the high frequency field strength variation is about ± 30%. Because of the high frequency of this disturbance the energy in the jitter oscillation remains low and the repelling action on the electrons is small.

The presence of the grooves tends to prevent the gliding type of multipactor because there exists no tangential incidence of electrons. Electrons can strike only near the crests of the ridges. The troughs should be free of multipactor because of lack of space. Under electron bombardment the crests should charge positively, if the secondary emission coefficient is above unity, and the grooves negatively, because electrons accumulate, resulting in an alternating dc field which focuses electrons away from the window.

4.7 .2 Manufacture Of Grooved Windows

Two methods were used to manufacture grooved windows. The first method consisted of forming the window in alumina powder prior to the firing process. A specific amount of powder was pressed between grooved, hardened and polished steel plates. After firing, the outer cylindrical edge was ground to size but

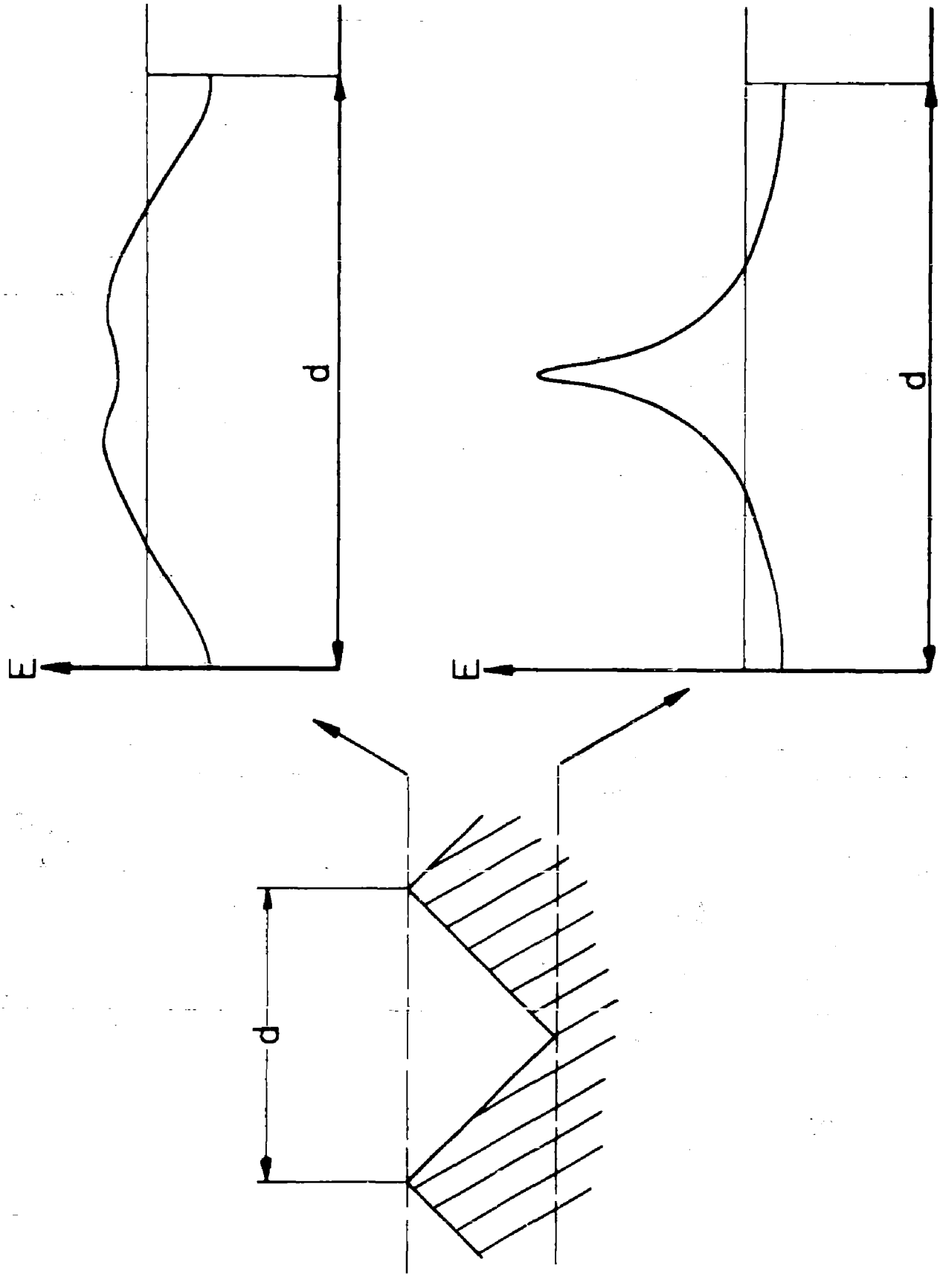

Fig. 29 Field Strength Variation Across Top and Bottom of Grooves

the groove surfaces did not require finishing. This method was used for making alumina windows. The second method, used on silica windows, consisted of grinding the surface of a plain disc with a diamond contour wheel followed by a firepolishing. A photograph of a grooved window is given in Fig. 30.

4.7.3 High Power Experiments On Grooved Windows

Most of the experiments on grooved windows were carried out in Task B using the Stanford Ring $R_e$sonator. The results are summarized in Table 8.

The first three windows tested were grooved alumina windows all of which supported multipactor. No discharge was visible near the bottom of the grooves, the luminosity being concentrated at the crests. Fig. 31 contains a series of photographs taken at intervals during the rise in power. It can be seen that the greatest discharge glows occur at the lower powers (6 to 8 megawatts). The luminosity is concentrated in the outer region of the window at these powers due to the variation in field strength across the surface. At higher levels a more uniform glow is evident.

The first two windows failed at 34 and 36 megawatts equivalent transmitted power because of internal arcing. The failures originated at the bottom of some of the grooves not at the crests where the multipactor takes place. It is believed that the puncturing is a run away condition starting at small overheated spots caused by a localized impurity or by a semi-loose

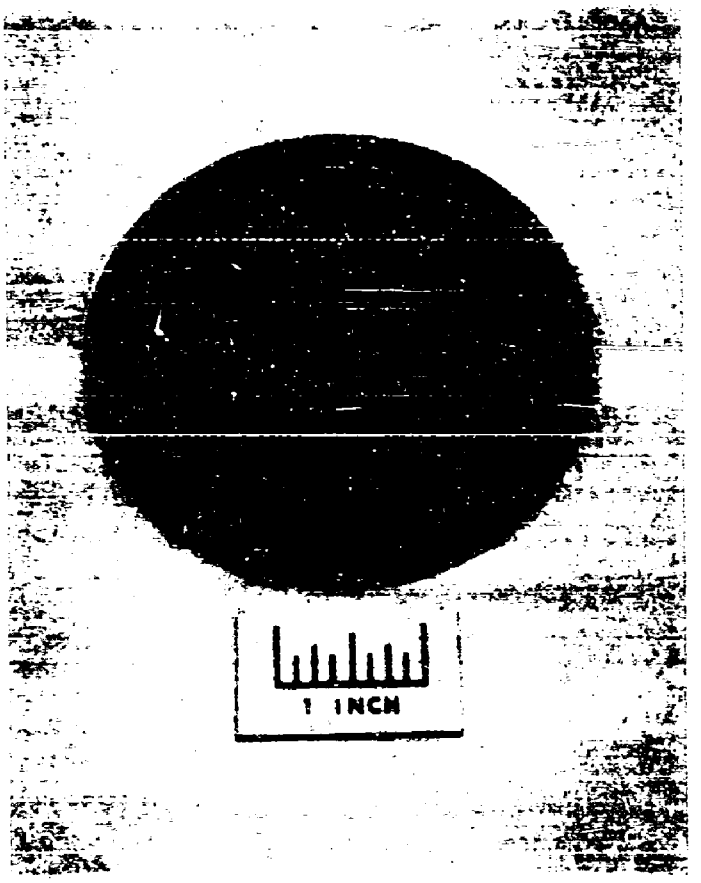

Fig. 30 Grooved Beryllia Disc.

TABLE 8

UNCOATED GROOVED WINDOWS
SUMMARY OF TEST RESULTS

* Re-test

nr.	Material	Surface	Coating	Failure At Peak Mw	Failure At Ave. kW	Highest Power Peak Mw	Highest Power Ave. kW	Multi-pactor	Remarks
B 1	AL 300	Grooved	No	34.	6.0	34.	6.	Yes	
B 2	AL 300	Grooved	No	36.	6.5	36.	6.5	Yes	
B 3	AL 300	Grooved Sandblasted	No	28.	20.0	78.	14.	Yes	
B 9	Silica	Grooved	No	No Failure		84. 40.	15. 43.	No	
B 10	Silica	Plain Sandblasted	No	63.	11.5	63.	11.5	Yes	
B 11	Silica	Grooved	No	No Failure		88. 39.	15.6 42.	No	
B 13	Silica	Grooved	No	No Failure		80. 39.	14. 42.	No.	
B 13*	Silica	Grooved	No	Failure		-	-		Destroyed by over-voltage due to mismatch.
B 16	Silica	Narrow Grooved 0.030"	No	No Failure		88. 41.	15.6 44.	No	
B 17	Silica	Grooved vertical	No	65.	12.	65.	12.	Yes	
B 18	Silica	Grooved .015"	No	-	-	88. 41.	16. 44.	No	
B 19	Silica	Grooved fire-polished		-	-	88. 41.	16. 44.	No	

AL 300 GROOVED WINDOW #2, WITHOUT COATING

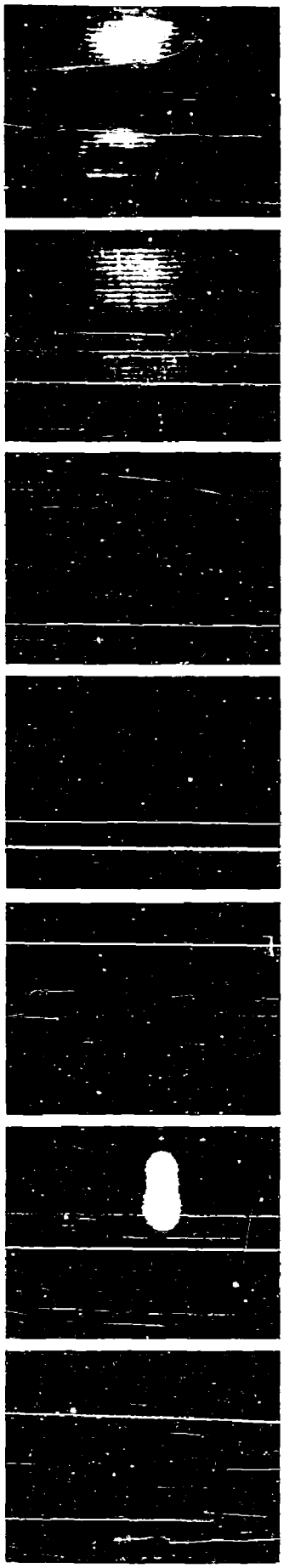

6 MEGAWATTS

8 MEGAWATTS

10 MEGAWATTS

10-13 MEGAWATTS
(SURFACE ARCING)

35-40 MEGAWATTS

48 MEGAWATTS
(INTERNAL ARCING)

BACKLIGHTED
(WINDOW DAMAGED)

Fig. 31

ceramic particle on the surface. The damage is thus indirectly connected to the multipactor through the temperature rise of the window. The third window to be tested was first sandblasted to remove loose particles. This window withstood 78 megawatts and failed after the average power was raised to 20 kilowatts equivalent at a peak pulse power of 28 megawatts.

A number of grooved silica (Amersil Optical Grade) windows were tested. Most of these had 90° v grooves with 1.5 millimeter pitch but on window B16 (Window No. 16 in Task B) the pitch was reduced to 0.75 millimeter and on Window B18 to 0.37 millimeter. Faint discharges were observed at low power levels (3 to 10 megawatts) but at higher powers these disappeared completely. Fig. 32 shows a series of photographs taken during the testing of Window B9. With very long exposures (40 seconds f 32 ASA 3000) a faint luminosity at the lower power levels can be observed, which disappears completely at higher energy levels. The 4th picture shows the reflection of a waveguide arc in the granular structure caused by the grinding of the grooves. The last picture had an exposure time of 3 minutes at f 8 for the film sensitivity of ASA 3000.

Window B10 had plain surfaces which were roughened by sandblasting. The object was to determine if sandblasting could replace the more complicated grooving. A negative result was obtained when tested at high power, the windows showed multipactor and failed.

From theoretical considerations discussed in Section 4.7.1 it is clear that window

SILICA WINDOW #9 WITHOUT COATING

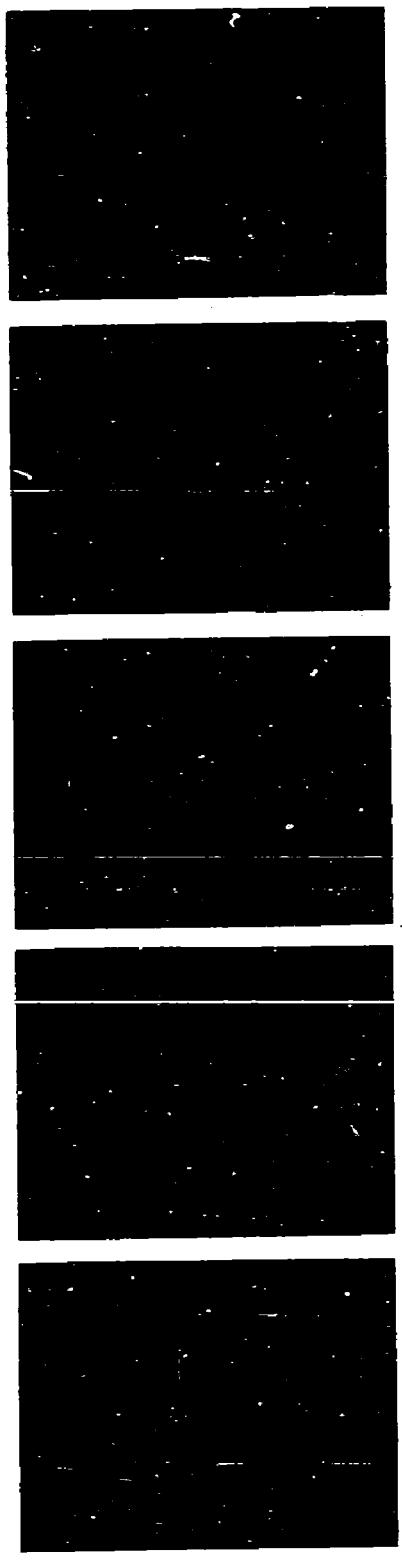

3-5 MEGAWATTS

9-14 MEGAWATTS

18-24 MEGAWATTS

30-43 MEGAWATTS
(WINDOW ILLUMINATED
BY ARC IN WAVEGUIDE)

84 MEGAWATTS

Fig. 32

grooving will suppress multipactor if the grooves are perpendicular to the direction of the electric field but not otherwise. In order to demonstrate this experimentally, window B17 was assembled with the grooves vertically, that is, parallel to the electric field. During the high power test this window showed considerable multipactor and failed.

The failure of window B10 occurred at the center of the disc and appeared to be thermal in nature. The destruction is illustrated in Fig. 33. The voids in the material shown in the enlargements indicate that local melting of the material had occurred. The destruction in window B13 occurred at the edge of the window and no plastic deformations as in window B10 could be found. It is likely that the destruction started at the window edge due to the mismatch which occurred during operation. The damage is shown in Fig. 34.

Experiments with surface grooves in quartz and beryllia were carried out during Task C. Grooves were made by grinding the window surface with a diamond contour wheel having a 90° v-shaped profile to give a groove pitch of 1.5 mm.

During a test on the grooved quartz window some multipactor was observed during the initial operation in the region of 0.1 Mw to 0.6 Mw equivalent transmitted power. As the power was increased the discharge glow moved from the center to the edges of the disc where the electric intensity is weaker. This indicates that the discharge occurs when the average distance traveled by an electron is less than the groove pitch.

WINDOW NO. 10 (AMERSIL, OPTICAL GRADE)

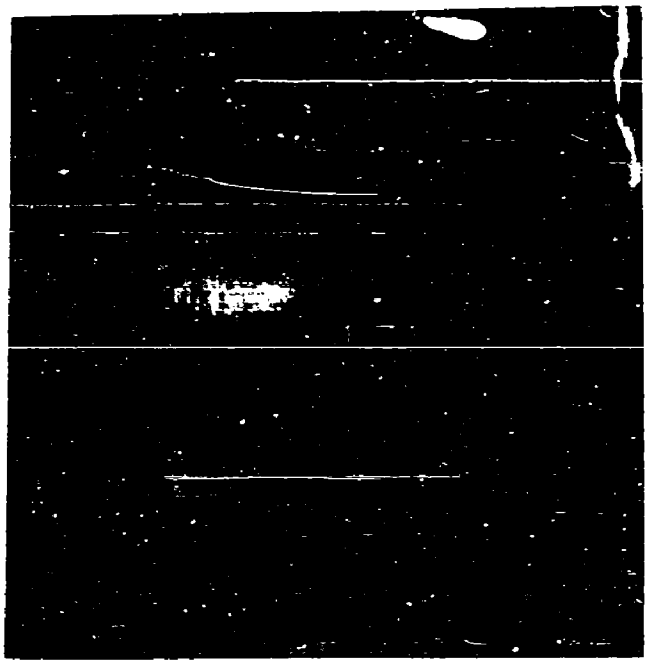

3 X

40 X

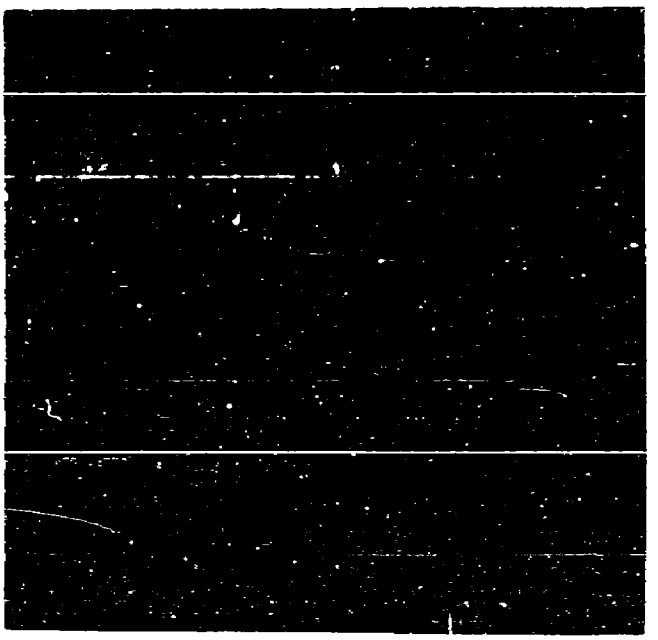

40 X

Fig. 33

WINDOW NO. 13 (AMERSIL, OPTICAL GRADE)

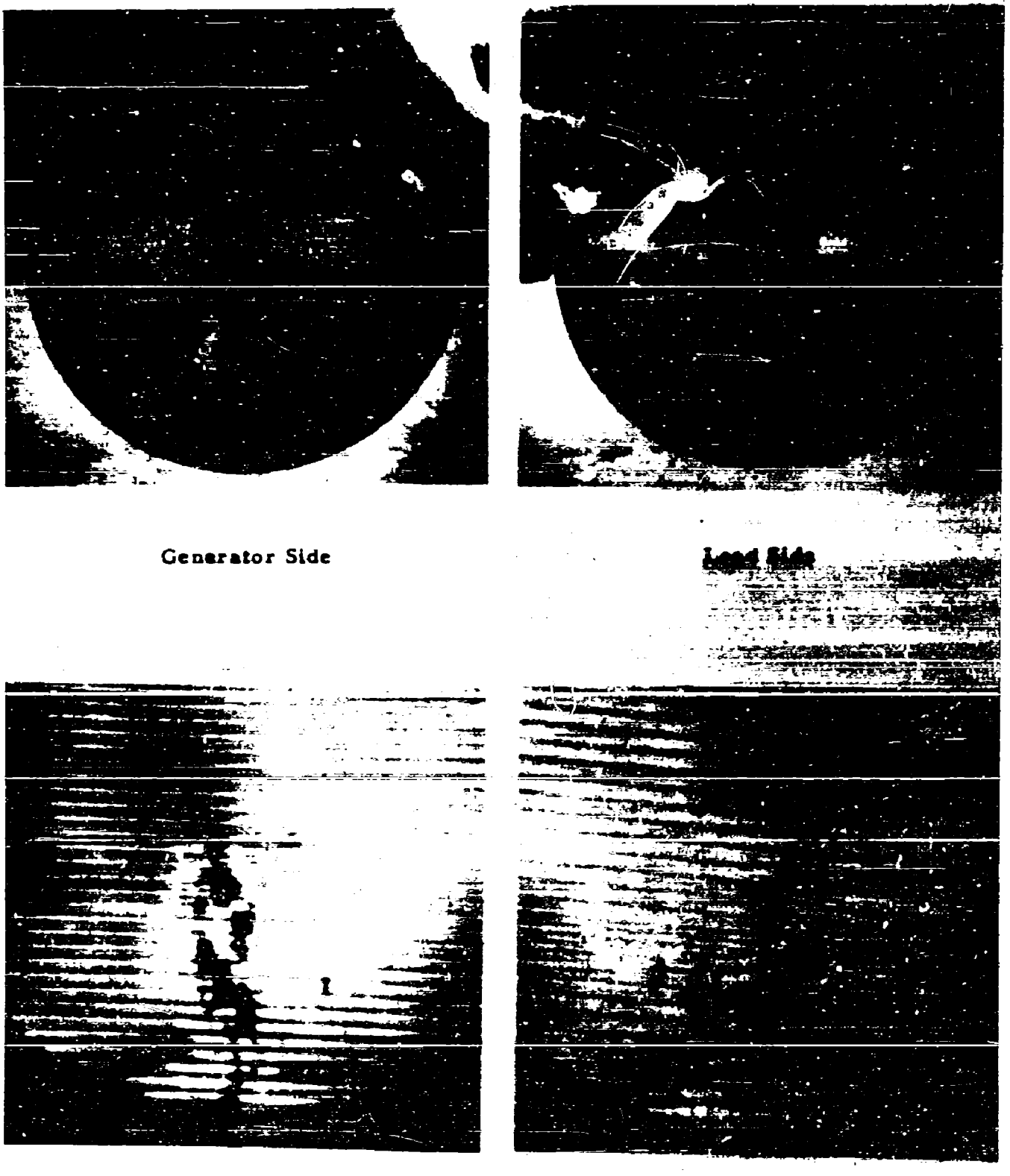

Generator Side

Load Side

Fig. 34

For greater electron distances the multipactor is effectively suppressed. Conditioning of the window surface occurred and after a period of operation the window was free of multipactor. A linear plot of power dissipated versus the square of the field strength was obtained and is shown in Fig. 35. The application of a crossed magnetic field of about 300 gauss caused some nonlinear effects at low power levels but these disappeared after a period of operation.

With the grooved beryllia window, multipactor occurred and was not eliminated even after several hours of operation. Measurements were taken after 1-1/2 hours and 4 hours operation and the results are given in Fig. 36. There is little difference in the two plots. The intensity of the discharge increased with power but a decrease occurred in the region of 5 Mw equivalent transmitted power. At this point, the grooves apparently had some inhibiting effect on the multipactor but this was not sufficient to eliminate the discharge completely. At higher powers the intensity increased again.

4.7.4 Coatings On Grooved Windows

Since surface grooves in alumina did not suppress multipactor, the effect of applying surface coatings in addition to the grooves was tried in Task B. Coatings were applied to the crest of the ridges only by sputtering titanium monoxide. Windows so treated showed no multipactor and were capable of taking the full power of the ring resonator, i.e., 85 megawatts peak at 15 kilowatts average equivalent

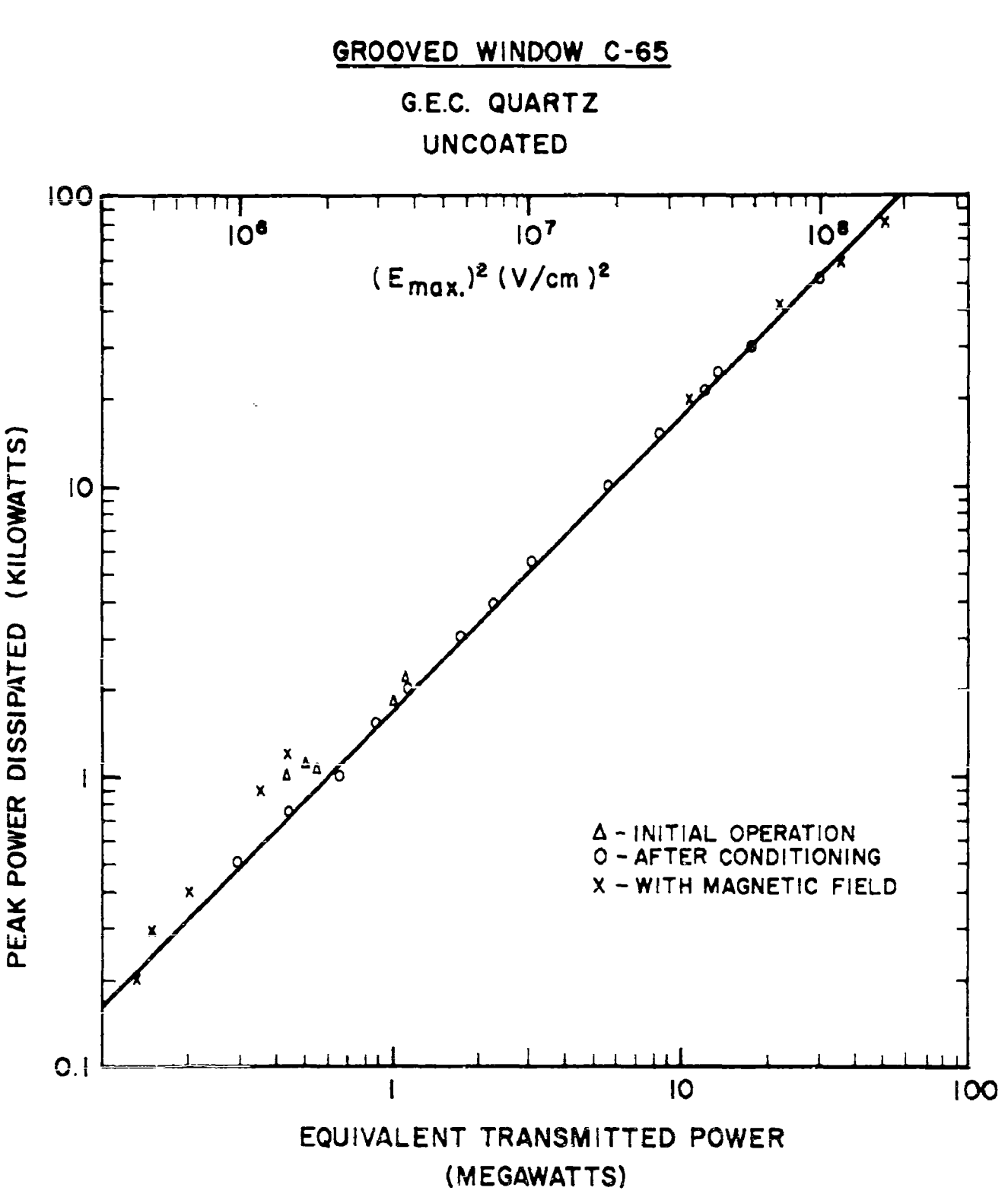
GROOVED WINDOW C-65
G.E.C. QUARTZ
UNCOATED
100
10
1
0.1
10^6
10^7
10^8
$(E_{max.})^2$ (V/cm)^2
PEAK POWER DISSIPATED (KILOWATTS)
Δ - INITIAL OPERATION
O - AFTER CONDITIONING
X - WITH MAGNETIC FIELD
1
10
100
EQUIVALENT TRANSMITTED POWER
(MEGAWATTS)

Fig. 35

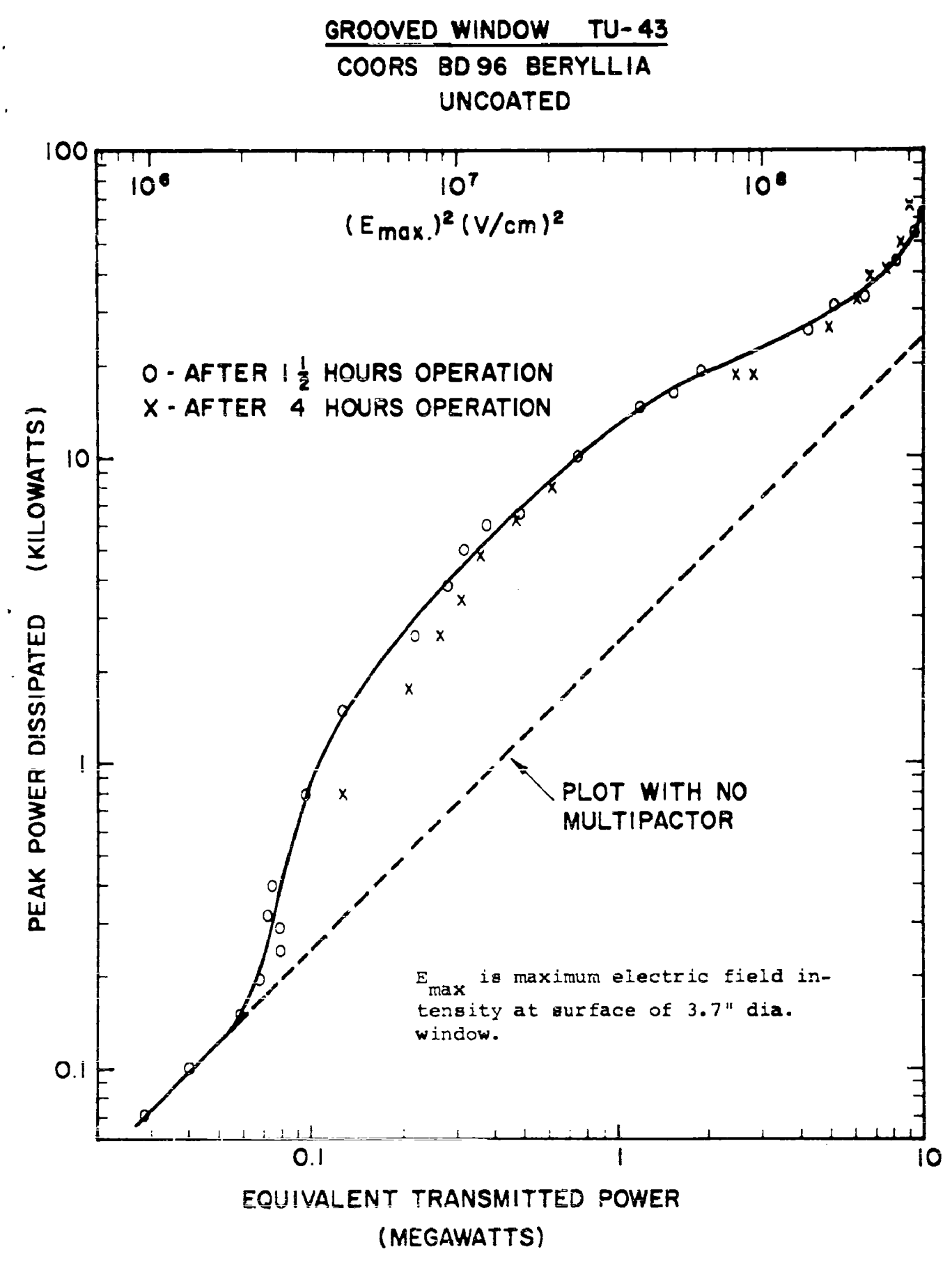
GROOVED WINDOW TU-43
COORS BD 96 BERYLLIA
UNCOATED
100
10
1
0.1
10^6
10^7
10^8
$(E_{max.})^2$ (V/cm)^2
O - AFTER 1 ½ HOURS OPERATION
X - AFTER 4 HOURS OPERATION
PEAK POWER DISSIPATED (KILOWATTS)
PLOT WITH NO MULTIPACTOR
E_{max} is maximum electric field intensity at surface of 3.7" dia. window.
0.1
1
10
EQUIVALENT TRANSMITTED POWER
(MEGAWATTS)

FIG. 36

transmitted powers and by increasing the pulse rate 40 megawatts at 43 kilowatts average.

Window B6 was coated on half the surface only. This was done in order to demonstrate visually the suppression of the multipactor by the coating. The effect is evident in Fig. 37. The left half is coated and shows no multipactor. During operation the multipactor suppression gradually spread across the whole of the window until it was eventually eliminated altogether. Thereafter the window remained completely quiet at power levels from 3 to 17 megawatts. The irregular bright lines in the 3rd and 4th pictures of Fig. 37 are faults in the photographic material.

4.8 Experiments With Other Window Coatings

4.8.1 Silicon Oxide Coatings

Multipactor was completely suppressed on all of the grooved silica windows that were tested at high power. It was therefore of interest to see if a surface coating of silica on grooved alumina windows would eliminate multipactor. Silica coatings would introduce no appreciable resistive losses which exist to some extent on titanium suboxide coatings, and for this reason the coating thickness would not be critical. Two coating methods were tried:

(a) Vacuum evaporation coating with silicon monoxide by vaporizing from a tantalum boat followed by heating in air in order to transform at least the surface of the coating into silica, (SiO_2).

AL 300 GROOVED WINDOW #6 HALF COATED WITH Ti_2O_3

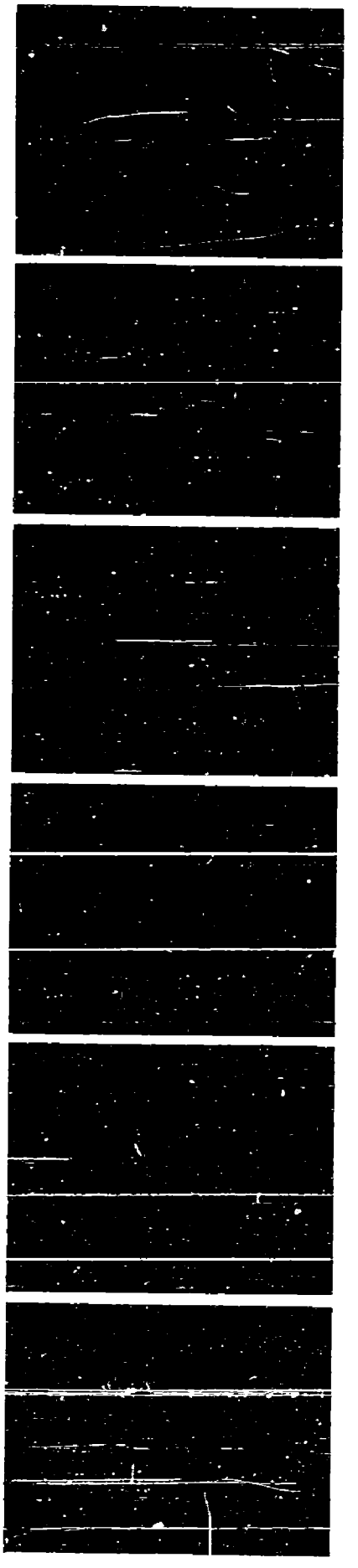

3 MEGAWATTS

5 MEGAWATTS

6-9 MEGAWATTS

11-18 MEGAWATTS

15 MEGAWATTS

45-52 MEGAWATTS

Fig. 37

TABLE 9

COATED GROOVED WINDOWS
SUMMARY OF TEST RESULTS

nr.	Material	Surface	Coating	Failure At Peak Mw	Failure At Ave. kW	Highest Power Peak Mw	Highest Power Ave. kW	Multi-pactor	Remarks
B 4	AL 300	Grooved	Yes	No Failure		85. 40.	15. 43.	No	
B 5	AL 300	Grooved	Yes	63.	11.5	63.	11.5	No	Window loose in fitting.
B 6	AL 300	Grooved	Half	No Failure		70.	12.5	No	
B 14	AL 300	Grooved	SiO_2+SiO	80.	14.	80. 41.	14. 44.	Yes	
B 15	AL 300	Grooved	SiO_2	91.	16.	91. 40.	16. 43.	Yes	

(b) Reactive sputtered coating of the window with pure silica by sputtering silicon in an atmosphere of equal parts of argon and oxygen.

The first method is well known for protective coating of metal mirrors and also as a dielectric coating for vapor deposition condensers. The structure of the layers obtained is that of silica with atomically dispersed silicon. This method was used to coat a grooved alumina window (No. B14), which was then tested at high power in the ring resonator. The operation of the window was relatively stable but multipactor was obtained which did not disappear. However, the discharge was weaker than on an uncoated window. It was thought that the excess silicon might have had an effect on the secondary emission and therefore the pure silica coating by process 2 was tried.

In this method a high frequency plasma (20 megacycles) was generated in an argon oxygen mixture at a pressure of 10^{-3} Torr. The target was transistor-grade silicon and the bombarding ion energy 1200 electron volts. The structure of the coating, according to Sinclair and Peters [13], is that of silicon glass. The coating thickness was estimated to be a few thousand Angstroms. A coating applied by this method was tested on window B15 at high power. The result was essentially the same as that of window B14 coated by method A. Multipactor was obtained but was less intense than that obtained with an uncoated window.

The reason for the difference in multipactor behavior between grooved windows of pure silia and alumina with silica coatings is not clear. Either the coatings were too thin and the microfield of the base material still affected the secondary electron emission of the surface, or the difference in the dielectric constant (a factor of 2.6) has considerable effect on the field distortion at the surface.

4.8.2 Diffusion Coatings

In addition to vacuum deposition and sputtering, another method of preparing titanium suboxide coatings on ceramic surfaces was developed independently by the Processing and Materials Laboratory at Eitel-McCullough, Inc., following a method specified by Dr. Leonard Reed. The method consists of spraying the surface to be treated with a solution containing crushed TiO_2 and subsequently firing at 1420-C in hydrogen. During heat treatment diffusion of the titanium into the ceramic occurs and an intermediate phase is formed between the ceramic and the surface coating. Due to the hydrogen atmosphere reduction of the TiO_2 occurred leaving the required titanium suboxide surface coating. It was thought that coatings applied in this manner might have greater stability and offer advantages in production. Accordingly, sample coatings were tested in this program.

As this procedure produces thick coatings which tend to produce excessive losses in the window, the coating was applied in the form of dots to reduce the overall amount of material on the disc surface.

In spite of this precaution, increased window losses were observed. The coating was tested on several windows during Task C, but was not successful in eliminating multipactor. In the first window tested, C42, multipactor started at an equivalent transmitted power of about half a megawatt and increased in intensity as the power was raised. The whole ceramic surface was illuminated by a pink glow and the dark spots of the coating could be clearly seen. It appeared that multipactor occurred between the dots where the discharge was brightest. Although some conditioning was observed, multipactor was not eliminated. At an equivalent transmitted power of 9 megawatts, arcing between the dots occurred in addition to the steady multipactor and prevented further increase in power. In window C42 which had a lighter coating similar results were obtained except that in this unit no arcing between the dots was observed.

It appeared that the multipactor discharge may have been confined to the area between the dots. Accordingly, a continuous coating was tested (window C62) but severe multipactor was again obtained.

The coatings produced by this method were rather thick and in order to avoid excessive window losses it was necessary to reduce the thickness by etching. This may have removed most of the titanium suboxide leaving only the intermediate phase which probably has very different secondary emission properties.

4.8.3 The Effect Of A Brazing Process On Window Coatings

Most of the coatings tested during this program were applied to windows which had already been brazed into an assembly. In many tube designs, especially at the higher microwave frequencies, windows are located in inaccessible positions which would make them difficult to coat after assembly. The solution to this problem would be to coat the ceramic prior to brazing into the tube structure, provided the brazing pro-process was not detrimental to the coating performance. Since brazing takes place in a reducing atmosphere it was anticipated that titanium coatings would survive the process. A titanium-hydrogen reaction occurs at elevated temperatures but this reaction is reversible. Thick coatings are liable to peel off due to volumetric changes associated with the titanium hydride phase, but thin coatings should not be affected.

A beryllia window coated by evaporating titanium to a resistivity of 10^6 ohms/square showed no multipactor when tested in a standard cavity. The window was removed, heated to 750°C in dry hydrogen, assembled in another test unit and reprocessed. On testing at high power no multipactor occurred.

An alumina and a beryllia disc were coated by evaporating titanium to resistivities of 10^8 and 10^6 ohms/square respectively, prior to brazing into assemblies. On subsequent testing at high power severe multipactor was obtained with the alumina window. The beryllia window supported a little multi-pactor initially which cleared up after a short period of operation.

One sputtered titanium monoxide coating was tested; this was applied to an alumina disc in an argon atmosphere prior to brazing the disc into assembly. This coating suppressed multipactor after an initial period of conditioning.

Of the 4 coatings subjected to brazing cycles, 3 retained their multipactor suppression properties and one did not. The reason for the failure is uncertain; the coating was thinner than the others but sufficiently thick to suppress multipactor under normal conditions. It is the practice to remove parts from the brazing furnace when the temperature has fallen to 100-200°C. This may have been hot enough to cause excessive oxidation of the titanium film in air.

From these results it can be tentatively concluded that titanium coatings will survive a brazing process in dry hydrogen. Further experiments under controlled conditions will be necessary to confirm this.

4.9 Arcing At The Window Seal

4.9.1 The Arcing Problem

The maximum peak power that could be dissipated in the window cavities during Tasks A and C was invariably limited by arcing at the metal-dielectric junction either in vacuum or in SF_6 at 20 pounds per sq. inch. This arcing occurred at the top and bottom of the cavity, corresponding to the regions of maximum electric intensity in the TE_{111} mode.

The threshold power for arcing varied somewhat from window to window but for pulse widths of 20 microseconds, generally occurred

when the maximum electric field strength at the window surface was in the region of 25 to 31 kv/cm corresponding to a transmitted power of 20 to 30 Mw peak. These field strengths are enhanced at sharp points and ridges in the region of the metal-dielectric seal and it is believed that this is responsible for initiating breakdown.

The nature of the window braze has a considerable influence on the arcing threshold. Normally windows were sealed into cylinders with a minimum of braze material but with one assembly (C36) a large amount of braze was used which formed thick fillets at the seal. This resulted in arcing at the junction, due to enhancement of the electric field at the edge of the fillet, at field strengths equivalent to a transmitted power of only 6 Mw peak.

The arcing threshold is also dependent on the pulse width. During high power experiments on window cavities the rectified RF pulse was monitored on an oscilloscope. Arcing at the window seal was observed to shorten the pulse. At the sparking threshold, the last 1 or 2 microseconds are chopped off the normal 20 microseconds pulse. On increasing the input power a greater portion of the pulse is chopped off, but a considerable increase in power is required to reduce the complete pulse. Typical pulse distortions are illustrated in Fig. 38.

It seemed probable that with shorter pulse widths higher peak powers would be obtained. Accordingly, the modulator delay line was modified in a temporary manner to provide shorter pulses. A number of window units were then tested, the peak power for arcing

(a) 20 μs PULSE , ARCING THRESHOLD

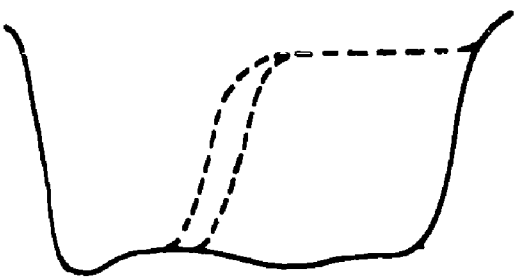

(b) 20 μs PULSE , PEAK POWER INCREASED 50 %

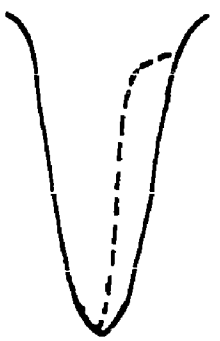

(c) 3 μs PULSE , ARCING THRESHOLD (HIGHER POWER)

DISTORTION OF RECTIFIED R.F. PULSE DUE TO ARCING

Fig. 38

being measured at 3, 10 and 20 microsecond pulse widths. The results are shown in Fig. 39. Since the actual values varied from unit to unit they have been plotted as a percentage of the threshold power for arcing at a pulse width of 3 microseconds. It can be seen that a considerable reduction in peak power occurs as the pulse width is increased. Decreasing the pulse width from 20 to 3 microseconds enabled the peak power to be increased by an average of 80%. These results indicate that, at the power levels of interest, time intervals of in the order of several microseconds are required for the density of charged particles in the vicinity of the window seal to build up to the arcing level and that the threshold power for arcing is critically dependent on the charged particle density under the conditions mentioned.

4.9.2 Methods Of Increasing The Arcing Threshold

In order to increase the peak power handling capability of the windows various methods of reducing the electric intensity at the metal-dielectric junction were tried. One attempt to weaken the electric field at the seal was by the use of arc suppressor rings situated near the ceramic surface. A window design employing such rings is shown in Fig. 40. The object of the rings is to divert electric field lines from the junction, thereby reducing the chance of arcing at this point.

A window assembly built to this design was tested in a unit pressurized with SF_6 gas on both sides of the ceramic but the results were disappointing. Arcing occurred at a

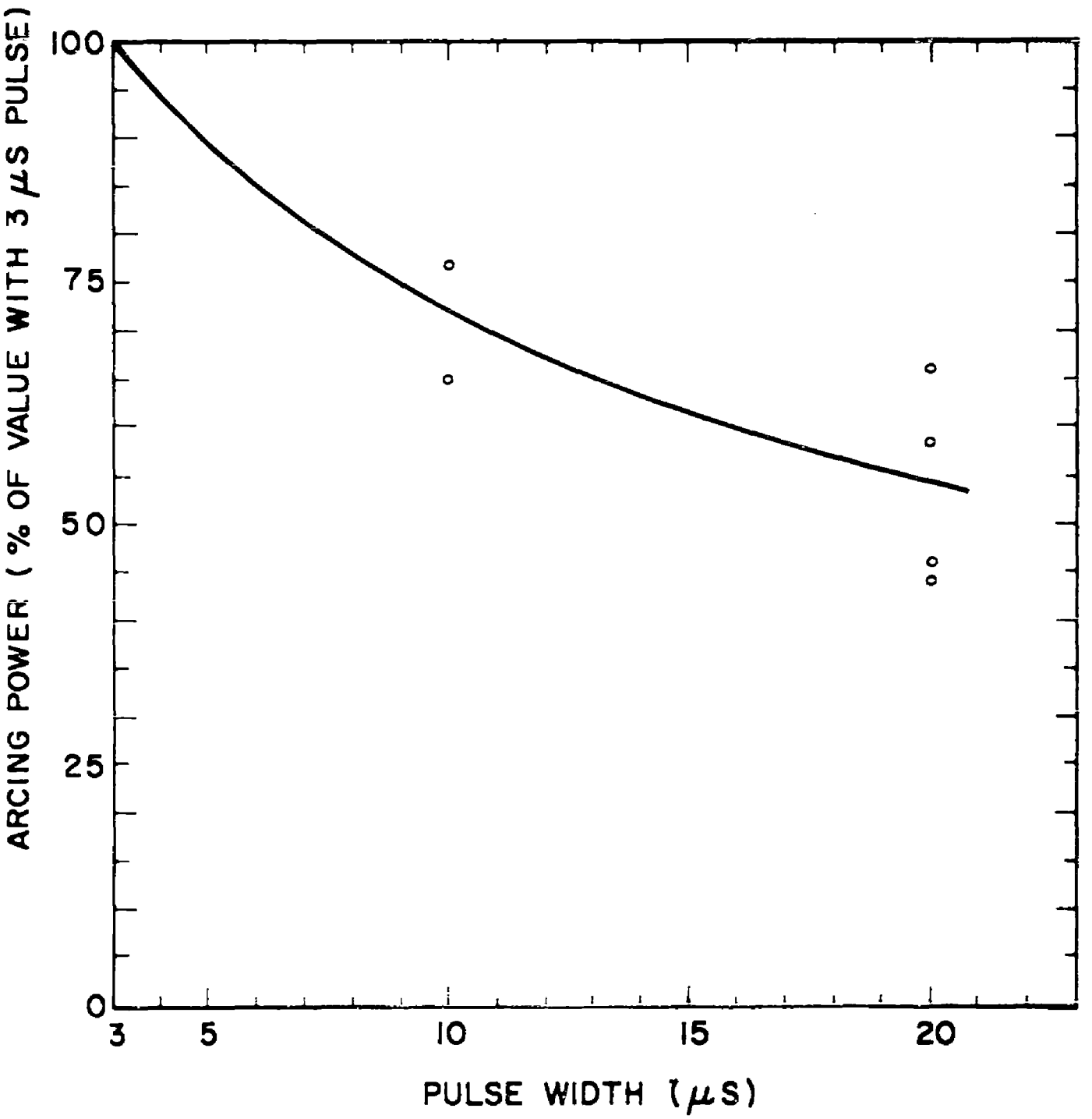

EFFECT OF PULSE WIDTH ON
PEAK POWER FOR ARCING

FIG. 39

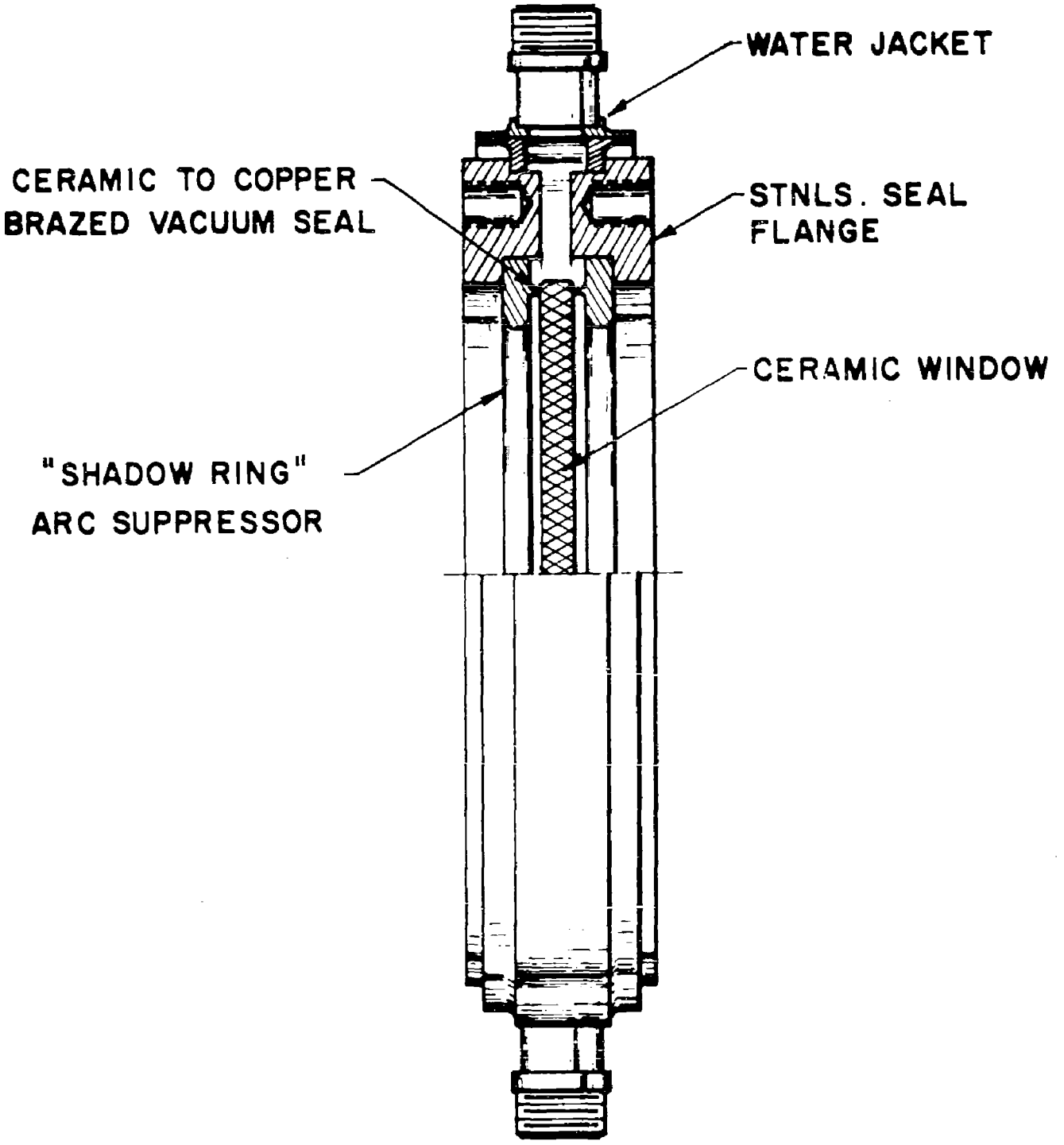

WINDOW CAVITY WITH ARC SUPPRESSOR RINGS

Fig. 40

comparatively low power. The breakdown appeared to originate at the uneven edge of the metalizing which in this design extended over part of the ceramic face. It is probable that the seal geometry could be improved by modifying the design but work on this window was stopped in favor of more promising methods.

Another way of reducing the electric intensity at the seal is by means of dielectric fillets adjacent to the ceramic and the metal cylinder.

The arrangement is shown in Fig. 41. Due to the higher permittivity the electric intensity has a lower value in the dielectric and the metal-dielectric junction is effectively transferred to a position of weaker standing electric field. One problem is to find a suitable material which can be applied to the window after brazing. It should bond to metal and ceramic, have a high dielectric strength, a low loss factor and withstand a high temperature bakeout under vacuum. Most epoxy resins are unsuitable because of the temperature requirement. However in order to test the principle, a window containing fillets of Araldite 502 was assembled in a modified test unit which could be pressurized with SF_6 gas on both sides of the ceramic. When tested at high power with a 20 microsecond pulse width this unit withstood field strengths equivalent to 35 Mw peak transmitted power prior to breakdown. This is about 30% higher than the usual arcing limit. Arcing caused cracking in the Araldite fillets which permanently reduced the peak power handling capability of the window. The success of this approach will depend on the development of a suitable dielectric material and application technique.

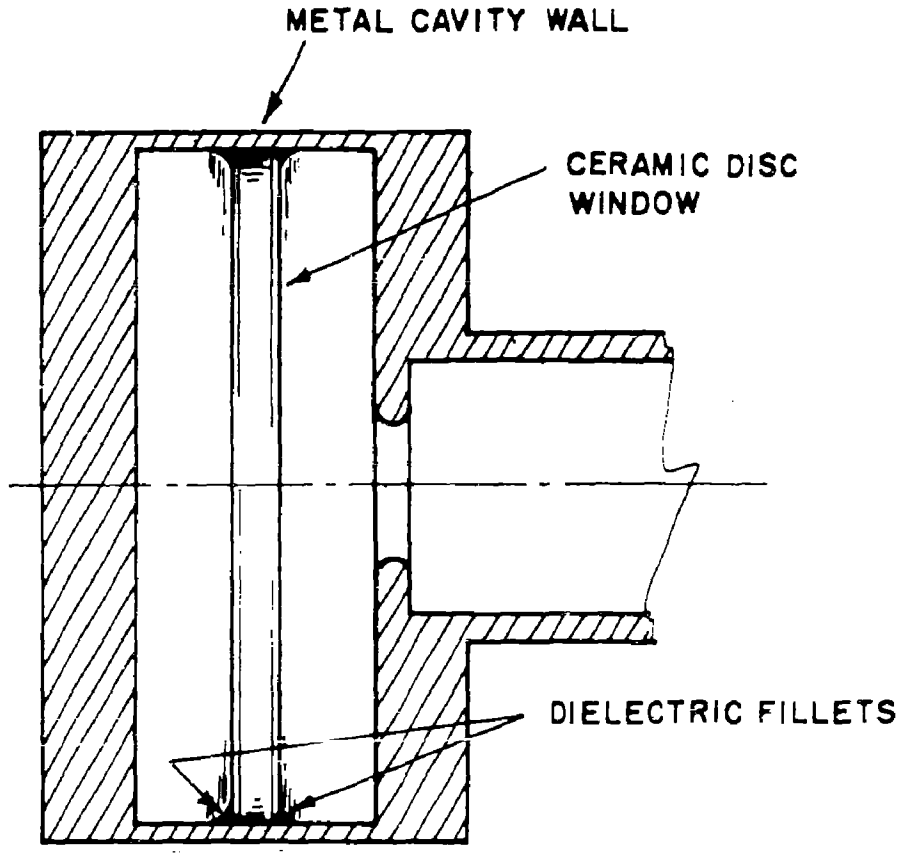

DIELECTRIC FILLETS AT CERAMIC-METAL JUNCTION IN RESONANT CAVITY

Fig. 41

4.10 Alternative Window Designs

4.10.1 Flanged (or "H") Window

Another approach to solving the arcing problem was to use a completely different window geometry in which the metal dielectric junction is located in a position of weak electric field. Such a design is shown in Figs. 42 and 43. A specially shaped ceramic is used which has an H type cross section. The external surfaces of the ceramic are metalized and copper-plated to form the waveguide wall. To evaluate the design an alumina ceramic part was manufactured and the test cavity assembled by clamping the ceramic between end plates.

The first high power test was carried out in air at atmospheric pressure. Arcing occurred at an equivalent transmitted power of 20 megawatts peak which compares with the arcing threshold of about 2 megawatts peak for a standard window under similar conditions. The arc resulted from the breakdown of air, it occurred at the ceramic surface in the center of the disc at the position of maximum electric intensity and was observed as a bright blue streamer. The arc was concentrated at the disc center and did not extend to the outer edge where all previous breakdowns had been observed.

By introducing SF_6 gas at atmospheric pressure into both sides of the cavity, the breakdown strength was improved and higher peak powers were possible. Under these conditions similar arcing occurred. The equivalent transmitted power was 112 megawatts peak and 280 kW average for this test. The average power dissipated was kept below 100 watts to avoid damaging the ceramic through overheating.

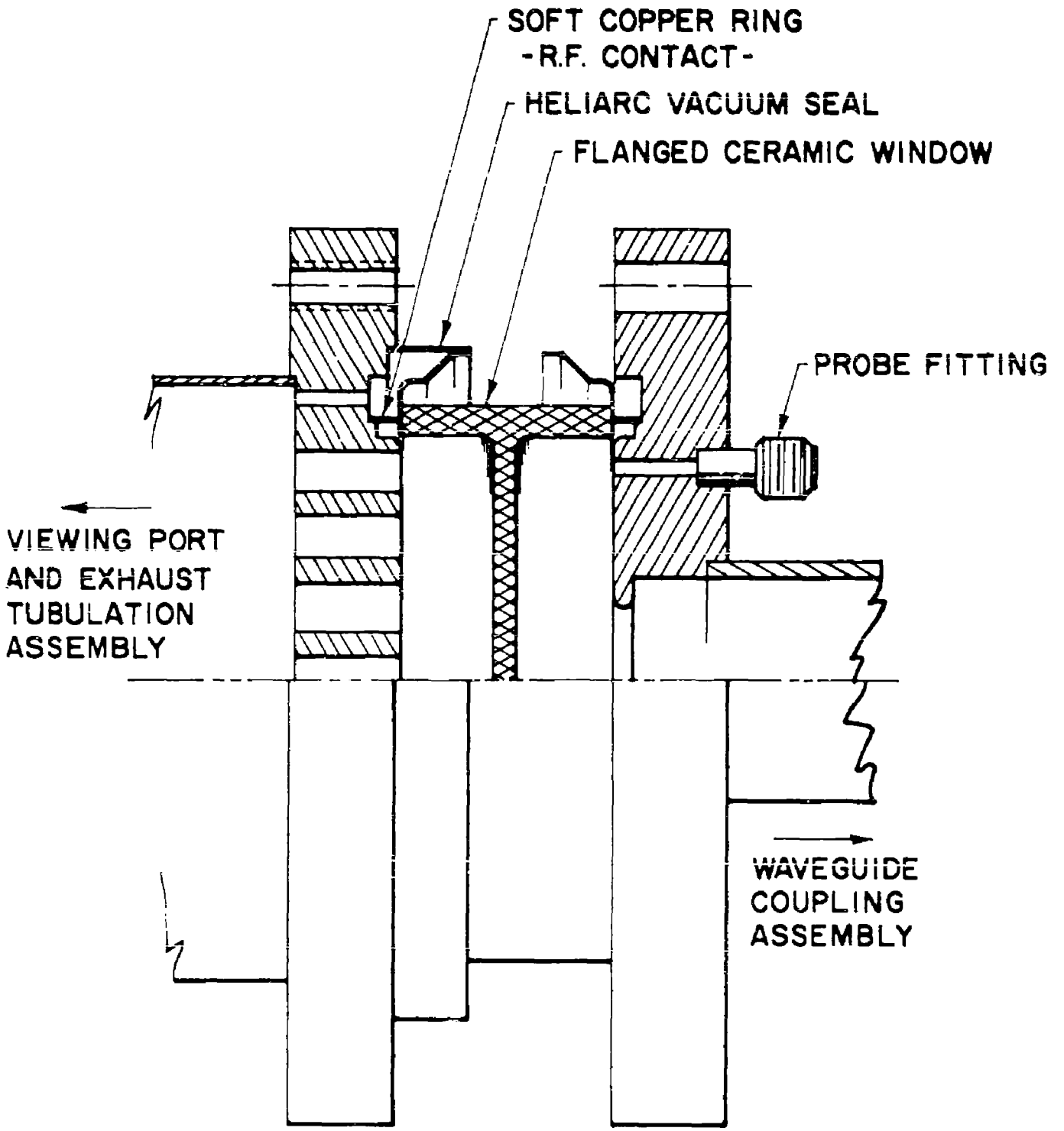

FLANGED (H-TYPE) WINDOW ASSEMBLY

VACUUM VERSION

FIG. 42

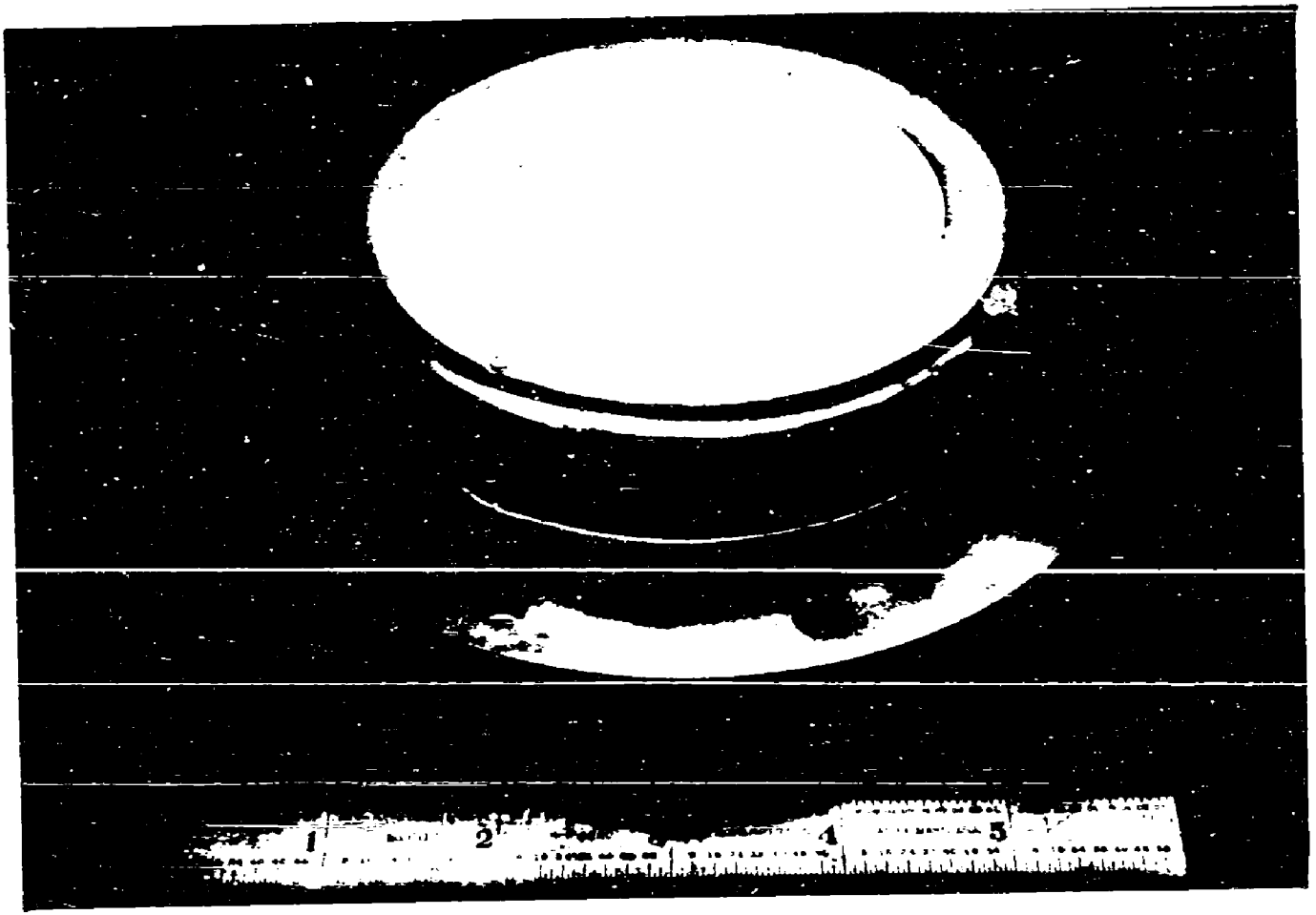

Fig. 43 "H" Window Assembly

To enable the window to be examined under vacuum conditions, one of the seals was modified to provide a vacuum-tight joint. Prior to assembly the ceramic was coated by evaporating titanium to a resistivity of 10^7 ohms/square to eliminate multipactor discharges. A standard test unit was then assembled and processed in the normal way.

During the first high power test on the vacuum version of this window, some arcing occurred at the sealing ring even though the seal was apparently located in a position of weak electric field. This arcing was found to be originating at the sharp edge of the heliarc ring which was brazed on to the end of the ceramic. On removing this edge no further breakdowns were obtained. The window was then capable of supporting peak powers up to an equivalent of 100 megawatts transmitted power without arcing.

4.10.2 Dome Window

Having demonstrated that surface coatings can successfully eliminate multipactor on flat disc windows, it was decided to extend the experimental work to include curved surfaces also. Cone or dome-shaped windows offer certain advantages compared with discs (e.g., they have greater potential bandwidth) but have been out of favor for high power applications in recent years because of their tendency to support strong multipactors which result in failures due to overheating.

To demonstrate that evaporated titanium surface coatings can successfully eliminate multipactor on curved surfaces, experiments

were carried out with a dome-shaped alumina ceramic. This was assembled in a cylindrical resonant cavity as shown in Fig. 44. A photograph of the dome mounted on a flange is given in Fig. 45. Prior to assembly the inner curved surface of the ceramic was coated by evaporating titanium to prevent the multipactor. This side of the window cavity was then evacuated, the other side being pressurized with SF_6 gas during high power testing. As the peak power was increased intermittent multipactor occurred at the lower levels, but disappeared after conditioning. At a power dissipation of about 10 kilowatts peak corresponding to 7 megawatts peak transmitted power, heavy loading of the cavity occurred preventing further increase in power. A bright glow which was concentrated at one position at the edge of the window was observed and could be intensified by a magnetic field. It is not clear whether this loading was due to arcing or a multipactor type discharge. If the latter, it was of an unusual type since it was concentrated in one region. Possibly a two-surface multipactor occurred between the base plate and the spot on the ceramic which may have been coated too thinly. To investigate this a further test was planned in which the base plate was coated with titanium in addition to the ceramic, to eliminate the possibility of a two-surface multipactor. Unfortunately, the ceramic dome was cracked during processing and the experiment could not be performed. Time did not permit the building of a new test unit.

Since multipactor was eliminated at the lower power level, the experiment indicates that the coating was successful. The nature of this spurious discharge needs to be investigated in further tests.

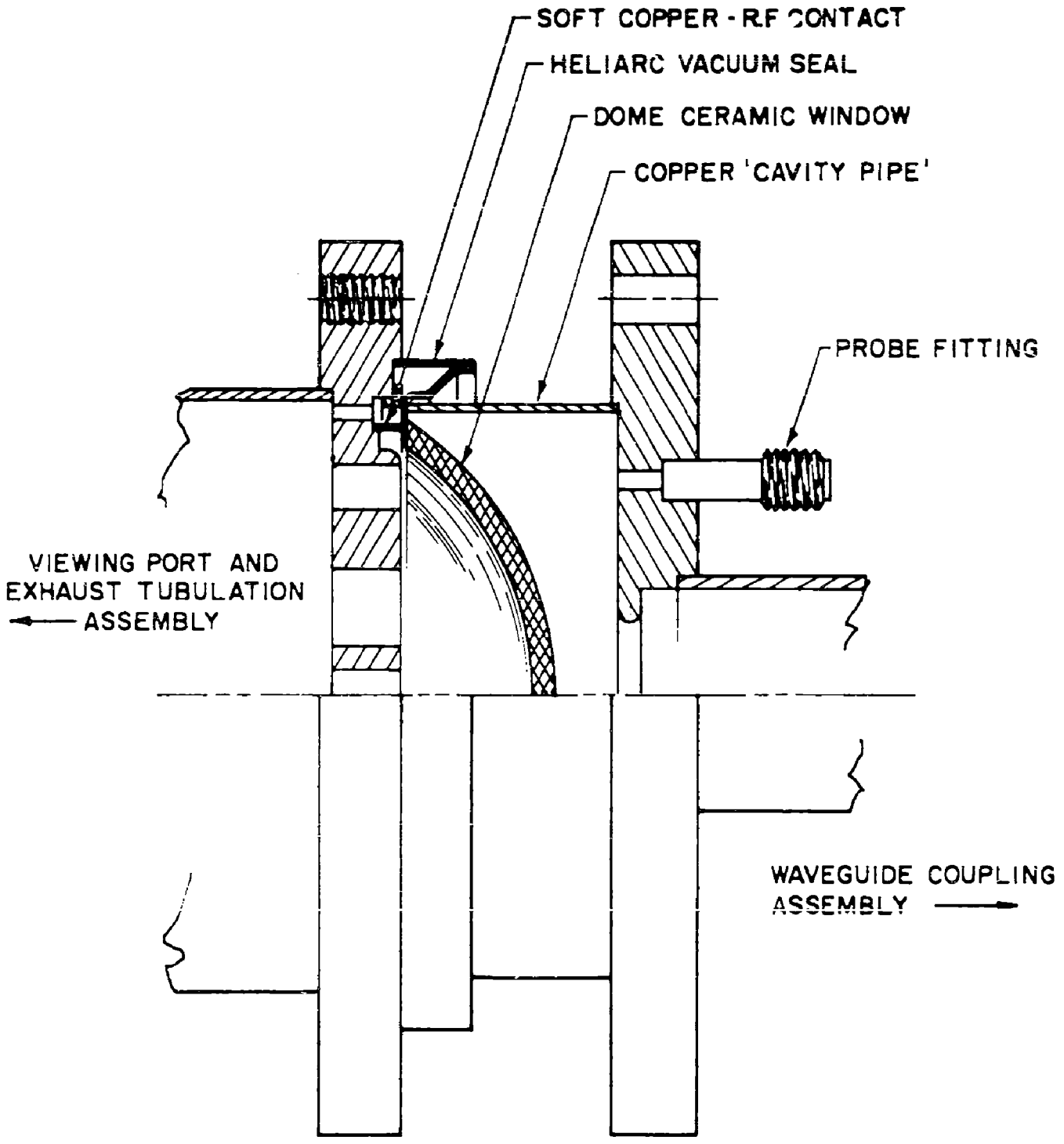

Fig. 44 DOME WINDOW TEST UNIT ASSEMBLY

Fig. 45 "Dome" Window Assembly

5. CONCLUSIONS

This section commences with a general discussion of the results of the investigation and ends with a summary of the conclusions.

Prior to the inception of this work it was known that discharges are liable to occur at microwave windows when operated at high power, but the nature of such discharges was not well understood. A single-surface multipactor mechanism had been suggested to explain excessive heat dissipation at ceramic cylinders used in certain types of klystron cavities and it seemed likely that a similar mechanism could occur at flat disc windows used in waveguides. The results of the present work confirm this speculation. It is clear that multipactor discharges invariably occur when microwave windows are operated at high power unless steps are taken to eliminate them.

A simple theory based on the motion of an electron in an RF and static electric field appears to offer a satisfactory explanation which is in accordance with experimental observations. The critical factors which determine the power level at which a multipactor will commence are the maximum energy which free electrons may gain from the electric field, the secondary emission characteristics of the window surface, and the value of the force which returns electrons to the surface. In the absence of a magnetic field this force is dependent on static charges at the window. When the maximum electron energy is greater than the first cross over potential of the secondary emission characteristic curve, multipactor is likely to occur. The secondary emission properties vary considerably with surface conditions, the effect of adsorbed gas, for example, can be expected to increase the secondary yield. This explains the conditioning process which is observed during a multipactor. A sustained discharge at a window surface removes adsorbed gas, thus lowering the secondary yield, and increasing the first cross over potential. Subsequently, higher electron energies or higher transmitted powers are necessary to start a discharge.

Multipactor is detrimental to window performance because it results in excessive heat dissipation at the window (which may cause window failure) and also liberates large amounts of gas which causes a deterioration in the vacuum of a sealed-off tube, and increases the possibility of arcing.

Multipactor at waveguide windows can be eliminated by surface coatings of titanium suboxide. The coatings may be applied by evaporating titanium in vacuum or by sputtering titanium monoxide in an argon or a mercury atmosphere. Both methods produce satisfactory coatings if certain precautions are taken. The vacuum evaporation method is the simpler, but the nature of the coating produced is dependent on the system pressure and the rate of evaporation, which must be kept constant if reproducible results are to be obtained. The sputtering method requires more equipment which must be set up and maintained very carefully. Sputtered coatings are also dependent on pressure and sputtering rate. No difficulty has been experienced with the adhesion of evaporated or sputtered coatings since only thin films are employed.

Both types of coating may be controlled by monitoring the resistance of a test strip during deposition. This will allow reproducible coatings to be obtained provided the conditions of deposition do not vary. The sputtering current and time provide an alternative method of monitoring the coating thickness but changes in the geometry or ambient pressure will cause variations.

Since the coatings are thin films they are subject to change on exposure to air due to oxidation but subsequent bakeout under vacuum causes a reduction of the oxide. The final oxygen content of the films is dependent on the time and temperature of the vacuum bakeout and the degree of initial oxidation. The conditioning observed with coated windows is probably connected with changes in the film in addition to the removal of adsorbed gas. Bombardment with electrons will tend to reduce the coating thus decreasing the secondary yield.

Grooves cut in the surface of a window perpendicular to the electric field decrease the intensity of multipactor at alumina, beryllia and quartz surfaces but the discharge is completely eliminated only in the case of quartz. This is not fully understood. It is possible that variations in the field-shaping method may eliminate multipactor at alumina and beryllia.

During the course of the investigation it became apparent that the main limitation to the peak power handling capability of the windows tested was arcing at the metal-dielectric seal. The arcing threshold was dependent on the nature of the seal and the pulse width. It is speculated that arcing is originated by field emission currents which occur due to local enhancement of the electric field at sharp points and ridges at the metal-dielectric seal. Secondary charged particles will be generated by bombardment of adjacent surfaces and collisions with stray molecules. Arcing occurs when the charged particle density reaches a critical level. During a multipactor discharge more charged particles are available and from theoretical considerations the arcing threshold would appear to be lower.

To summarize, the main conclusions of the work are briefly stated in the following:

Multipactor at waveguide windows of alumina, beryllia or quartz is liable to occur at transmitted powers above about 100 kw peak (the corresponding value of E/ω being 1.05 volts per cm. per Mc. The threshold power is largely independent of frequency. Multipactor is accompanied by the liberation of gas. An analysis of gases liberated during a multipactor discharge at an alumina surface indicates that the gas evolution is a secondary effect of the multipactor and results from outgassing of the window surface.

Multipactor can be eliminated by coating the window surface by evaporating titanium in vacuum, or sputtering titanium monoxide in an argon or a mercury atmosphere.

Coating thickness can be effectively controlled by monitoring the surface resistivity during deposition. For coatings prepared by evaporating titanium at a pressure of 10^{-5} Torr a resistivity range of 10^6 to 10^{10} ohms/square is suitable for alumina and beryllia windows. For quartz with an optical finish the lower limit of resistivity needs to be increased to avoid additional RF losses. Definite limits of coating resistivity for quartz have not been established. Sputtered titanium monoxide coatings with resistivities in the range 10^7 to 10^{10} ohms/square are suitable for alumina and beryllia windows.

Window coatings have been tested up to peak field strengths equivalent to 100 Mw peak transmitted power and average dissipations equivalent to over 300 kW of average transmitted power. Some coatings require a period of conditioning on first exposure to high power microwaves, but the final performance of such coatings is satisfactory.

Grooves cut in the window surface perpendicular to the electric field eliminate multipactor at quartz windows and decrease the intensity of multipactor at alumina and beryllia windows. Of the three groove sizes, 1.50, 0.75 and 0.37 mm, the smallest is to be preferred. Multipactor can be eliminated on grooved alumina windows by coating the crests with titanium suboxide.

The peak power capacity of the windows tested was limited by arcing at the metal-dielectric seal. An increase in the threshold power for arcing was achieved by coating the seal area with dielectric. Better results were obtained with a specially shaped window of "H" cross section in which the metal-dielectric junction was located in a position of weak electric field. A window of this design supported field strengths equivalent to 100 Mw peak power without arcing.

6. RECOMMENDATIONS

From the work carried out during this investigation, it is apparent that multipactor is a major problem with high-power microwave windows. It has been demonstrated that multipactor can be eliminated by certain window treatments. Such methods have been thoroughly evaluated and shown to give consistent results.

Certain areas of the work merit further investigation. It has been shown that the window coatings are subject to change under certain environments and the ability of coatings to withstand normal tube production processes has not been fully evaluated. While some coatings have been subjected to brazing processes and retained their ability to eliminate multipactor, others have not and the reasons for this inconsistency are not clear.

It is conceivable that other coatings and application methods would be successful in eliminating multipactor and offer improvements over the methods presently used. Coatings which were not subject to change on exposure to various environments would be an advantage. However, it should be pointed out that all coatings and surfaces are subject to contamination. It is the upper most film which determines the secondary emission properties of the surface. Thus any processes carried out subsequent to window coating which may result in the deposition of other materials (e.g., any heating or brazing process) is liable to alter the surface condition.

Although grooved windows have met with limited success during this program, the method has worked well with one material and partially eliminated multipactor at the other window materials tested. A variation on this approach may provide a more efficient means of multipactor suppression. The method has the advantage of not being subject to changes when exposed to various atmospheres, though surface contamination could cause a discharge in borderline cases where the multipactor is only just suppressed.

The role of gases evolved at the window during a discharge has not been fully explained. The evidence so far indicates that gas evolution is a secondary effect, but it is possible that gases may be more closely involved in the discharge. Gases adsorbed on the window depend on previous treatment and attention to such treatment may offer means of improving the window. For example, varuum firing the ceramic at high temperature prior to assembly may reduce the gas content.

Another major problem which has been emphasized by the present work is arcing at the window seal. Windows which had been made multipactor-resistant by suitable coatings invariably failed due to arcing at this point. Further studies on arcing at the seal and its dependence on such factors as metalizing, brazing and local geometry are recommended. Some progress with this problem has been achieved under the present contract by the use of a new window design which is less subject to arcing. It is believed that further work using this approach would be worthwhile.

7. REFERENCES

1. D. H. Preist and R. C. Talcott, "On The Heating Of Output Windows Of Microwave Tubes By Electron Bombardment" - IRE Trans. E.D. Vol. 8, p. 243, July 1961.

2. R. C. Talcott, "The Effects Of Titanium Films On Secondary Electron Emission Phenomena in Resonant Cavities and at Dielectric Surfaces" - IRE Trans. E.D. Vol. 9, p. 405, September 1962.

3. D. H. Preist, "Multipactor Effects And Their Prevention In High-Power Microwave Tubes" - Microwave Journal, Vol. 6, No. 10, p. 55, October 1963.

4. P. T. Farnsworth, "Television By Electron Image Scanning" - Journal of the Franklin Institute, Vol. 218, No. 4, p. 411, October 1934.

5. Gill, E. W. B., and von Engel, A., "Starting Potentials of High Frequency Gas Discharge at Low Pressure" - Proc. Royal Soc. London, Vol. A-192, p. 446, 1948.

6. A. J. Hatch and H. B. Williams, "The Secondary Electron Resonance Mechanism of Low Pressure High Frequency Gas Breakdown" - Journal Appl. Physics, Vol. 25, 1954.

7. D. J. Goertz, Jr., "Ultra-High Vacuum Components For The Proposed Stanford Two-Mile Linear Accelerator" - Amer. Vac. Soc. Symposium Trans. Pergamon Press, New York, p. 16, 1960.

8. I. R. Kanicheva and V. V. Burtsev, "Investigation Of Transmission Of 0.5-16 kev Electrons Through Collodian and Gold Films" - Soviet Physics Solid State, Vol. 1, No. 8, p. 1146, February 1960.

REFERENCES (Cont'd)

9. H. Bruining "Physics And Applications Of Secondary Electron Emission" - Pergamon Press, New York, Ch. 3, 1954.

10. W. L. Bond, "Notes On Solution Of Problems in Odd Job Vapor Coating" - Jour. Opt. Soc. of America, Vol. 44, No. 6, p. 429, June 1954.

11. L. Holland and L. Laurenson, "Secondary Electron Emission of Evaporated Titanium Films" - Nature, Vol. 199, p. 274, June 1963.

12. A. D. Pearson, "Studies On The Lower Oxides of Titanium" - J. Phys. Chem. Solids, Vol. 5, p. 316, 1958.

13. W. R. Sinclair and F. G. Peters, "Preparation of Oxide Glass Films by Reactive Sputtering" - J. Amer. Cer. Soc. Vol. 46, p. 20, 1963.

14. L. E. Hollander and P. L. Castro, "Anistropic Conduction in Nonstoichiometric Rutile (TiO_2)" - Phys. Review, Vol. 119, p. 1882, September 1960.

8. IDENTIFICATION OF KEY AND TECHNICAL PERSONNEL

The hours worked by all those participating in the program for the period July 1, 1962 through June 30, 1964 are as follows:

D. Preist	1,036 hours
R. Talcott	386 "
J. Soderstrum	192 "
J. Zegers	2,105 "
B. Hill	869 "
K. Scholz	991 "
J. Leidigh	110 "
I. Coutts	1,079 "
A. McConn	293 "
R. Lindquist	113 "
B. Barnaby	101 "
P. Fletcher	460 "
R. Hayes	1,408 "
O. Heil	1,079 "
G. Brauns	250 "
B. Morozovsky	1,269 "
S. Zott	802 "

APPENDIX I

Mathematical Analysis Of Multipactor Motion On A Single Dielectric Surface With No Static Magnetic Field

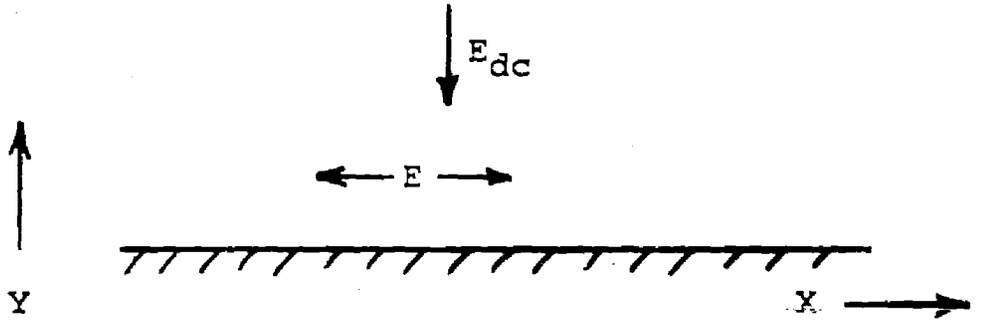

Let v_o be the initial velocity of a secondary electron, having components v_{ox} and v_{oy} in the x and y directions.

Let E be an alternating electric field parallel to the surface.

Let E_{dc} be a static electric field normal to the surface.

The differential equations of motion for an electron will be:

$$\frac{d^2x}{dt^2} = \frac{e}{m}\left[E \sin \omega t\right] \qquad (1)$$

$$\frac{d^2y}{dt^2} = \frac{e}{m}\left[E_{dc}\right] \qquad (2)$$

where

e is electron charge, m is electron mass, ω is frequency in radians per second.

Also, let

$$\frac{e}{m} \cdot E = A,$$

$$\frac{e}{m} \cdot E_{dc} = B.$$

Then, rewriting,

$$\dot{x} = A \sin \omega t,$$

$$\ddot{y} = B.$$

Also, let t_o be the time when the electron leaves the surface.

The solutions to these equations are:

$$x = \frac{-A}{\omega^2} [\sin \omega t - \sin \omega t_o] + \frac{A}{\omega^2} \cos \omega t_o [\omega t - \omega t_o] + v_{ox} (t - t_o),$$

$$y = \frac{-B}{2} (t - t_o)^2 + v_{oy} (t - t_o),$$

giving the displacements at time t, and

$$\frac{dx}{dt} = \frac{-A}{\omega} (\cos \omega t - \cos \omega t_o) + v_{ox}$$

$$\frac{dy}{dt} = B (t - t_o) + v_{oy}$$

giving the velocities.

Maximum velocity in the x direction occurs when

$\omega t = \pi\ (2n + 1)$, where n is any integer, and $\cos \omega t_o = 1$,

giving:

$$v_{x\ max} = 2 \frac{e}{m} \frac{E}{\omega} + v_{ox}$$

This may be expressed in electron volts V by using the following formula:

$$eV = \frac{1}{2} m v^2$$

In the practical case where the initial velocity of the electron is small compared to its final velocities, the following equation gives a very close approximation to $V_{x\ max}$

$$V_{x\ max} = 2 \frac{e}{m} \left(\frac{E}{\omega}\right)^2$$

In terms of f, rather than ω, this becomes, numerically,

$$V_{x_{max}} = 8.88 \times 10^{13} \left(\frac{E_p}{f}\right)^2 \quad \text{volts}$$

where E_p is in volts per cm.

where f is in cycles per second.

APPENDIX II

Analysis of the Window Cavity

The field equations in the dielectric-loaded cavity of Fig. 11 may be written in the following form:

For the vacuum section:

$$H_z = A\, J_1 (kr) \cos \phi \sin \beta_1 z \qquad A\ 1$$

$$E_r = j \frac{\omega\mu}{rk^2} A\, J_1 (kr) \sin \phi \sin \beta_1 z \qquad A\ 2$$

$$E_\phi = j \frac{\omega\mu}{k} A\, J_1' (kr) \cos \phi \sin \beta_1 z \qquad A\ 3$$

$$H_\phi = \frac{-\beta_1}{rk^2} A\, J_1 (kr) \sin \phi \cos \beta_1 z \qquad A\ 4$$

$$H_r = \frac{+\beta_1}{k} A\, J_1' (kr) \cos \phi \cos \beta_1 z \qquad A\ 5$$

For the dielectric section:

$$H_z = A\, J_1 (kr) \cos \phi \cos \beta_2 y \qquad A\ 6$$

$$E_r = j \frac{\omega\mu}{rk^2} A\, J_1 (kr) \sin \phi \cos \beta_2 y \qquad A\ 7$$

$$E_\phi = j \frac{\omega\mu}{k} A\, J_1' (kr) \cos \phi \cos \beta_2 y \qquad A\ 8$$

$$H_\phi = \frac{-\beta_2}{rk^2} A\, J_1 (kr) \sin \phi \sin \beta_2 y \qquad A\ 9$$

$$H_r = \frac{+\beta_2}{k} A\, J_1' (kr) \cos \phi \sin \beta_2 y \qquad A\ 10$$

where $k = \frac{1.84}{a}$

where a is radius of guide

For TE modes the boundary condition requires that the normal derivaties of H_z be zero at all conducting walls, hence, $J_1'(ka) = 0$. For the required field pattern ka is given by the first root. The propagation constant β is then obtained from $\beta^2 = \omega^2 \mu\epsilon - k^2$.

At the vacuum-dielectric boundary tangential components of E and H must be continuous. By equating these quantities the following equation is obtained which gives the conditions for resonance:

$$\beta_2 \tan \beta_1 p = -\beta_1 \cot \beta_2 q \qquad \text{A 11}$$

Stored energy in the dielectric-loaded cavity

A general expression for stored energy is given in equation 9, Sec. 4.3.5. For the particular TE_{111} mode cavity under consideration this becomes:

$$U = \frac{\epsilon}{2} \int_0^L \int_0^{2\pi} \int_0^a \left| E_r^2 + E_\phi^2 \right| \; r \; dr \; d\phi \; dz \qquad \text{A 12}$$

where E_r and E_ϕ are given by equation 2 and 3 respectively in the vacuum sections, and by equations 7 and 8 respectively in the dielectric sections. Thus for the E_r component:

$$U_r = \frac{\epsilon}{2} \int_0^L \int_0^{2\pi} \int_0^a \left[\frac{\omega\mu}{k^2} A \frac{J_1(kr)}{r} \sin \phi \sin \beta_z \right]^2 r \; dr \; d\phi \; dz \qquad \text{A 13}$$

Performing the integration,
the total stored energy due to the E_r component is:

A 14

$$U_r = \frac{\varepsilon_o \omega^2 \mu^2 \pi}{k^4} A^2 C \left[\left(\frac{p}{2} - \frac{\sin 2\beta_1 p}{4\beta_1} \right) + \varepsilon_r \left(\frac{q}{2} + \frac{\sin 2\beta_2 q}{4\beta_2} \right) \right]$$

where $$C = \int_o^a \frac{J_1^2 (kr)}{r} dr$$

Repeating for the E_ϕ component gives the following expression:

A 15

$$U_\phi = \frac{\varepsilon_o \omega^2 \mu^2 \pi}{k^2} A^2 D \left[\left(\frac{p}{2} - \frac{\sin 2\beta_1 p}{4\beta_1} \right) + \varepsilon_r \left(\frac{q}{2} + \frac{\sin 2\beta_2 q}{4\beta_2} \right) \right]$$

where $$D = \int_o^a r \left[J_1' (kr) \right]^2 dr$$ A 16

The total stored energy is given by the sum of U_r and U_ϕ.

Power Dissipated in the Cavity

End Walls

The expression for the power loss in one end wall of the cavity is:

$$P_{end} = R_s \int_o^{2\pi} \int_o^a \left| H_\phi (z = o) \right|^2 + H_r \left| (z = o) \right|^2 r \, dr \, d\phi$$

where H_ϕ is given by equation 4 and H_r by equation 5.

Evaluating the integral we have for the H_ϕ component:

$$\frac{R_s}{2} \frac{\beta_1^2}{k^4} \pi A^2 C$$

and for the H_r component

$$\frac{R_s}{2} \frac{\beta_1^2}{k^2} \pi A^2 D$$

The total end wall loss is

$$P_{end} = \frac{R_s \beta_1^2}{k^2} \pi A^2 \left[\frac{C}{k^2} + D \right]$$

Side Walls

The expression for the power loss in the side walls of the cavity is:

$$P_{side} = R_s \int_0^L \int_0^{2\pi} \left| H_\phi (r = a) \right|^2 + \left| H_z (r = a) \right|^2 d\phi \, dz$$

H_ϕ is given by equations 4 (vacuum section) and 9 (dielectric section) and H_z by equations 1 (vacuum section and 6 (dielectric section). Evaluation of the integral gives the following:

One vacuum section

H_ϕ component $\frac{R_s}{2} \frac{\beta_1^2 \pi A^2}{k^4} \left(\frac{J_1 (ka)}{a}\right)^2 \left[\frac{p}{2} + \frac{\sin 2 \beta_1 p}{4\beta_1}\right]$

H_z component $\frac{R_s}{2} \pi A^2 J_1^2 (ka) \left[\frac{p}{2} - \frac{\sin 2 \beta_1 p}{4\beta_1}\right]$

1/2 dielectric section

H_ϕ component $\frac{R_s}{2} \frac{\beta_2^2 \pi A^2}{k^4} \left(\frac{J_1 (ka)}{a}\right)^2 \left[\frac{q}{2} - \frac{\sin 2\beta_2 q}{4\beta_2}\right]$

H_z component $\frac{R_s}{2} \pi A^2 J_1^2 (ka) \left[\frac{q}{2} + \frac{\sin 2\beta_2 q}{4\beta_2}\right]$

The total side wall loss is the sum of the losses due to each component give above.

Dielectric loss

The dielectric loss is given by the following integral:

$$P_{dielectric} = \int_{vol.} \frac{\sigma E^2 \, dv}{2}$$

where σ is the volume resistivity. Since $\sigma = \omega \varepsilon \tan \delta$ we can write

$$P_{dielectric} = \omega \tan \delta \int_{vol.} \frac{\varepsilon E^2}{2}$$

$$= \omega \tan\delta \text{ x stored energy in dielectric.}$$

APPENDIX III

Effects Of Power Flow On Electron Behavior

Let v be the instantaneous velocity in the direction perpendicular to the propagation of an electromagnetic wave obtained by an electron from the field. Since the corresponding kinetic energy is supplied by the propagating wave, this amount of electromagnetic energy is missing from the wave. Expressed in terms of the electron mass m, the equivalent mass of the missing energy is $mv^2/2c^2$ (for non-relativistic electron velocities). But in this exchange process not only the energy is conserved but also the momentum attached to this energy. The electromagnetic energy absorbed by the electron has the above-mentioned mass

$$\frac{m \quad v^2}{2 \quad c^2}$$

and the velocity of the energy propagation of the wave, which is c for a planar wave and the group velocity

$$c.\frac{\lambda}{\lambda_g}$$

in a waveguide wave (λ is the free space wavelength and λ_g the guide wavelength). The momentum of the wave, mass x velocity, must equal the forward momentum of the electron:

$$\frac{m\ v^2}{2\ c^2} .c\ \frac{\lambda}{\lambda_g} = m\ v_f \qquad (1)$$

where v_f is the forward component of the electron velocity. We obtain for the forward velocity of the electron:

$$v_f = \frac{v^2}{2c} \cdot \frac{\lambda}{\lambda_g} \quad \text{or} \quad v_f = v \frac{\beta}{2} \cdot \frac{\lambda}{\lambda_g} \quad \text{with} \quad \beta = \frac{v}{c}$$

For the free space wave $\frac{\lambda}{\lambda_g}$ becomes one and disappears out of the equations.

If we express the kinetic energy of the electron in direction of the field in electron volts as Ue, and the kinetic energy in the forward direction as $U_f e$ we obtain the following:

$$\frac{m v_f^2}{2} = U_f e = \frac{m v^2}{2} \cdot \left(\frac{v \lambda}{2c \lambda_g}\right)^2 = Ue \cdot \left(\frac{v \lambda}{2c \lambda_g}\right)^2 \qquad (2)$$

$$\text{or } U_f = U\left(\frac{v \lambda}{2c \lambda_g}\right)^2 = U\left(\frac{\beta \lambda}{2 \lambda_g}\right)^2$$

$$\text{since } U = \frac{m v^2}{2 e} \; ; \; v^2 = U \frac{2 e}{m}$$

$$U_f = U^2 \frac{}{2 mc^2} \left(\frac{\lambda}{\lambda_g}\right)^2 \qquad (3)$$

for $e = 1.602 \times 10^{-12}$ erg. V^{-1}

$m = 9.107 \times 10^{-28}$ g

$c = 2.998 \times 10^{10}$ cm sec^{-1}

$$U_f = 9.7795 \times 10^{-7} \, U^2 \left(\frac{\lambda}{\lambda_g}\right)^2$$

It can be seen that the forward energy of the electron in electron volts is proportional to the square of the electron energy in the direction of the E field. This relation is of course valid for any moment during the oscillating cycle, because the law of conservation of energy and momentum is valid at any moment. Fig. 19 shows, in the bottom row, electron velocities in the E field direction for electrons released at different phase angles and therefore having different mean dc velocities added to the ac velocity. The phase angles at the time of release of the electrons are given. These were chosen to yield dc velocity rises in five equal steps from picture to picture. The resulting forward velocities are shown in the top row.

We reccgnize the frequency doubling effect in v_f due to the square relationship in the first case and we see that more of the fundamental frequency gets mixed in, as the dc velocity in the bottom row grows, until finally the mixed-in fundamental has reached twice the amplitude of the second harmonic, which remains constant in amplitude through all the pictures. The peak forward velocity at 0° phase angle is four times that for 90°, with all intermediate values possible, which means energy-wise a factor of sixteen. Similar electron motions have been computed by D. Churchill using an analogue computer. (3)

If we consider the possible sources of electrons which may move down a waveguide and arrive at a window, we conclude that field-emitted electrons from the waveguide walls will probably be most prevalent. We shall therefore consider the conditions under which such electrons are most likely to be released, that is to say, at the time when the transverse electric field is a maximum. These electrons will tend to travel down the waveguide since they acquire no net dc transverse velocity across the guide. Secondary electrons on the other hand, conceivably released by multipactor at the time of zero electric field, will tend to cross the waveguide quite rapidly and therefore are less likely to reach the window.

---

(3) Sperry Gyroscope Co., Electron Tube Div., Great Neck, N. Y. "Investigation of Microwave Window Failure Mechanisms and Their Elimination" - Second Quarterly Progress Report, U.S. Army Signal Research and Development Lab., Fort Monmouth, Contract No. DA-36-039 SC-78314, covering period 1 Sept. 1959 - 1 December 1959, prepared by D. Churchill.

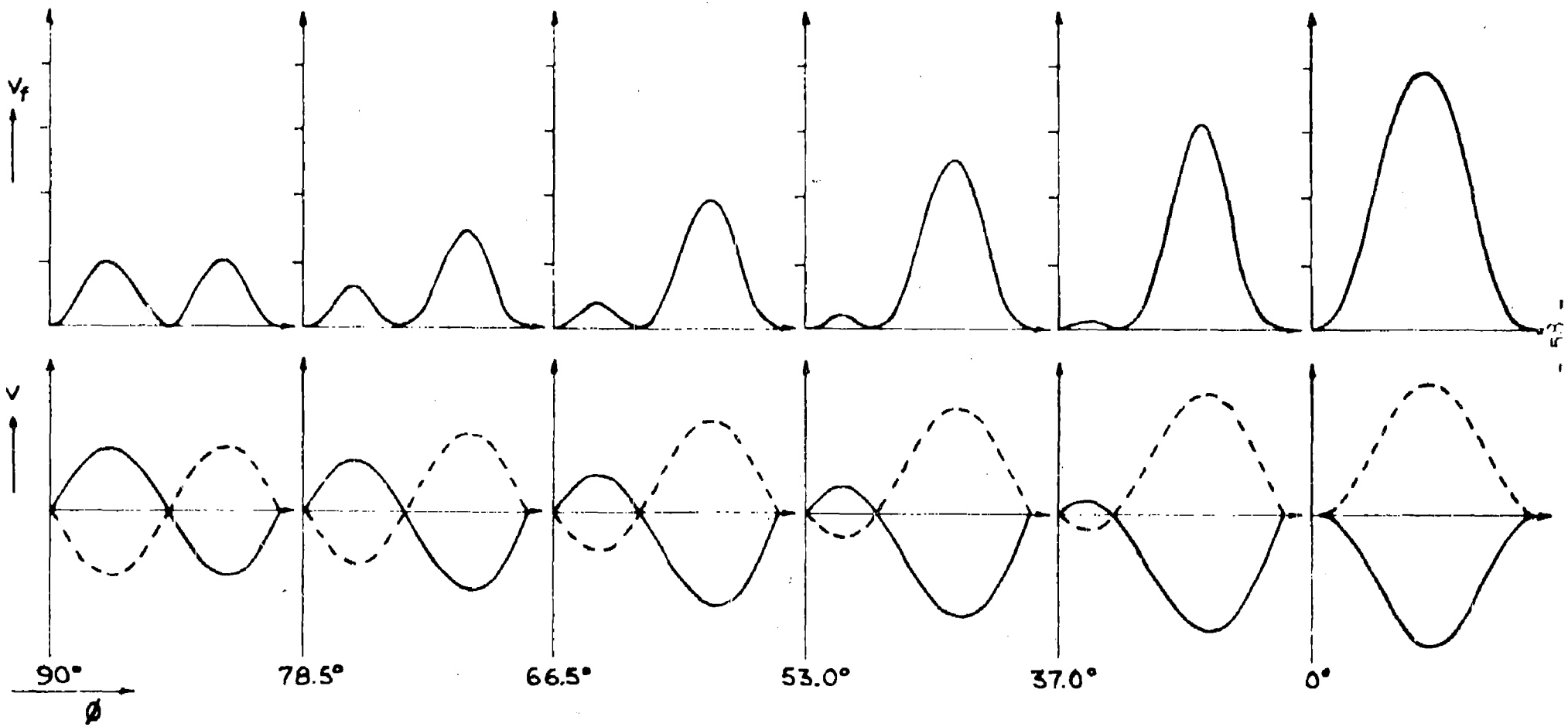

Fig. A III.1

The energy U of the oscillating electron is proportional to the square of the electric field and for that reason U_f, the forward energy, goes up as the fourth power of the electric field. The peak energy U of an electron oscillating without dc velocity released at the time of peak electric field, $\phi = 90°$, in a high frequency field with a peak value of E_p is:

$$U = \frac{e}{2m} \left(\frac{E_p}{\omega} \right)^2 \qquad (4)$$

This formula is obtained by looking at the momentum m v given to the electron during a quarter of a cycle which equals the average force acting on the electron $e E_f \cdot \frac{2}{\pi}$ multiplied by the time

$$\frac{1}{4f} = \frac{2\pi}{4\omega} .$$

$$\frac{eE_p}{\pi} \cdot \frac{2}{\pi} \cdot \frac{2\pi}{4\omega} = \frac{eE_p}{\omega} = m\ v$$

The energy of the electron is:

$$\frac{\text{Momentum}^2}{2\ m} = U\ e = \left(\frac{eE_p}{\omega} \right)^2 \frac{1}{2\ m} \qquad (5)$$

giving:

$$U = \frac{e}{2m} \left(\frac{E_p}{\omega} \right)^2 \qquad (6)$$

In units: Volt, cm, sec this becomes numerically:

$$U = 8.790 \times 10^{14} \left(\frac{E_p}{\omega} \right)^2$$

$$U = 2.2265 \times 10^{13} \left(\frac{E_p}{f} \right)^2$$

For the peak forward equivalent volts of the electron we obtain, by combining equations (3) and (6):

$$U_f = \left(\frac{e}{2m} \right)^3 \frac{1}{c^2} \left(\frac{E_p}{\omega} \right)^4 \left(\frac{\lambda}{\lambda_g} \right)^2$$

and numerically:

$$U_f = 7.570 \times 10^{23} \left(\frac{E_p}{\omega} \right)^4 \left(\frac{\lambda}{\lambda_g} \right)^2$$

or

$$U_f = 4.857 \times 10^{20} \left(\frac{E_p}{f} \right)^4 \left(\frac{\lambda}{\lambda_g} \right)^2$$

where f is in cycles per second.

In order to give an idea of the magnitude of this effect, some numerical values, closely related to our experimental conditions, are given in Table I

TABLE A.III.1

85 Megawatts Through A Window Area of 45.6 cm^2
(3" diameter round window)

	Free Planar Wave	Round Waveguide(TE_{11}) *
Wavelength	λ 10.5 cm	λ_g 17.78 cm
Peak-E-Field on Axis	26700. Volt/cm	70600.
Peak-H-Field on Axis	89. Gauss	172.3 Gauss *
For an Electron Liberated at Peak of E-Field:		
Max e.V in direction of E	1946. eV	13606. eV
Max e.V perpendicular to E (Radiation Pressure)	3.62 eV	63.25 eV
Amplitude (peak-to-peak)	0.292 cm	0.773 cm
Peak β of electron	8.72%	23.06%
For an Electron Liberated at Zero E-Field:		
Max e.V in direction of E	7796. eV	54600. eV
Max e.V perpendicular to E	58.2 eV	1012. eV
Distance Travelled per half cycle	0.325 cm	0.861 cm
Peak β of Electron	17.45%	46.7%

* Assumes travelling wave in matched waveguide.

The first column shows a planar wave carrying an energy of 85 megawatts per 45.6 cm^2 which is the area of a 3-inch window. The second column represents the values in a round 3-inch waveguide TE_{11} mode. The window is assumed to be thin having no standing wave energy surrounding it. For a resonant window having a Q of about three and sitting in the middle of the window box, the forward energies have to be multiplied by Q to give the real values. To understand this we have to look at the peak E-field, which is greater by the factor Q, whereas the peak H-field retains its old value, because the standing wave has no magnetic field in the middle of the cavity. The oscillating energy of the electron is greater by the factor three. However, since the magnetic deflection of the electron into the forward direction results from an H-field, which is not increased, the forward energy increases in this case only proportional to the oscillating energy, that is, by the factor three. We have up to this case, always intentionally ignored the magnetic field deflection which is, of course, responsible for all forward motions and we have used the simpler law of conservation of momentum. But we can also look in the last case only at the momentum transfer and get the right answer. The presence of the standing wave energy in the window box reduces locally the group velocity of the propagating wave. The energy transport velocity is smaller. For the same power flux this means an increased momentum of the electro-magnetic wave. The standing wave energy in the window box is longitudinal. But going from the planar wave to the waveguide wave we also add some standing wave energy in the transverse direction, which is responsible for the reduced group velocity in the waveguide. It is known that the waveguide wave can be understood as two planar waves cutting the guide axis at the angle α where $\cos \alpha = \frac{\lambda}{\lambda_g}$. The electric fields of the two waves add directly to the axis, whereas the magnetic fields combine vectorially to a field value reduced by the factor $\cos \alpha$ or $\frac{\lambda}{\lambda_g}$. The overbalance

of the electric field over the magnetic field stems from the standing wave energy, which in this case is transverse to the waveguide, but has the same effect as the longitudinal standing wave in the window box. We obtain the same forward effect on the electrons either looking at the momentum connected with the group velocity or at the unbalance of electric and magnetic field. The factor in both cases is $\frac{\lambda_g}{\lambda}$. The values in Table I are non-relativistic. Only for the rather energetic electrons in the waveguide released at zero E-field does the relativistic effect make a small difference. All the electron energies given for the waveguide case are by a factor Q bigger in the window box. Q is about 3 for the alumina windows and considerably less for silica windows. The forward effects on electrons grow very rapidly with energy and relativistic treatment becomes necessary. Very roughly we can say, an electron which would receive 511 kV energy, that is the relativistic energy-equivalent of the electronic mass, would have forward energies comparable to transverse energies, because the momentum of the radiation absorbed by the electron and the momentum of the electron become the same.

The conclusion can be drawn that the radiation pressure effect on electrons can be neglected at low powers, but becomes appreciable at higher power levels, and can affect the nature and magnitude of the multipactor discharge. On output windows, it tends to suppress and on input windows it tends to favor multipactor. Electrons get lifted off the window surface by this effect on the input window and carried back by the dc charge field of the surface, which is always stronger than the radiation effect. Electrons have, during that time a chance to pick up oscillating energy from the field to effectively knock out new secondaries. On the output window the radiation pressure plus the dc field tend to bring electrons back rather quickly.

(O. Heil)

APPENDIX IV

Sample Calculations Of Equivalent Transmitted Power In Resonant Cavity

From measurements of power dissipated in the cavity, and Q measurements, the equivalent transmitted power may be calculated by two methods.

Using Method (1)

The unloaded Q of the resonant cavity is measured. (Q_2). A similar cavity, when inserted in a waveguide terminated in a matched load, will have a Q which will be called Q_1. The two situations are represented graphically in Fig. A.IV.1.

Both cavities are assumed to be matched at this resonant frequency in what follows.

The parameter $\frac{R}{Q}$ has been used for the two cases. This factor, relating impedance to stored energy, depends only on geometry.

Consider the first case (transmitting power). We can speak of an equivalent voltage V_1 effective between the two points A and B at opposite sides of the window and in the plane of the E vector. (TE_{111} mode assumed). We can also imagine an $\frac{R}{Q}$ value and a shunt impedance R, also referred to A and B.

We can write:

$$P_{T_1} + P_{d_1} = \frac{V_1^2}{R_1}$$

$$= \frac{K.\ E_1^2}{\frac{R}{Q}\ Q_1} \qquad \text{A.IV.(1)}$$

where P_{T_1} is power transmitted to load

" P_d is power dissipated in cavity

" k is a constant relating E to V.

Consider now the second case. Here all the power is absorbed in the cavity losses. We can write:

$$P_{d_2} = \frac{V_2^2}{R_2}$$

$$= \frac{KE_2^2}{\frac{R}{Q} \cdot Q_2} \qquad \text{A.IV.(2)}$$

If we assume $\frac{R}{Q}$ and K to be the same in both cases, we can combine equations (1) and (2) to give:

$$\frac{P_{T_1} + P_{d_1}}{P_{d_2}} = \left(\frac{E_1}{E_2}\right)^2 \cdot \frac{Q_2}{Q_1} \qquad \text{A.IV.(3)}$$

For the same field strength at the window in both cases, $P_{d_1} = P_{d_2}$ and

$$\frac{P_{T_1}}{P_{d_2}} = \frac{Q_2}{Q_1} - 1 \qquad \text{A.IV.(4)}$$

Since P_{d_2} can be measured, either by a directional coupler or calorimetrically, and Q_2 and Q_1 can be measured on a cold test bench, P_{T_1} can be calculated.

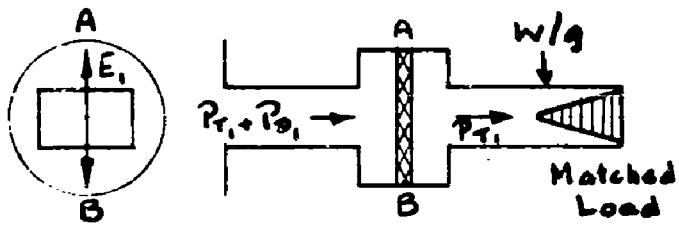

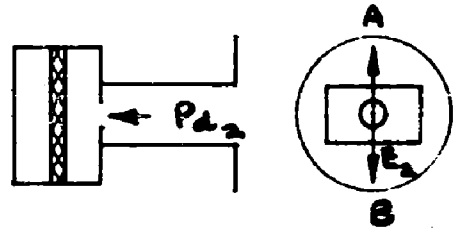

Q_1	Q_2
$\frac{R}{Q}$	$\frac{R}{Q}$
E_1	E_2
V_1	V_2
P_{T_1}	P_{d_2}
P_{d_1}	

Window transmitting power P_{T_1} and absorbing power P_{d_1}.

Window absorbing power P_{d_2}.

Fig. A.IV.1.

We note that $\frac{R}{Q}$ was assumed to be the same in the two cases. This is not strictly true, because in case 1 the coupling irises between the cavity and the waveguide will be larger than in case 2, and therefore the geometry is different and the calculation is to this extent approximate.

Method (2)

In Appendix II, and also in Section 4.3.5 a relationship between window field strength and total cavity loss has been derived:

$$P_{diss} = \frac{\omega U}{Q_o} = \frac{\omega}{Q_o} \int_{vol.} \frac{\varepsilon}{2} E^2 \, dv \qquad \text{A.IV.(5)}$$

Since the total cavity loss can be measured directly, and so can ω, and Q_o, the stored energy $\int \frac{\varepsilon}{2} E^2 \, dv$ may be computed for a given P_d.

From Appendix II the stored energy may also be calculated in terms of E^*, the maximum electric field at the window surface. Therefore E^* may be calculated for a given measured value of P_{diss}.

To obtain the equivalent power transmitted we may now assume the window to be in a round waveguide, matched to a load at one end. If the window did not perturb the waveguide fields, we could write:

$$P_T = 1.99 \times 10^{-3} \sqrt{1 - \left(\frac{\lambda}{3.41a}\right)^2} \, a^2 E^{2\,*} \qquad \text{A.IV.(6)}$$

---

* The most useful reference for this equation has been found to be "The Relative Power-Carrying Capacity of High Frequency Waveguides", by H. M. Barlow, Proceedings of the IEE, Part 3, Vol. 99, No. 57, January 1952.

Where a is guide radius in cm.

Where E is peak electric field strength, in volts/cm.

Where P_T is power flow in watts.

(This is equation (3), page 16)

Therefore for the value of E calculated from equation (5) above, we may calculate a corresponding value of P_T.

We note that this will be accurate only when the window does not perturb the waveguide, which will be true only for a window of infinitesimal thickness, if ϵ is greater than unity. This calculation is therefore approximate when used with a real window.

A sample calculation

For a typical non-multipactoring coated window the following results were obtained: (Window No. TU 49, from 7th Quarterly Progress Report, Fig. 6, page 7b, Coors BD 96 Beryllia Window with evaporated titanium coating).

Average power dissipated in window box	100 watts
duty cycle	10^{-2}
Peak power dissipated	10 kilowatts
Q_2	1100
Q_1	3

From method (1) above, equation (4):

$$P_{T_1} = P_{d_2}\left(\frac{Q_2}{Q_1} - 1\right)$$

$$= 10 \text{ kw} \times \frac{1099}{3}$$

$$= \underline{3.66 \text{ MW}}$$

Using Method (2)

To calculate the stored energy in the cavity in terms of the maximum electric field strength at the window we proceed as follows:

From Appendix II, equations A 14 and A 15, using the following values for the constants:

$\epsilon_o = 8.85 \times 10^{-12}$ farads per meter

$\omega = 2\pi \times 2.7 \times 10^{9}$ c.p.s.

$\mu = 1.26 \times 10^{-6}$ henrys per meter

$k = \frac{1.84}{a}$

$a = 4.7 \times 10^{-2}$ meters

$p = 1.62 \times 10^{-2}$ meters

$q = 2.54 \times 10^{-3}$ meters

$\epsilon_r = 6.65$ (for BeO)

$\beta_1 = 40.8$

and performing the numerical integrations for the factors C and D, which become

$$C = \int_o^a \frac{1}{r} J_1^2 (kr)\, dr = 0.2817$$

$$D = \int_o^a r \left(J_1' (kr)\right)^2 dr = \int_o^a \frac{r}{k^2} \left[\frac{d}{dr}\left(J_1 (kr)\right)\right]^2 dr$$

$$= 0.1226/k^2$$

$$= .7977 \times 10^{-4}$$

We arrive at the following numerical values for stored energy, in terms of the field amplitude factor A in the equations A II (1-10):

$$U_r \text{ (air)} = 3.26 \times 10^{-12} \quad A^2$$

$$U_r \text{ (dielectric} = 20.65 \times 10^{-12} \quad A^2$$

$$U_\phi \text{ (air)} = 1.42 \times 10^{-12} \quad A^2$$

$$U_\phi \text{ (dielectric} = 9.00 \times 10^{-12} \quad A^2$$

$$\text{Total stored energy} = 34.33 \times 10^{-12} \quad A^2 = U_{total}$$

We wish to know this quantity in terms of the maximum electric field at the window, given by equation A II 2, putting $\phi = \frac{\pi}{2}$.

We will denote this field strength by E^*.

$$E^* = 170.0\ A \quad \text{(from Appendix II, Equation (1))}$$

Therefore $U_{total} = 1.183 \times 10^{-15}\ E^{*2}$

We now use the relationship

$$Q_o = \frac{\omega U_{total}}{P_{diss}}$$

to obtain U_{total} in terms of P_{diss} (measured) and Q_o ($Q \times Q_L$, measured).

For the case discussed, Q_o was 2200 and P_{diss} was 10^4 watts.

This gives $U_{total} = 1.3 \times 10^{-3}$.

Hence $E^{*2} = 1.1 \times 10^{12}$

and $E^{*} = 1.05 \times 10^{6}$ v/meter

$= 1.05 \times 10^{4}$ v/cm.

Also, $\frac{E^{*2}}{P_{diss}} = \frac{1.1 \times 10^{8}}{10^{4}} = 1.1 \times 10^{4}$ $(v/cm)^2$ per watt

If this field strength existed in a matched circular waveguide of 4.7 cm radius carrying the $TE_{1,1}$ mode at 2700 Mc, the corresponding power transmitted would be (from equation A.IV.(6))

$$P_T^* = 3.15 \times 10^{-2} E^{*2}$$

$$= 3.15 \times 10^{-2} \times 1.1 \times 10^{8} \text{ (in cm. units)}$$

$$= 3.47 \times 10^{6} \text{ watts}$$

We can refer to this as the "equivalent transmitted power" corresponding to the field strength E^* at the window surface.

Minimum Power Level for Multipactor

It is of interest to calculate the equivalent transmitted power corresponding to the critical field strength at which multipactor begins. This is related to the secondary emission characteristic of the dielectric, and particularly to the lowest value of primary electron energy required to release one secondary electron per primary ($\delta = 1$). See Section 4.2.2, page 9.

The mean of several measurements gave a typical value of P_{diss} at the threshold of multipactor, when encouraged by magnetic fields (which cannot accelerate electrons and therefore cannot reduce the electric field required for multipactor) of 0.4 kw. Using the relationship above for $\frac{E^{*2}}{P_{diss}}$

We find $E^{*2} = 1.1 \times 10^4 \times 400$

and $E = 2.1$ kv/cm

The corresponding equivalent transmitted power is 138 kw.

We note that for a window scaled linearly in dimensions with wavelength, this "threshold power level" for the onset of multipactor will remain the same for all wavelengths. This is the minimum peak power level at which the gliding single-surface can be expected with an uncoated Alumina or Beryllia window. In practice, it has been found that the actual threshold power level is often greater than this, probably due to the presence of thin films of substances on the window surface, such as decomposed diffusion pump oil, which may fortuitously reduce the secondary emission, albeit in an unpredictable manner.

(D. Preist)

APPENDIX V

Procedure For The Coating of Waveguide Windows by Evaporating Titanium in Vacuum

1.0 OBJECTIVE

This specification standardizes the procedure for coating the vacuum side of waveguide windows used in high-power microwave tubes.

2.0 REFERENCES

The following procedures form part of this specification:

Chemical Cleaning Procedure "E"
Ceramic Assembly cleaning procedure
Chemical Cleaning Procedure "P"
Titanium cleaning procedure
Chemical Cleaning Procedure "R"
Ceramic window assembly cleaning procedure

3.0 APPLICABILITY

The coating is used for the suppression of multipactor at microwave windows. The use of the coating is recommended for the windows of high-power microwave tubes operating at peak power levels above 100 kW.

4.0 MATERIALS

The materials required are included in Section 5 (Equipment), and in the appropriate chemical cleaning specifications.

5.0 EQUIPMENT

The following equipment is required for the coating process:

5.1 Vacuum evaporator station - Veeco VE 400 or equivalent.

5.2 Filament. Standard titanium getter wound as used on Eimac High-Power Klystrons. See Eimac drawing No. 106217.

5.3 Surface resistivity monitor. This should be a rectangular bar about 2" x 1/4" x 1/8" made of the same material as is the window to be coated. The ends of the bar should be metalized for about 1/4" on one face.

5.4 Megohmeter. General Radio, D-C Amplifier and Electrometer Type 1230-A or equivalent instrument for the measurement of high resistance.

6.0 PROCEDURE

6.1 The window or window assembly should be thoroughly cleaned before a coating is applied. The appropriate chemical cleaning procedures should be used where necessary. Procedure "E" is used for plain ceramic windows. Procedure "R" is used for window assemblies and Procedure "P" for cleaning windows which have been previously coated with titanium. Windows which have been clean-fired or brazed into assemblies will generally not require further cleaning if standard tube cleanliness precautions have been observed.

Windows and monitors should be handled with cotton gloves during assembly in the vacuum chamber to avoid contamination of the surfaces.

6.2 Connect the filament. For most work the filament wire is bent to a U-shape and the ends tied to the heater terminals on the vacuum chamber base-plate (see Fig. 1). In certain cases (e.g., for coating ceramic cylinders) a single filament is required with connections at the top and bottom (see Fig. 2).

6.3 Prior to coating, the filament should be pre-heated for cleaning purposes and to ensure that the titanium is heated evenly. Pump the vacuum chamber to a pressure below 10^{-6} Torr and heat the filament to the evaporating temperature by slowly increasing the filament current to 55 amperes. Hold for 1 minute, turn off filament supply, allow filament to cool for at least 30 minutes before admitting air to the vacuum chamber. If uneven heating of the titanium wire results in beading, the filament should be discarded. Once a filament has been processed in this way it is suitable for several evaporations.

6.4 Place the window to be coated in the vacuum chamber facing the filament. The window should be located centrally with respect to the filament (see Fig. 1) and spaced from the filament a distance greater than twice the window diameter. In cases where the window is partly shielded by the containing waveguide it may be necessary to modify the arrangement. An example is the pill-box window shown in Fig. 2. In this case a single element filament is employed and the structure placed so that the filament is in direct "line of sight" to all points on the window surface.

Parts of the containing waveguide which will be subsequently sealed (e.g., heliarc joints) should be shielded from the filament with a metal mask.

6.5 Place the surface resistivity monitor either next to the window or on the opposite side of the filament (positions A or B in Fig. 1, position C in Fig. 2). The monitor should be the same distance from the filament as is the window to be coated and should be exposed to the same portion of filament. If necessary, parts of the filament should be screened from the monitor as shown in Fig. 2.

6.6 Close the vacuum chamber and pump to a pressure better than 10^{-6} Torr. Liquid nitrogen must be used. Slowly increase the filament voltage until

the evaporating temperature is reached. As the filament is heated the pressure will increase and should be about 10^{-5} Torr during evaporation. If the pressure rises above this value the filament should be outgassed below the evaporating temperature. Evaporation is indicated by a steady decrease in the monitor resistance measured by the Megohmeter, the process is continued until a surface resistivity in the range 10^{7} to 10^{6} ohms/square is obtained.* The rate of evaporation will depend on the filament temperature on the filament temperature which should be adjusted for a total evaporation time of 1-2 minutes. The system should be allowed to cool for at least 30 minutes before admitting air. During this cooling period the monitor resistance will increase; this is a normal occurrence.

6.7 The window should be coated just before tube assembly and processing. If storage is necessary, the coated window should be placed in a plastic bag to protect the coating.

* Note: The surface resistivity of a coating is defined as the resistance of any square area of coated surface. It is independent of the size of the square. If the monitor is of the size specified in section 5 the resistance measured must be divided by 6 to obtain the equivalent surface resistivity in ohms/per square.

CHEMICAL CLEANING PROCEDURE "P"

Titanium Cleaning Procedure

This procedure pertains to chemical cleaning of all titanium component parts such as cylinders, sheets and disks. It can also be used to remove titanium films from ceramic surfaces.

A. EQUIPMENT

1. Suitable pyrex or polypropylene container

2. Titanium cleaning solution consisting of:

a.	Deionized water	890 mls	89 parts by volume
b.	Nitric acid	100 mls	10 parts by volume
c.	Hydrofluoric acid	10 mls	1 part by volume

3. Ammonium hydroxide solution consisting of:

a.	Deionized water	1000 mls	100 parts by volume
b.	Ammonium hydroxide	150 mls	15 parts by volume

B. PROCEDURE

1.	Degrease procedure "J"		
2.	Versene clean	140°F (60°C)	5 minutes
3.	Tap water rinse	140°F (60°C)	5 dips
4.	Immerse in titanium cleaning solution room temperature		2 minutes
5.	Tap water rinse - cold		5 dips
6.	Ammonium hydroxide dip - cold		10 seconds
7.	Tap water rinse - cold		5 dips
8.	Tap water rinse - cold		5 dips
9.	Deionized water rinse	140°F (60°C)	5 dips
10.	Deionized water rinse	140°F (60°C)	10 seconds
11.	Forced air dry		
12.	Cool and bag		

CHEMICAL CLEANING PROCEDURE "R"

Ceramic Window Assembly Cleaning Procedure

This procedure pertains to cleaning ceramic window assembly #173190 and similar assemblies, prior to incorporation into tubes. The component parts of this assembly are copper, ceramic and nickel.

A. EQUIPMENT:

1. Ultrasonic cleaner - bench type model.
2. Two 4000 ml beakers - or suitable pyrex or polypropylene container.
3. Freon TF cleaner - DuPont Company

B. PROCEDURE

1.	Ultrasonic Freon TF degrease		1 minute
2.	Scrub ceramic surfaces with alumina (Nortons 150 grit alundum)		
3.	Versene clean	140°F (60°C)	5 minutes
4.	Tap water rinse	140°F (60°C)	5 dips
5.	Tap water rinse - cold		5 dips
6.	Ammonium citrate clean	140°F (60°C)	5 minutes
7.	Tap water rinse - cold		5 dips
8.	Deionized water rinse - cold		5 dips
9.	Deionized water rinse	140°F (60°C)	5 dips
10.	Deionized water rinse	140°F (60°C)	10 seconds
11.	Forced air dry		
12.	Cool and bag		

CHEMICAL CLEANING PROCEDURE "E"

Ceramic Assembly Cleaning Procedure

This procedure pertains to cleaning ceramic assemblies prior to incorporation into tubes. Ceramic assemblies consist of ceramic parts attached to copper, copper nickel and nickel seal rings. Stubborn oxides on rings can be removed by Chemical Cleaning Procedure "R".

PROCEDURE

1.	Scrub ceramic surfaces with alumina (Norton's 150 grit alundum).		
2.	Spray rinse - tap water - cold		
3.	Versene clean	140°F (60°C)	5 minutes
4.	Tap water rinse	140°F (60°C)	5 dips
5.	Tap water rinse - cold		5 dips
6.	Deionized water rinse - cold		5 dips
7.	Deionized water rinse	140°F (60°C)	5 dips
8.	Deionized water rinse	140°F (60°C)	20 seconds
9.	Forced air dry		
10.	Cool and bag		

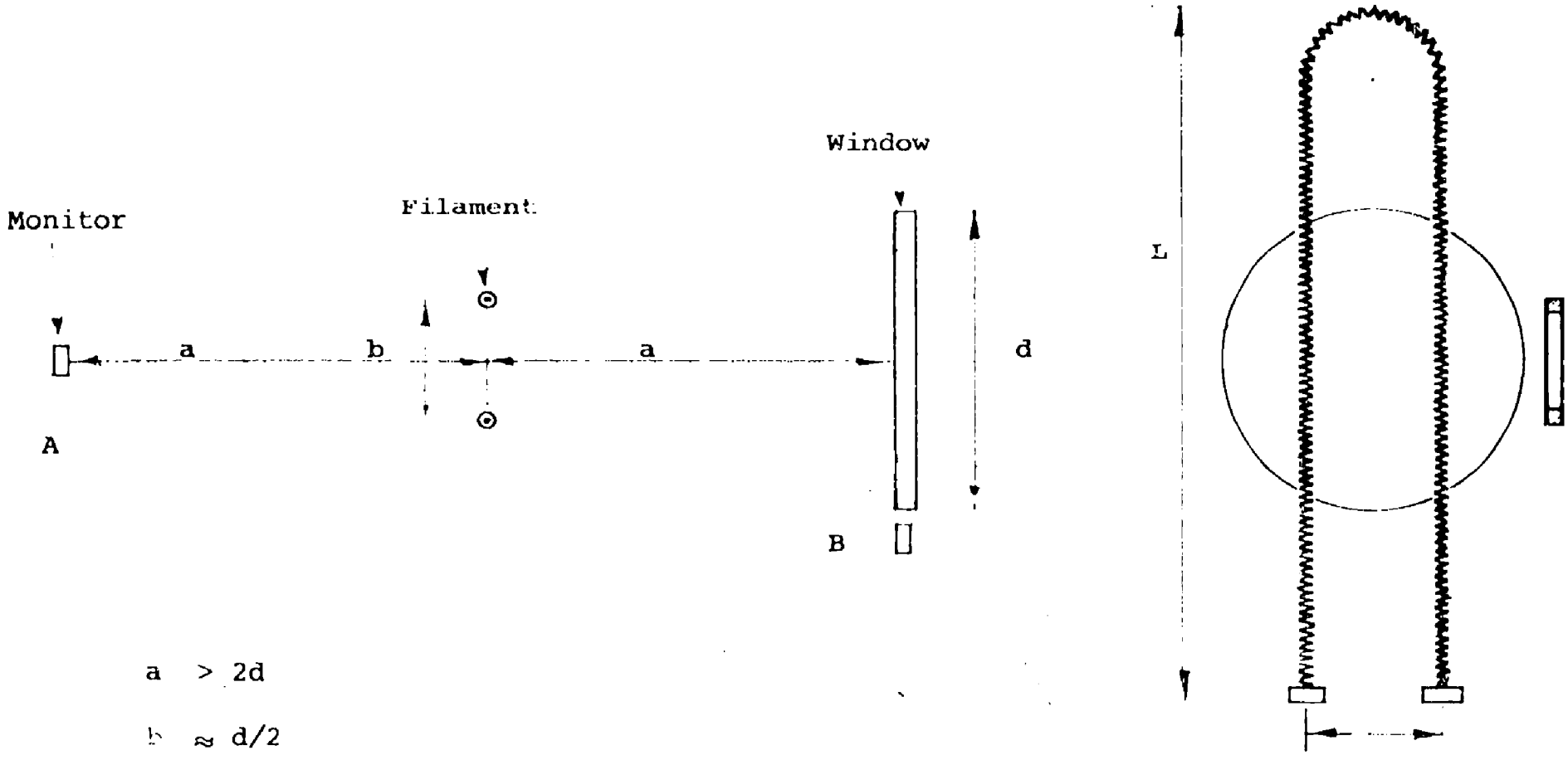

a > 2d

b ≈ d/2

L > 2d

Window Coating Arrangement

Fig. A-5-1

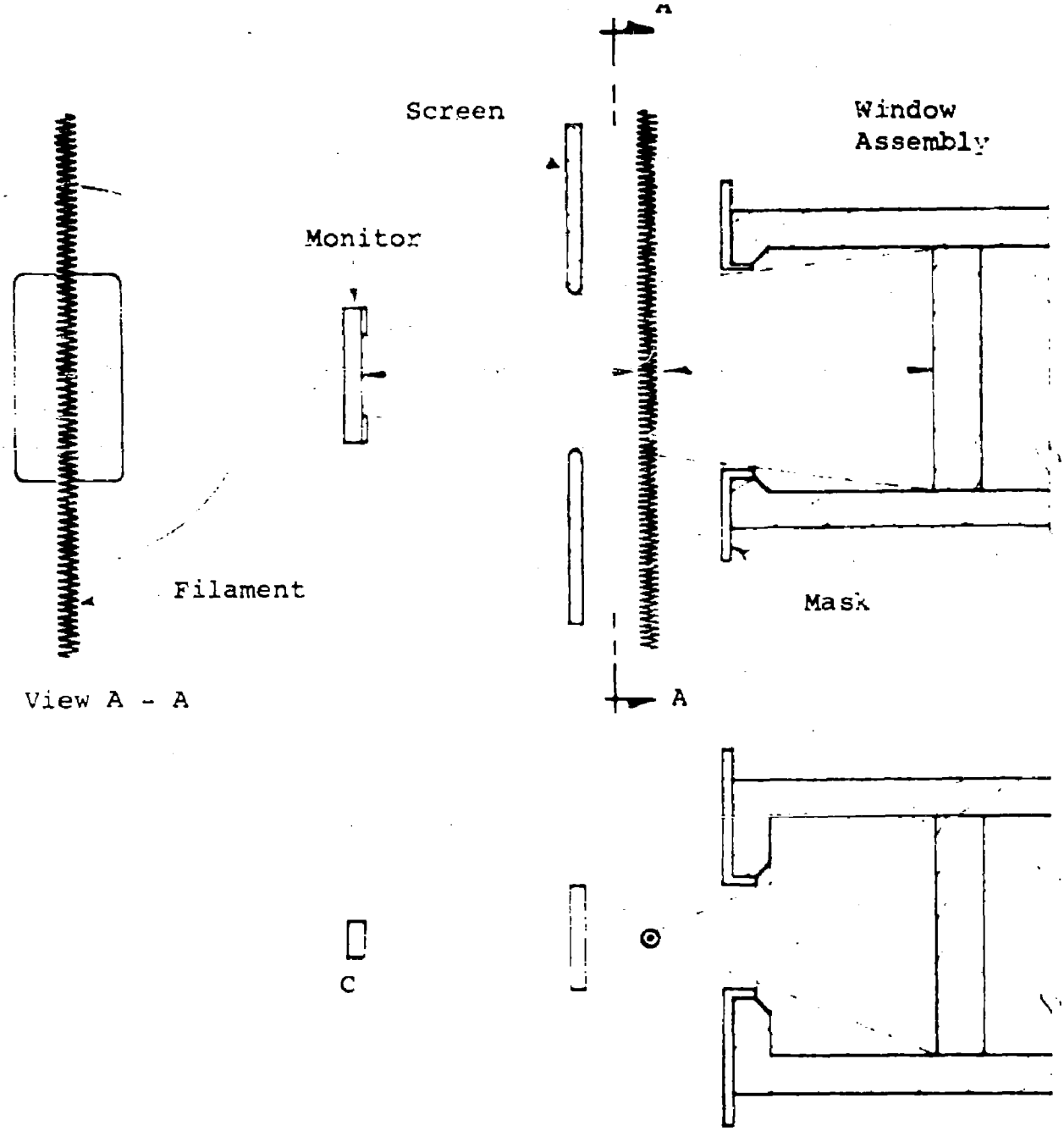

Fig. A-5-2

Alternative Window Coating Arrangement

No. 106217

SUPERSEDES 153147, 106115, 106116 173217

No.	DATE	CHNG No.	BY	DESCRIPTION.
	12-4 61	D674	EB	DRAWN - OBS. 153147 106115 106116 173217.
A	2-7 62	D687	NTM	ADDED 4KM50LB
B	10-9 62	D855	NTM	ADD 4KM50LC

UNLESS OTHERWISE SPECIFIED FRACTIONAL DIMENSIONS ± 1/64" DECIMAL DIMENSIONS ± .005" ANGULAR DIMENSIONS ± 1°

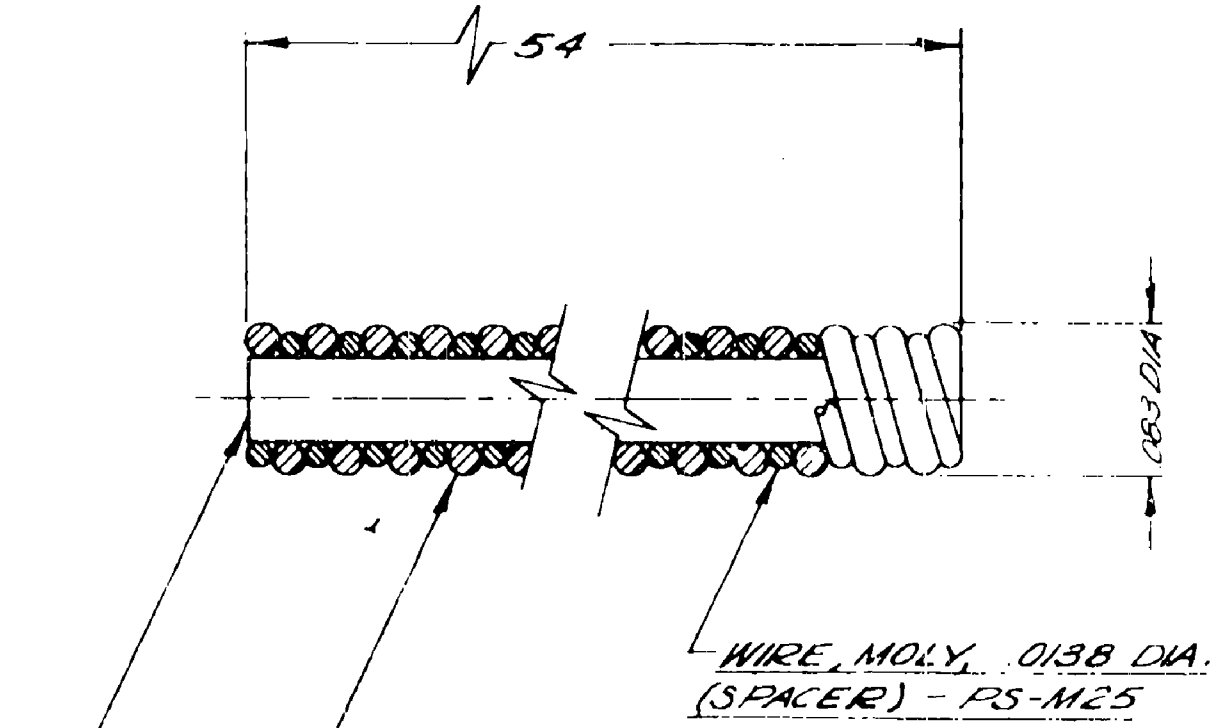

AMT REQ	TUBE TYPE	NEXT ASSEM. DWG.
	4KM50LB,LC	
	3KP10000LQ	
	4KM50000LA3	
	4KM50000LQ	
	4KM50000LR	
	3KM50000PA	
	4KM50000LF	
	4KMP10000LF	
	4KM170000LA	

EITEL-McCULLOUGH, INC.

☒ SAN BRUNO CALIFORNIA — Eimac TUBES — SALT LAKE CITY UTAH ☐

GETTER WOUND

DRWN. EB	DATE 12-4-61	SCALE 10X	FINISH	
CHKD.	DATE	MAT'L. NOTED		No.
SH.	BLK.	AL. WT.	GR. WT.	

No. 106217 CHANGE B

APPENDIX VI

Drawings For Test Cavity Model 3 as follows:

BP-1062-31	-	Waveguide Plug
AP-1062-33	-	Vacuum Seal - Copper Gasket
BP-1062-34B	-	Seal Flange/Water Jacket
BP-1062-38B	-	Window Coupling Plate Seal Flange
BP-1062-40	-	Window Coupler Assembly
BP-1062-41	-	Window Plate & Seal Flange
DP-1062-42	-	View Port - Window Assembly
DP-1062-43	-	Window Test Unit Assembly
AP-1062-44	-	Window Ceramic

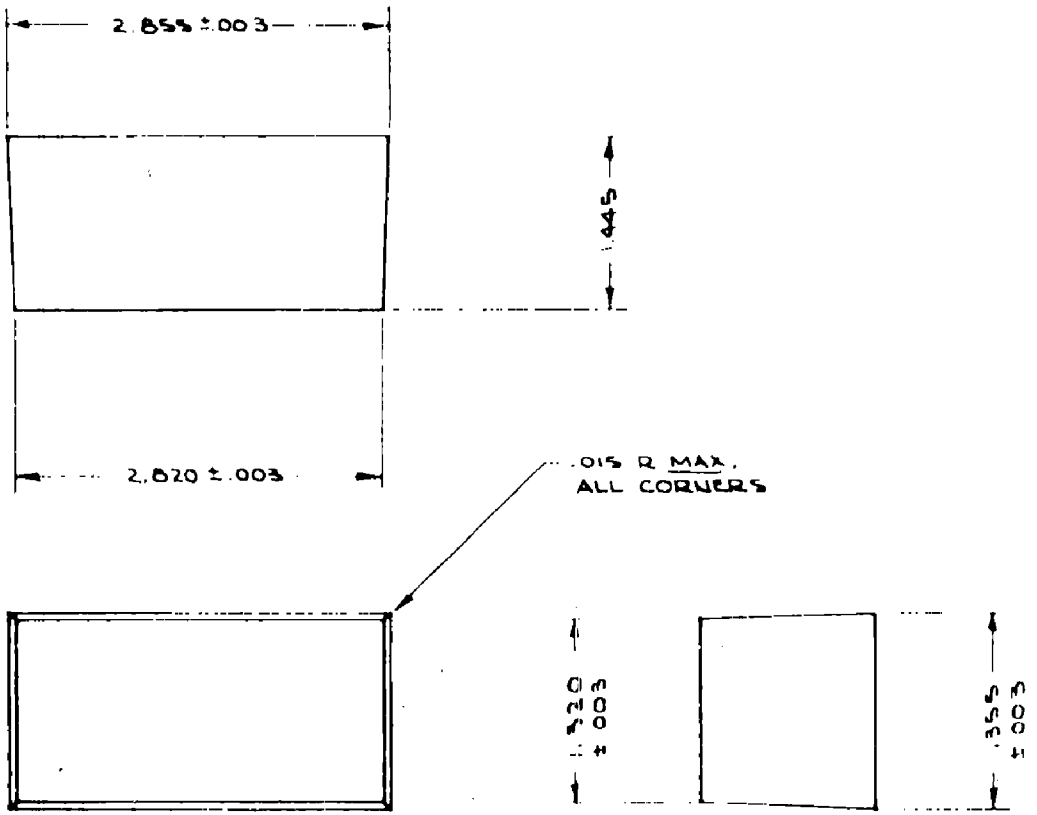

P-1062-31

ITEM	QTY	PART NUMBER
1		P-1062-29

TOLERANCES UNLESS OTHERWISE SPECIFIED
FRACTIONS ± 1/64 DECIMALS ± .005 ANGLES ± 1°

DO NOT SCALE DRAWING

DRAWN JJV 11-7-63 SCALE FULL
CHKD PRODN. CNTRL.
ENG. ACCP. PRODN. ACCP.
MATL. TEFLON
MATL SPEC NO
FINISH 63 OR BETTER

DESCRIPTION

This Document is the Property of Eitel-McCullough, Inc., and Shall Not Be Copied, Reproduced, Used in the Manufacture or Sale of Apparatus or Disclosed to Others Without Permission.

DIVISION:

EITEL-McCULLOUGH, INC.
SAN CARLOS, CALIFORNIA

WAVEGUIDE PLUG

B P-1062-31

NO.	DESCRIPTION OF CHANGE	ECO	DATE	BY

QTY	PRODUCT	NEXT ASSY. USED
1	P-1062-29	

3240-19 ER

QTY	PRODUCT	NEXT ASSY DWG	NO.	DESCRIPTION OF CHANGE	SCO	DATE	BY
2			1	ADDED ±.002		2-15-63	GEN

NOTE:
ANNEAL - FULL SOFT IN HYDROGEN ATM.

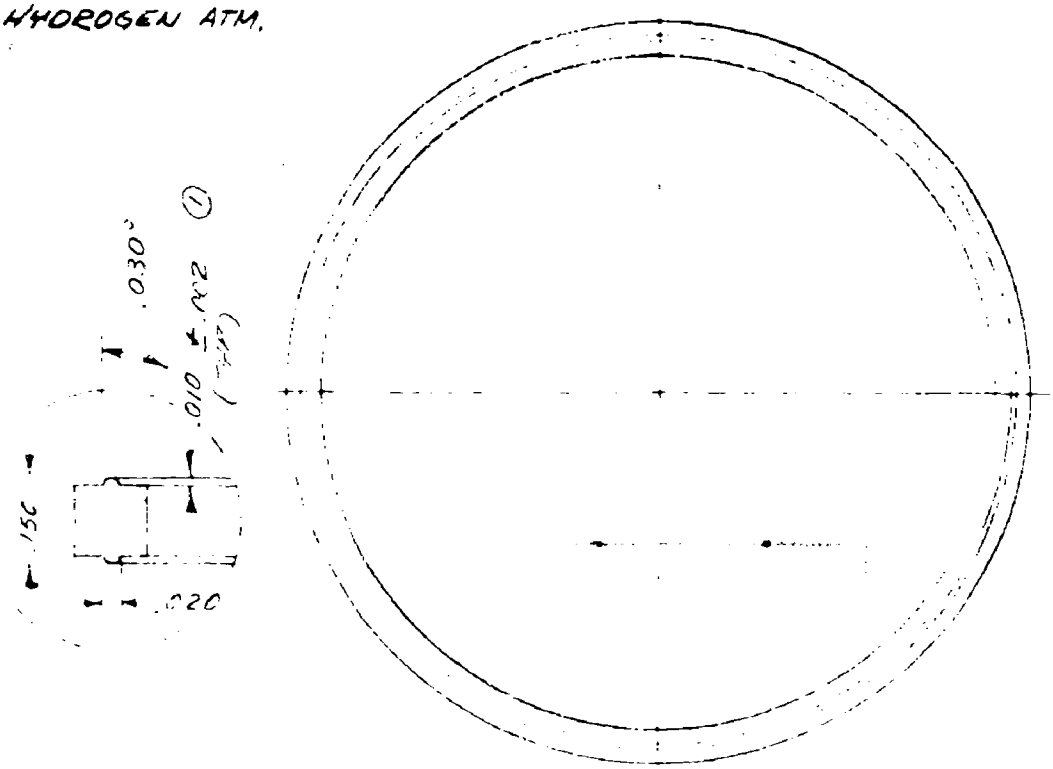

ITEM	QTY	PART NUMBER	DESCRIPTION

TOLERANCES UNLESS OTHERWISE SPECIFIED
FRACTIONS ± 1/64 DECIMALS ± .005 ANGLES ± 1°

DO NOT SCALE DRAWING

DRAWN RSN	2-7-63	SCALE DNS.	
CHKD.		PRODN. CHKD.	
ENG. APPD.		PRODN. APPD.	
MAT'L OFHC-COPPER			
MAT'L SPEC. NO.			
FINISH 63 UNLESS NOTED		BLK.	

DIVISION:

EITEL-McCULLOUGH, INC.
SAN CARLOS, CALIFORNIA

VACUUM SEAL COPPER GASKET

NO. A P-1052-33 CHANGE —

NO. P-1062-34 B

SUPERSEDES

"F (.257) DIA DRILL THRU.
TAP 3/8-18 UNC - 8 HOLES
EQUALLY SPACED ON 9.687 DIA. B.C.

NOTES:
1. CU. PLATE .005
2. CHASE HOLES AFTER PLATING
3. LAP SURFACE "A" TO 16 µ/c FINISH BEFORE AND AFTER PLATING -LEAVE .001 OF PLATING

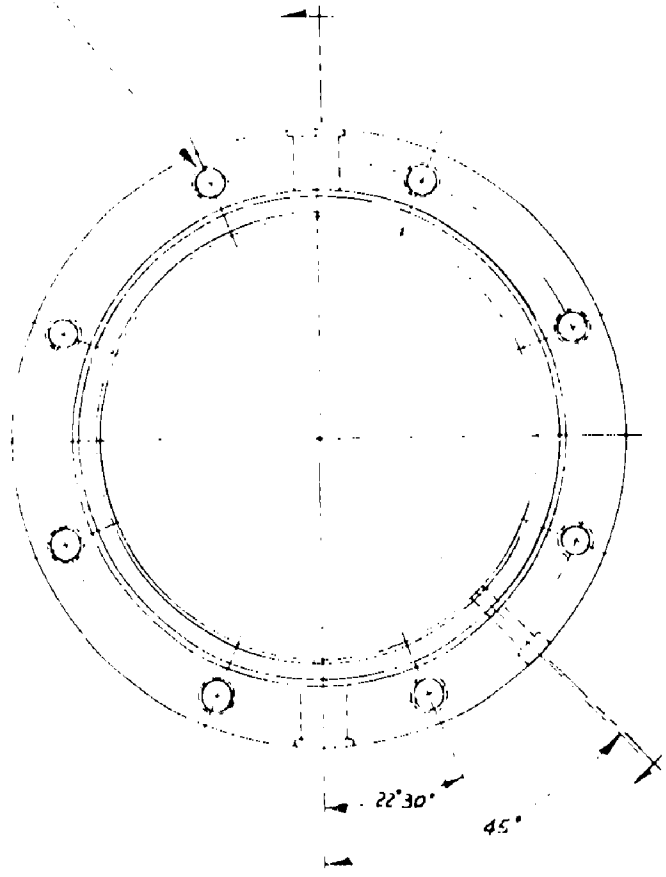

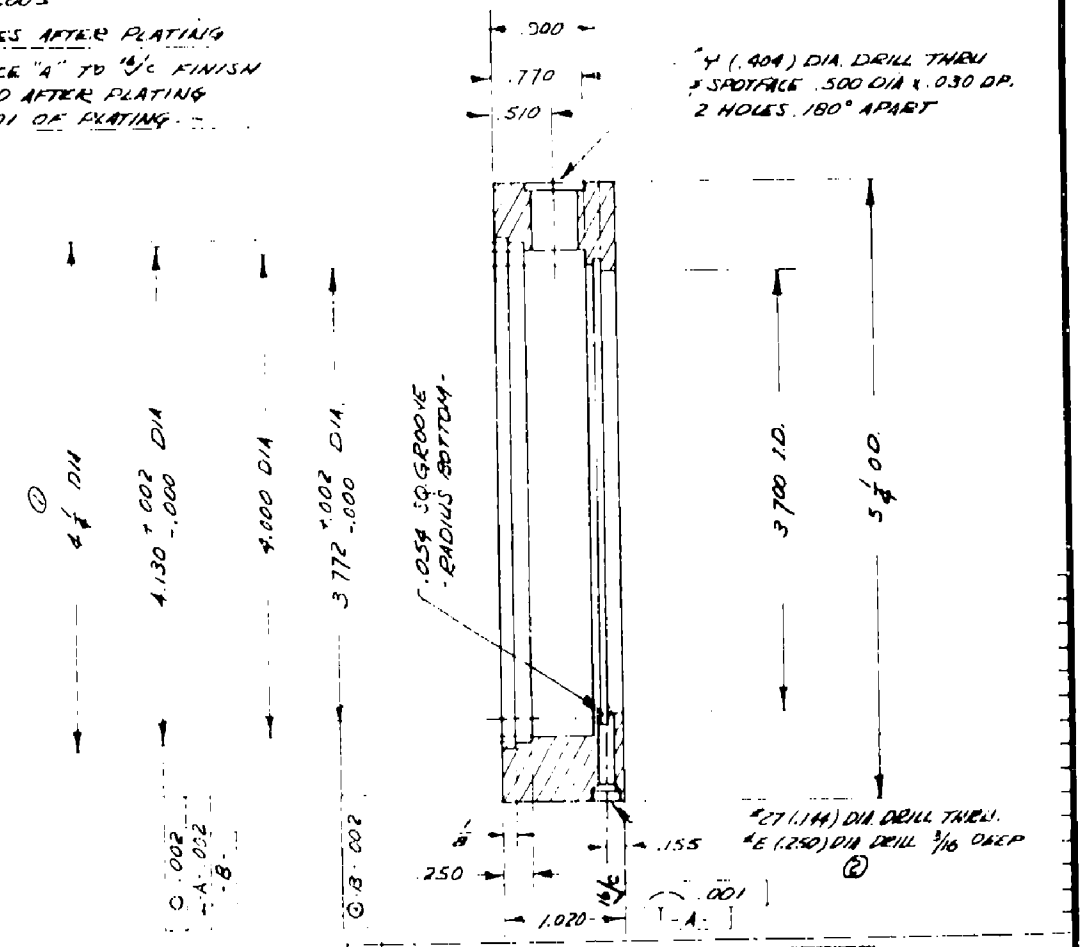

ITEM	QTY	PART NUMBER	DESCRIPTION

NO.	DESCRIPTION OF CHANGE	ECO	DATE	BY
2	CHANGED HANDLE HOLE	925	6-3	
1	REMOVED GROOVE + ADDED STEP	9-16-63		ASN

QTY	PRODUCT	NEXT ASSY. DWG
1	P-1062-37A	

TOLERANCES UNLESS OTHERWISE SPECIFIED
FRACTIONS ± 1/64 DECIMALS ± .005 ANGLES ± 1°

DO NOT SCALE DRAWING

DRAWN SSH 12-7-63 SCALE
CHKD PROGR. CHKD
ENG. APPD. PROGR. APPD.
MATL. 304 STNLS
MATL. SPEC. NO.
FINISH 125 UNLESS NOTED

DIVISION

EITEL-MCCULLOUGH, INC.
SAN CARLOS, CALIFORNIA

SEAL FLANGE / WATER JACKET

NO. B P-1062-34 B

CHANGE

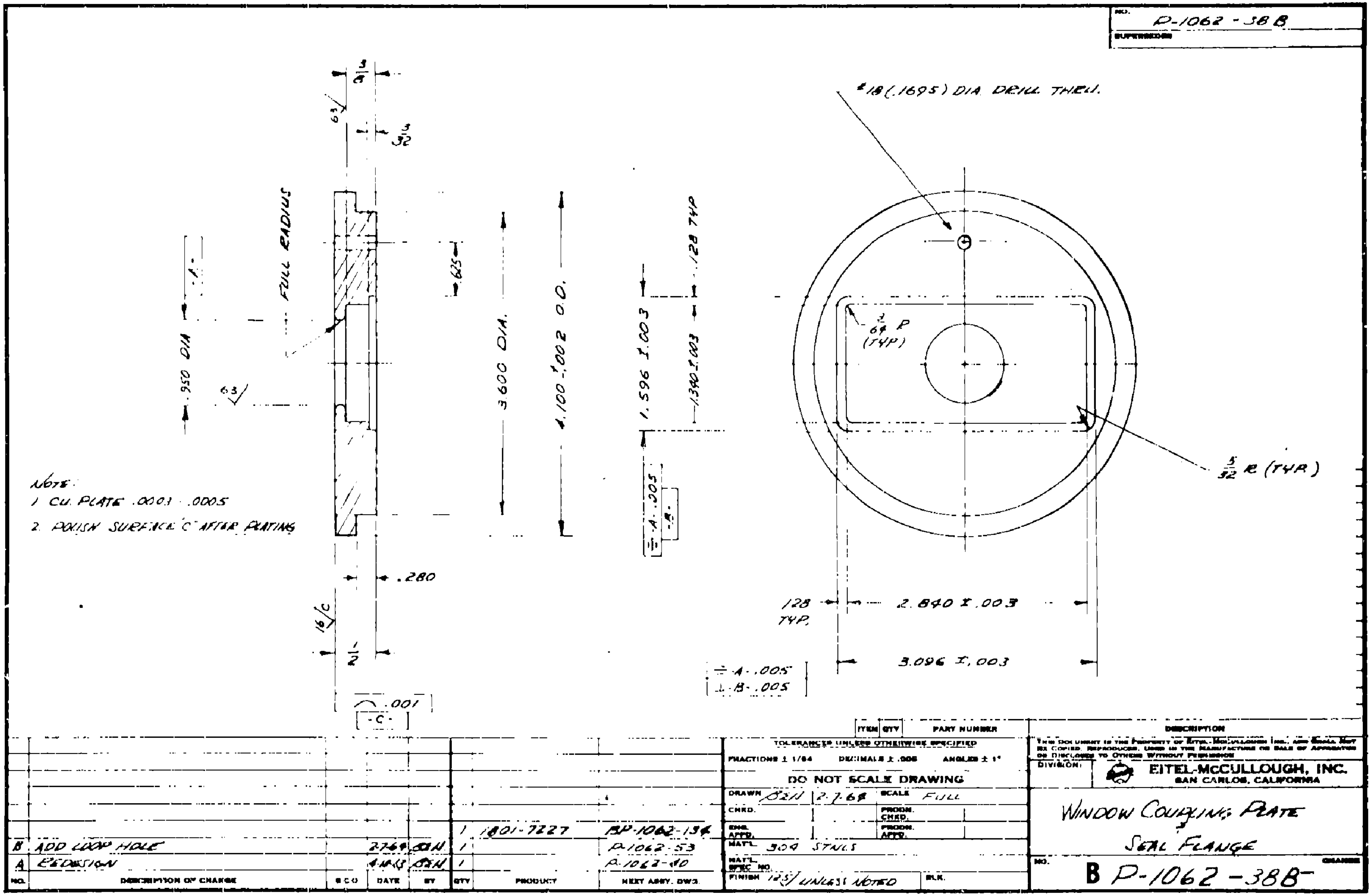
P-1062-38B
SUPERSEDES
#18 (.1695) DIA DRILL THRU.
3/64 R (TYP)
5/32 R (TYP)
.128 TYP
2.840 ±.003
3.096 ±.003
⊥ -A- .005
⊥ -B- .005
1.596 ±.003
1.340 ±.003
.128 TYP
-A- .005
-B-
4.100 ±.002 O.D.
3.600 DIA.
.625
3/8
3/32
63
.280
1/2
16/C
-C- .001
FULL RADIUS
63
.950 DIA
-A-
NOTE:
1 CU. PLATE .0003 - .0005
2. POLISH SURFACE "C" AFTER PLATING
ITEM QTY PART NUMBER
TOLERANCES UNLESS OTHERWISE SPECIFIED
FRACTIONS ± 1/64 DECIMALS ± .005 ANGLES ± 1°
DO NOT SCALE DRAWING
DRAWN BJH 2-7-63 SCALE FULL
CHKD.
PRODN. CHKD.
ENG. APPD.
PRODN. APPD.
MAT'L 304 STNLS
MAT'L SPEC NO.
FINISH 125/ UNLESS NOTED
BLK.
DESCRIPTION
THIS DOCUMENT IS THE PROPERTY OF EITEL-McCULLOUGH INC., AND SHALL NOT BE COPIED, REPRODUCED, USED IN THE MANUFACTURE OR SALE OF APPARATUS OR DISCLOSED TO OTHERS WITHOUT PERMISSION
DIVISION:
EITEL-McCULLOUGH, INC.
SAN CARLOS, CALIFORNIA
WINDOW COUPLING PLATE & SEAL FLANGE
NO. B P-1062-38B
CHANGE
1 1801-7227 BP-1062-134
1 P-1062-53
1 P-1062-40
QTY PRODUCT NEXT ASSY. DWG.
B ADD LOOP HOLE 2764 BJH
A REVISION 4-11-63 BJH
NO. DESCRIPTION OF CHANGE ECO DATE BY

NO. P-1062-40
SUPERSEDES

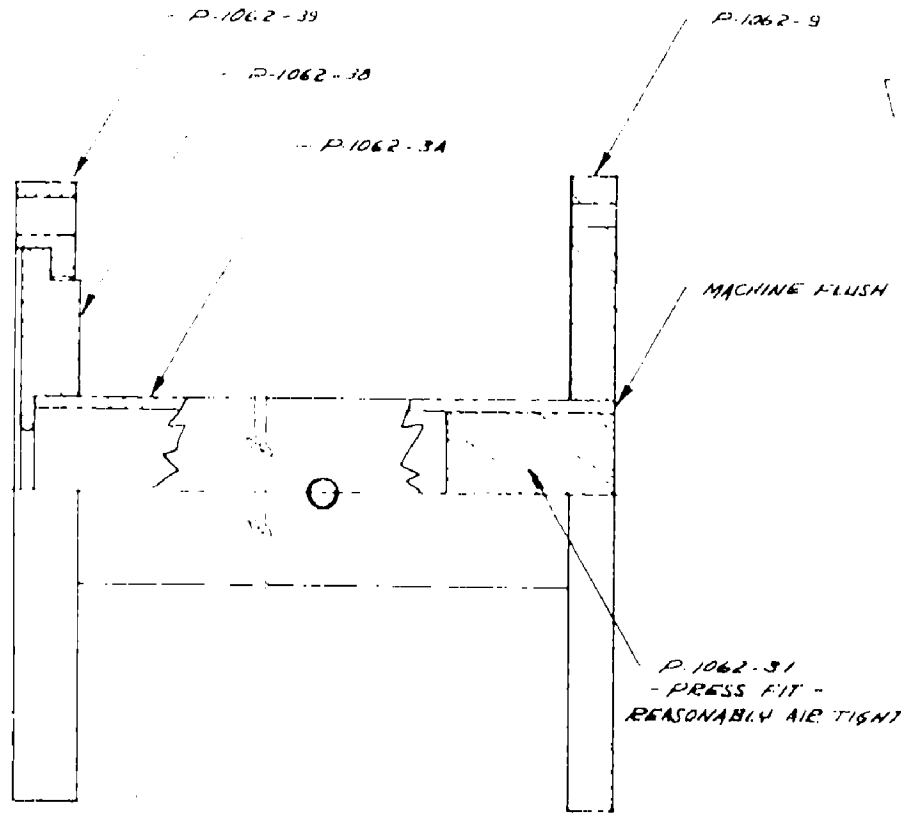

1/4 O.D. x 1/32 WALL x 1" LG
STNLS TUBING

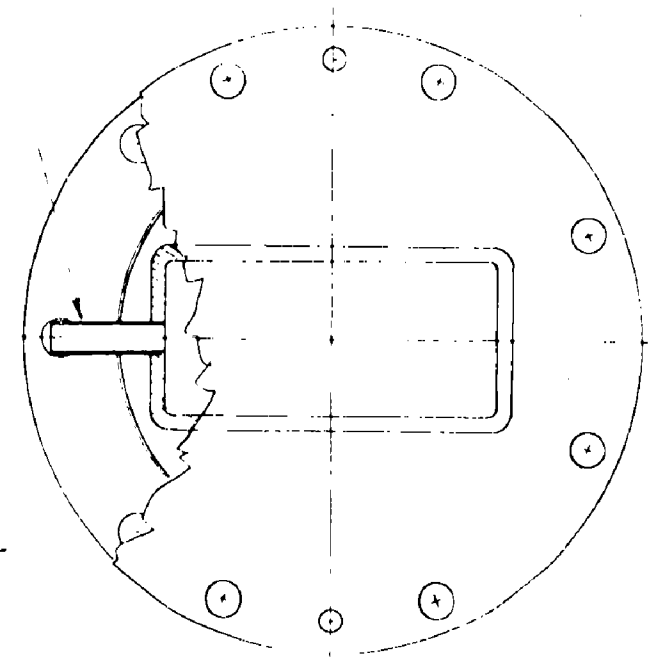

NO.	DESCRIPTION OF CHANGE	ECO	DATE	BY

QTY	PRODUCT	NEXT ASSY DWG
		P-1062-43

ITEM	QTY	PART NUMBER	DESCRIPTION

TOLERANCES UNLESS OTHERWISE SPECIFIED
FRACTIONS ± 1/64 DECIMALS ± .005 ANGLES ± 1°

DO NOT SCALE DRAWING

DRAWN JSH 2-11-63 SCALE FULL
CHKD.
ENG. APPD.
MATL. NOTED
PRODN. CHKD.
PRODN. APPD.
MATL. SPEC. NO.
FINISH BLK.

DIVISION

EITEL-MCCULLOUGH, INC.
SAN CARLOS, CALIFORNIA

WINDOW COUPLER ASSEMBLY

NO. B P-1062-40 — CHANGE

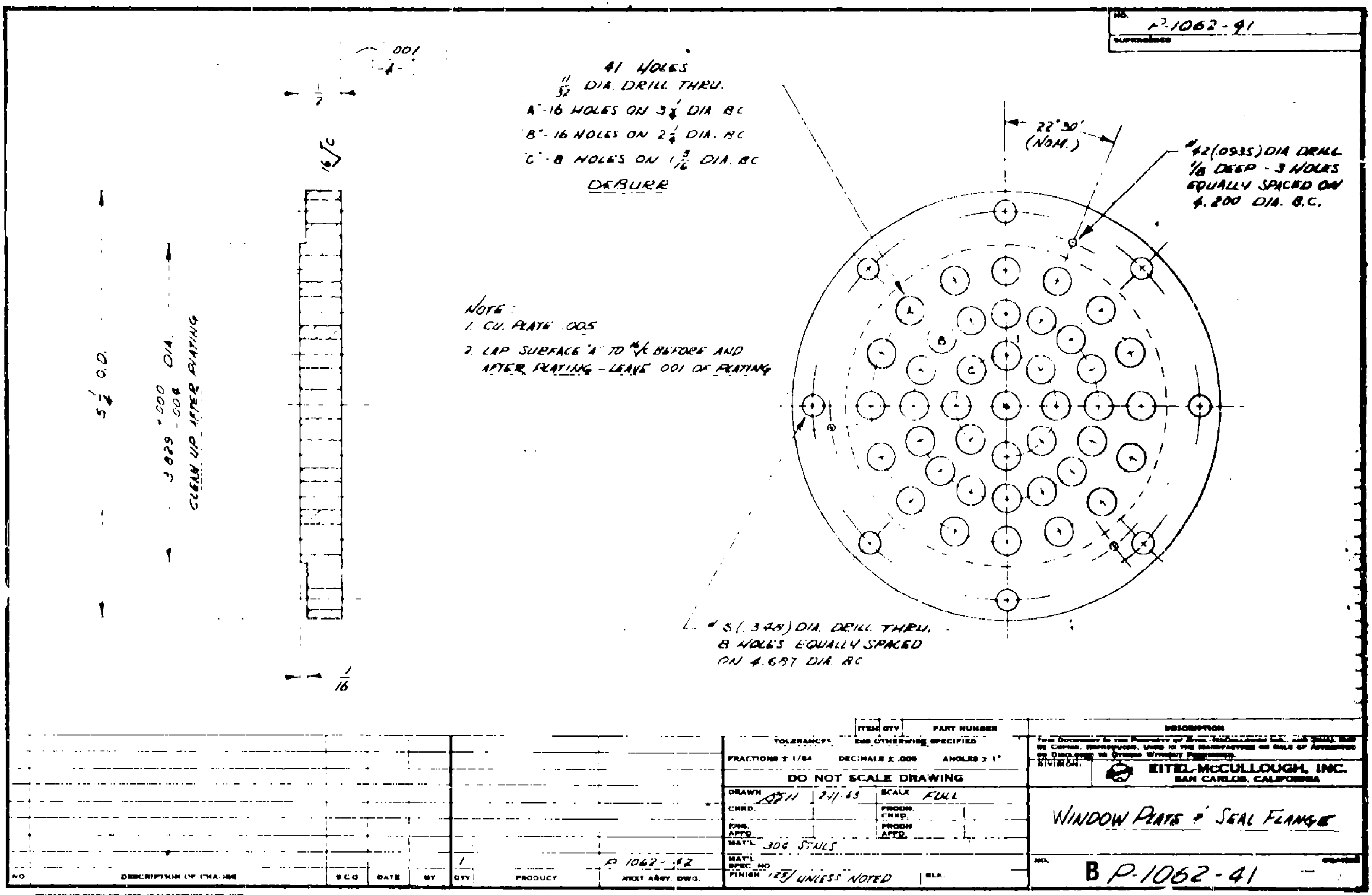
P-1062-41
41 HOLES
11/32 DIA. DRILL THRU.
"A" - 16 HOLES ON 3 1/4 DIA. BC
"B" - 16 HOLES ON 2 1/4 DIA. BC
"C" - 8 HOLES ON 1 3/16 DIA. BC
DEBURR
NOTE:
1. CU. PLATE .005
2. LAP SURFACE "A" TO 16 BEFORE AND AFTER PLATING - LEAVE .001 OF PLATING
22°30' (NOM.)
#42 (.0935) DIA DRILL 1/8 DEEP - 3 HOLES EQUALLY SPACED ON 4.200 DIA. B.C.
#S (.348) DIA. DRILL THRU. 8 HOLES EQUALLY SPACED ON 4.687 DIA. BC
5 1/4 O.D.
3.829 +.000 -.004 DIA.
CLEAN UP AFTER PLATING
.001
1/2
1/16
DO NOT SCALE DRAWING
TOLERANCES UNLESS OTHERWISE SPECIFIED
FRACTIONS ± 1/64 DECIMALS ± .005 ANGLES ± 1°
DRAWN 24-1-63
SCALE FULL
MAT'L 304 STNLS
FINISH 125/ UNLESS NOTED
1
P-1062-42
NEXT ASSY. DWG.
EITEL-McCULLOUGH, INC.
SAN CARLOS, CALIFORNIA
WINDOW PLATE & SEAL FLANGE
B P-1062-41

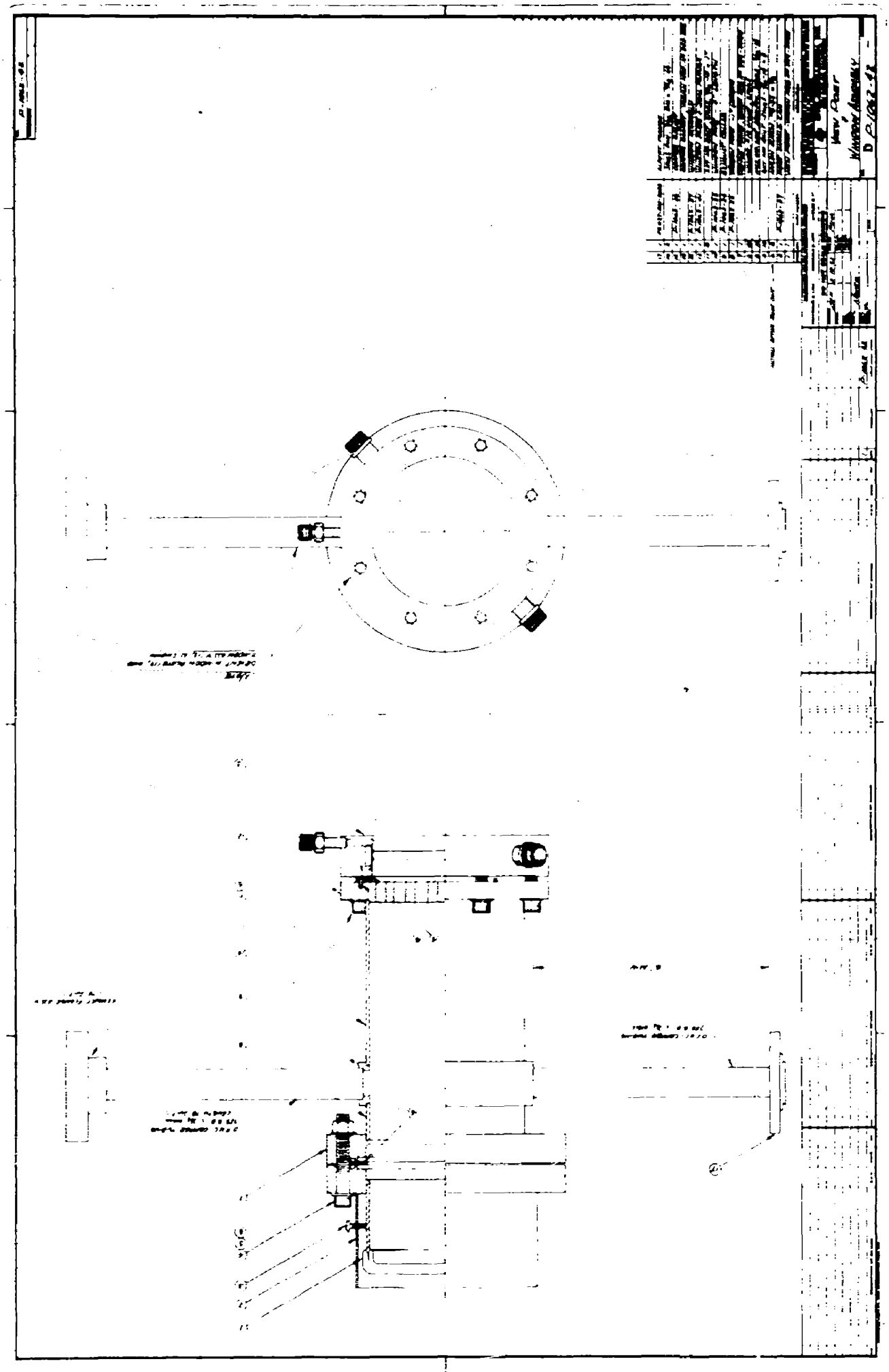

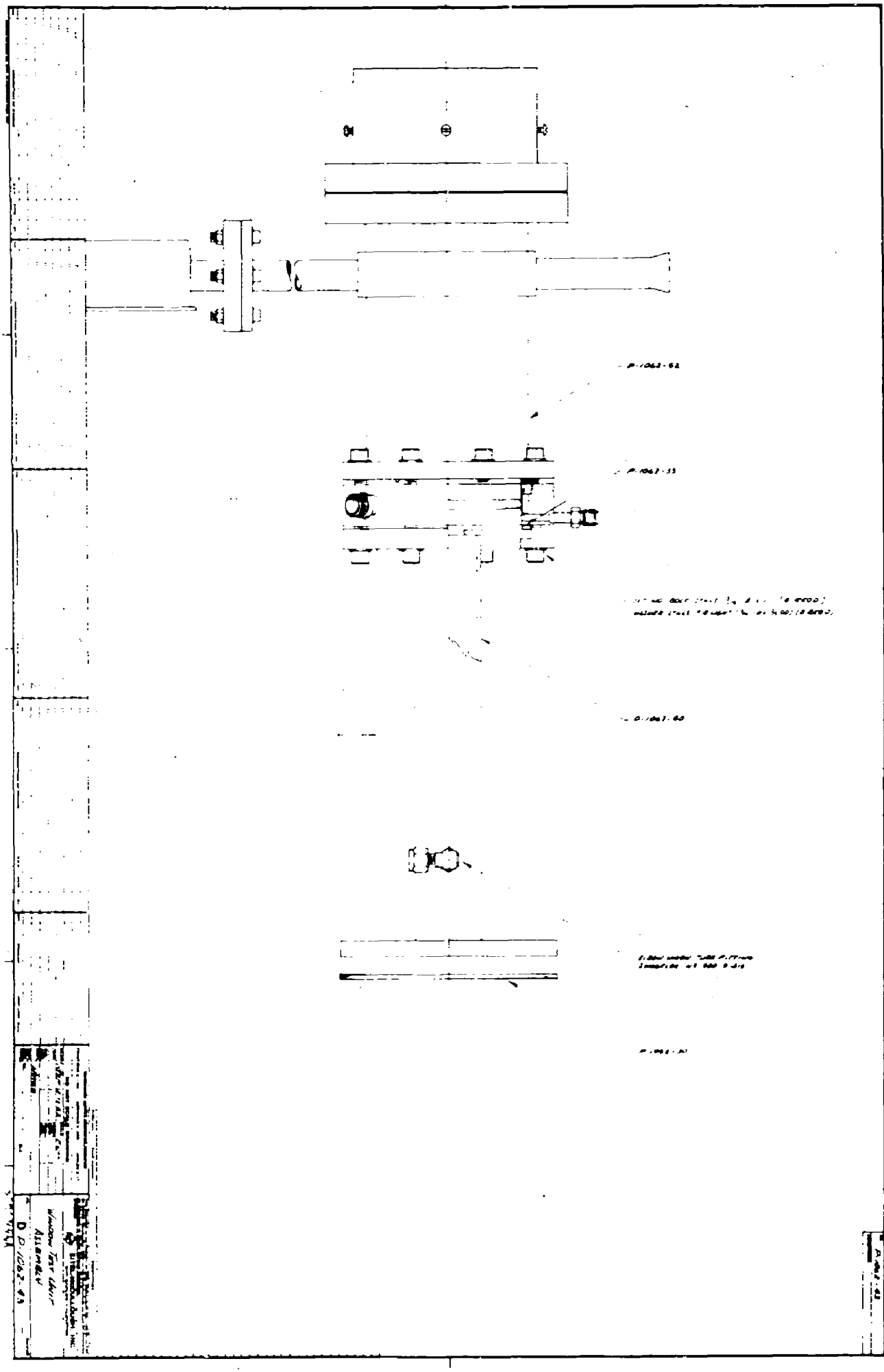

QTY	PRODUCT	NEXT ASSY DWG	NO.	DESCRIPTION OF CHANGE	ECO	DATE	BY

METALIZE @ EIMAC P800C .204 ø CU. PLATE
- DO NOT METALIZE CHAMFERED SURFACES -

.025 x 45° CHAMFER
- BOTH SIDES -

-B-	⌒ .003
⌒ .003	11-B-.003
⊥-A-.003	

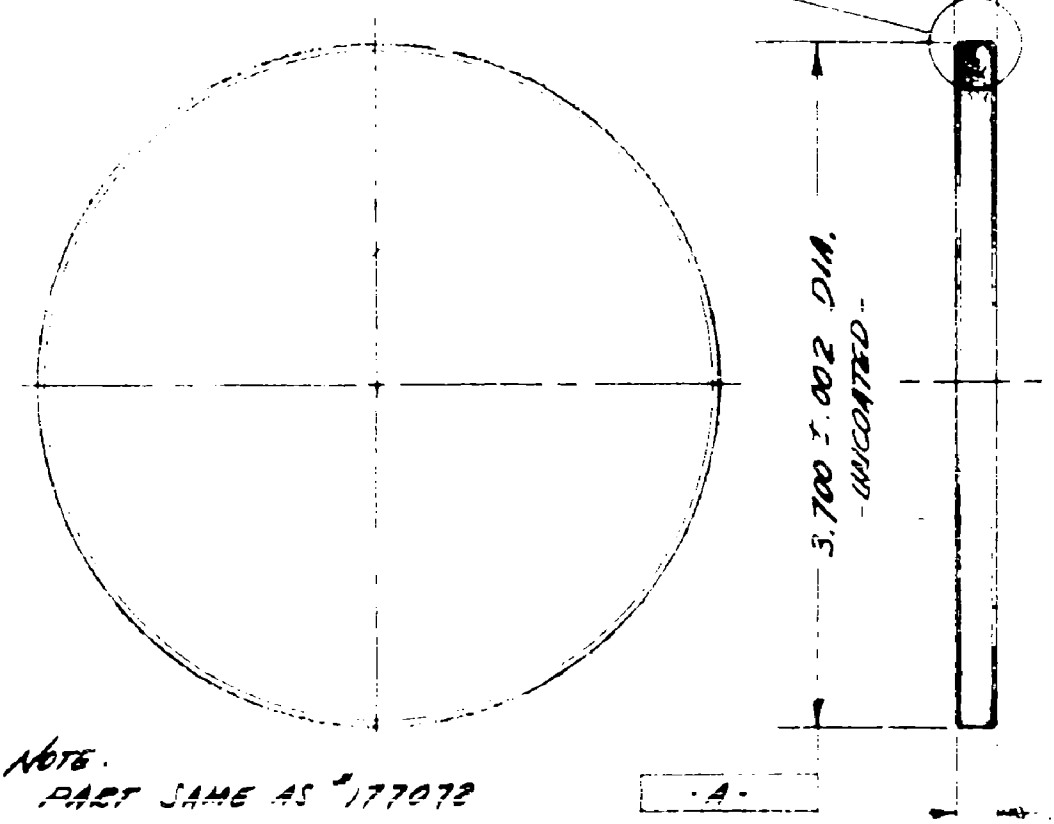

CAUTION-
BERYLLIUM OXIDE
TOXIC — CHECK WITH DEPT.
HEAD BEFORE HANDLING.

NOTE.
PART SAME AS #177072

ITEM	QTY	PART NUMBER	DESCRIPTION

TOLERANCES UNLESS OTHERWISE SPECIFIED
FRACTIONS ± 1/64 DECIMALS ± .005 ANGLES ± 1°

DO NOT SCALE DRAWING

DRAWN BSH	4-2-63	SCALE FULL	
CHKD.		PRODN. CHKD.	
ENG. APPD.		PRODN. APPD.	
MAT'L B&O CERAMIC DISK Nº 177071N			
MAT'L SPEC. NO.			
FINISH		BLK.	

DIVISION:

EITEL-McCULLOUGH, INC.
SAN CARLOS, CALIFORNIA

WINDOW CERAMIC

NO. A P-1062-44 —

DISTRIBUTION LIST

Contract DA 36-039 SC-90818 (E)	No. of Copies
OASD (R&E) Attn: Technical Library Rm. 3E1065, The Pentagon Washington 25, D. C.	1
Defense Documentation Center Attn: TISIA Bldg. 5, Cameron Station Alexandria, Virginia 22314	20
Advisory Group on Electron Devices 346 Broadway New York 13, New York 10013	3
Director U. S. Naval Research Laboratory Attn: Code 2027 Washington 25, D. C. 20390	1
Commanding Officer & Director U. S. Navy Electronics Laboratory San Diego 52, California	1
Chief, Bureau of Ships Department of the Navy Attn: 681A-1 Washington 25, D. C.	1
Systems Engineering Group Deputy for Systems Engineering Directorate of Technical Publications and Specifications (SEPRR) Wright-Patterson AFB, Ohio 45433	1
Commander, AF Cambridge Research Laboratories Attn: CCRR (1 cy) CCSD (1 cy) CRCZ (1 cy) L G. Hanscom Field Bedford, Massachusetts	3

No. of Copies

Commander, AF Cambridge Research Laboratories
Attn: CRXL-R, Research Library
L. G. Hanscom Field
Bedford, Massachusetts 2

AFSC Scientific/Technical Liaison Office
U. S. Naval Air Development Center
Johnsville, Pennsylvania 18974 1

Chief, U. S. Army Security Agency
Attn: AC of S, G4 (Tech Library)
Arlington Hall Station
Arlington 12, Virginia 2

Chief of Research and Development
OCS Department of the Army
Washington 25, D. C. 2

Deputy President
U. S. Army Security Agency Board
Arlington Hall Station
Arlington 12, Virginia 1

Commanding Officer
Harry Diamond Laboratories
Connecticut Avenue & Van Ness Street,N.W.
Washington, D. C. 20438
Attn: Library Room 211, Bldg. 92 1

Commander
U. S. Army Missile Command
Attn: Technical Library
Redstone Arsenal, Alabama 1

Commanding Officer
U. S. Army Electronics Materiel Support Agency
Attn: SELMS-ADJ
Fort Monmouth, New Jersey 07703 1

Director
USAEGIMRADA
Attn: ENGGM-SS
Fort Belvoir, Virginia 22060 1

	No. of Copies
Marine Corps Liaison Office U. S. Army Electronics Laboratories U. S. Army Electronics Command Attn: AMSEL-RD-LWR Fort Monmouth, New Jersey 07703	1
Director U. S. Army Electronics Laboratories U. S. Army Electronics Command Attn: Special Assistant for Research Fort Monmouth, New Jersey 07703	1
Director U. S. Army Electronics Laboratories U. S. Army Electronics Command Attn: AMSEL-RD-PR (Contracts) (1 cy) AMSEL-RD-PR (Tech Staff)(1 cy) AMSEL-RD-PRT(Mr. Kaplam)(1 cy) AMSEL-RD_PRG(Mr. Zinn) (1 cy) Fort Monmouth, New Jersey 07703	4
Director U. S. Army Electronics Laboratories U. S. Army Electronics Command Attn: Logistics Division (For: AMSEL-RD-PRM, Project Engineer) Fort Monmouth, New Jersey 07703	1
Commanding General U. S. Army Materiel Command Attn: R&D Directorate Washington, D. C. 20315	2
Commanding General U. S. Army Combat Developments Command Communications-Electronics Agency Fort Huachuca, Arizona 85613	1
Commanding General U. S. Army Combat Developments Command Attn: CDCMR-E Fort Belvoir, Virginia 22060	1

	No. of Copies
Hq. Electronics Systems Division Attn: ESTI L. G. Hanscom Field Bedford, Massachusetts	1
Director, Monmouth Office U. S. Army Combat Developments Command Communications-Electronics Agency, Bldg. 410 Fort Monmouth, New Jersey 07703	1
AFSC Scientific/Technical Liaison Office Attn: AMSEL-RD-LNA Fort Monmouth, New Jersey 07703	1
USAEL Liaison Officer Rome Air Development Center Attn: RAOL Griffiss AFB, New York 13442	1
Commander U. S. Army Research Office (Durham) Box CM - Duke Station Durham, North Carolina	1
Commanding Officer U. S. Army Engineering Research and Development Laboratories Attn: STINFO Branch Fort Belvoir, Virginia 22060	2
Director U. S. Army Electronics Laboratories U. S. Army Electronics Command Attn: AMSEL-RD_ADO-RHA Fort Monmouth, New Jersey 07703	1
Commanding Officer U. S. Army Electronics Research & Development Activity Attn: AMSEL-RD-WS-A White Sands, New Mexico 88002	1

	No. of Copies
Director, Materiel Readiness Directorate Hqs, U. S. Army Electronics Command Attn: AMSEL-MR Fort Monmouth, New Jersey 07703	1
Director U. S. Army Electronics Laboratories U. S. Army Electronics Command Attn: Tech Documents Center (AMSEL-RD-ADT) Fort Monmouth, New Jersey 07703	1
Director U. S. Army Electronics Laboratories U. S. Army Electronics Command Attn: AMSEL-RD-P Fort Monmouth, New Jersey 07703	1
Stanford University Microwave Laboratory, W.W. Hansen Labs Stanford, California Attn: Prof. S. Sonkin	1
Commanding Officer U. S. Army Electronics Materiel Agency Attn: SELMA-R2a 225 South 18th Street Philadelphia, Pennsylvania 19103	1
Advanced Research Projects Agency Office of Secretary of Defense Washington 25, D. C. Attn: Program Manager, AO 318	3
Chief, Bureau of Ships Department of the Navy Washington 25, D. C.	
Attn: Code 680	1
Attn: Code 335	1
Attn: Code 670B	1
Attn: Code 261B	1

	No. of Copies
Chief of Naval Operations Department of the Navy Washington 25, D. C. Attn: OP-07	1
Chief, Bureau of Naval Weapons Department of the Navy Washington 25, D. C. Attn: RRRE Attn: RAAV-4423 Attn: RREN-3 Attn: RNWC	 1 1 1 1
Applied Physics Laboratory Attn: Mr. William Dobbins Howard County, Maryland	1
Chief of Naval Research Department of the Navy Washington 25, D. C. Attn: 461 Attn: 427	 1 1
Director U. S. Naval Research Laboratory Washington, D. C. 20390 Attn: Dr. S. T. Smith, Code 5240 Attn: Mr. R. C. Guthrie, Code 5300	 1 1
Commander New York Naval Shipyard Naval Material Laboratory Brooklyn 1, New York Attn: Code 920	 1
Commander, Air Force Systems Command R & T Division Attn: Mr. S. Tepper, RTNC Bolling AFB, Washington 25, D. C.	 1
Commander Electronic Systems Division Air Force Systems Command Attn: ESRDE Bedford, Massachusetts	 1

	No. of Copies
Commander, Rome Air Development Center	
Griffiss AFB, New York 13442	
Attn: RCLTT	1
Attn: RCLS	1
Attn: RCLC	1
Attn: RCLTM	1
Attn: RALTP	1
Commander, Air Force Ballistic Missile Division	
Air Force Unit Post Office	
Attn: WDZRS	
Los Angeles 45, California	1
Zeus Project Liaison Officer	
Bell Telephone Laboratories	
Attn: Lt. Col. Lee G. Jones	
Whippany, New Jersey	1
Director	
U. S. Army Electronics Laboratories	
Fort Monmouth, New Jersey 07703	
Attn: AMSEL-RD-SR(Dir. Radar Div)	1
Attn: AMSEL-RD-SR(Dir. Cm Div)	1
Attn: AMSEL-RD-S(Dir. EP&M Div)	1
Attn: AMSEL-RD-N(Dir. Comm Dept)	1
Attn. AMSEL-RD-SC	1
Attn: AMSEL-RD-PEM	1
Commander	
U. S. Army Materiel Command	
Washington 25, D. C.	
Attn: AMCRD-RS-PE-E	1
Commanding Officer	
Frankford Arsenal	
Attn: ORDBA-FEL	
Philadelphia 37, Pennsylvania	1
Commander, Army Missile Command	
Attn: ORDXM-RMP	
Redstone Arsenal, Alabama	1

No. of Copies

Eitel-McCullough, Inc.
301 Industrial Way
San Carlos, California
Attn: Dr. George Caryotakis 1
Attn: Mr. Earl Shelton 1
Attn: L. Reed 1

Radio Corporation of America
Lancaster, Pennsylvania
Attn: Mr. E. E. Spitzer 1

David Sarnoff Research Center
RCA Laboratories
Princeton, New Jersey
Attn: Dr. L. S. Nergaard 1

General Electric Company
TWT Products Section
601 California Avenue
Palo Alto, California
Attn: Mr. S. E. Webber 1

Kane Engineering Laboratories
845 Commercial Street
Palo Alto, California
Attn: Mr. John Kane 1

Sylvania Electric Products, Inc.
Chief Engineer of Microwave Device Division
500 Evelyn Avenue
Mountain View, California
Attn: Dr. Rudy Hutter 1

Sylvania Electric Products, Inc.
East 3rd Street
Williamsport, Pennsylvania
Attn: Dr. John Whitmore 1

Sperry Electronics Tube Division
Sperry Rand Corporation
Gainesville, Florida
Attn: Dr. A. D. Sutherland 1

	No. of Copies
Manager, Applied Research Department Electron Tube Division Westinghouse Electric Corporation P. O. Box 746 Baltimore, Maryland Attn: Mr. G. R. Kilgore	1
Raytheon Company Attn: Mr. William C. Brown Waltham, Massachusetts	1
Varian Associates 611 Hansen Way Palo Alto, California Attn: Dr. T. Moreno	1
Attn: Dr. A. Staprans	1
Attn: Dr. E. W. Herold	1
S. F. D. Laboratories 800 Rahway Avenue Union, New Jersey Attn: Dr. J. Feinstin	1
Litton Industries 960 Industrial Road San Carlos, California Attn: Dr. J. F. Hull	1
Attn: Dr. A. Prommer	1
Hughes Aircraft Company Culver City, California Attn: Dr. L. M. Field, Microwave Tube Div.	1
Watkins-Johnson Company 3333 Hillview Avenue Palo Alto, California Attn: Dr. Rolf Peter	1
Field Emission Corporation McMinnville, Oregon Attn: Dr. F. M. Charbonnier	1

No. of Copies

Sperry Gyroscope Company
Division of Sperry Rand Corporation
Great Neck, Long Island, New York
Attn: D. Churchill 1
Attn: J. McLinden 1
Attn: Dr. V. R. Learned 1

General Electric Company
1 River Road
Schenectady, New York
Attn: R. Bondley, Knolls Research Laboratory 1
Attn: Mr. E. D. McArthur, Knolls Research Laboratory 1

Stanford Research Institute
Menlo Park, California
Attn: L. Feinstein 1

General Telephone and Electronics Corp.,
Bayside Laboratory
Bayside, New York
Attn: B. W. Leavitt 1

Mitronics, Inc.
132 Floral Avenue
Murray Hill, New Jersey
Attn: S. S. Cole 1

General Electric Company
3001 East Lake Road
Erie, Pennsylvania
Attn: J. J. Cacciotti 1

Ford Instrument Company
31-10 Thomas Avenue
Long Island City, New York
Attn: W. Franklin 1

Director, Lincoln Laboratory
P. O. Box 73
Lexington 73, Massachusetts
Attn: Dr. G. L. Guernsey 1

	No. of Copies
Stanford University Microwave Laboratory Stanford, California Attn: Prof. M. Chodorow, Director	1
Aerospace Corporation Los Angeles 45, California Attn: Dr. I. Getting	1
Los Angeles Air Procurement Center Attn: Administrative Contracting Officer The Rand Corporation 1700 Main Street Santa Monica, California	1
Project M Stanford University Stanford, California Attn: Mr. J. Jasberg	1
Polytechnic Institute of Brooklyn 55 Johnston Street Brooklyn 1, New York Attn: J. W. Triemamann	1
Physics Laboratory University of Utah Salt Lake City, Utah Attn: P. Gibbs (1 cy) Attn: G. Baker (1 cy)	2
Laboratory for Insulation Research Massachusetts Institute of Technology Cambridge, Massachusetts Attn: D. A. Powers	1
Battelle Memorial Institute 505 King Avenue Columbus 1, Ohio Attn: Defender Library	1
Cornell Aeronautical Laboratory, Inc. 4455 Genesee Street Buffalo 21, New York Attn: Mr. R. C. Beitz	1

No. of Copies

MITRE Corporation
Bedford, Massachusetts
Attn: Dr. R. F. Naka, Associate Technical
Director, Bldg. 2A-251 1

Chief, Army Research Office
Washington 25, D. C. 1

Hqs. U. S. Air Force
Attn: AFRST-EL-CS
Rm. 4D-335, Pentagon
Washington 25, D. C. 1

Director, R & D
Army Materiel Command
Attn: Development Division
Temporary Bldg. T, Gravelly Point
Washington 25, D. C. 1

Commander, EOAR
Attn: Lt. Col. O. R. Hill
Pouch Room, American Embassy
APO 230
New York, New York 1

Bell Telephone Laboratories, Inc.
Whippany, New Jersey
Attn: Mr. R. C. Newhouse 1

RCA Aerospace Communication and Controls Div.
P. O. Box 588
Burlington, Massachusetts
Attn: Mr. W. Ramsey 1

Jet Propulsion Laboratory
California Institute of Technology
4800 Oak Grove Drive
Pasadena, California
Attn: 05.00/31, Mr. I. E. Newland, Mgr.
Tech Reports Section 1

	No. of Copies
Microwave Associates Inc. Burlington, Massachusetts Attn: Grant St. John	1
Beryllium Corporation Box 1462 Reading, Pennsylvania Attn: Mr. Jack Blum	1
Scientific and Technical Information Facility Attn: NASA Representative (SAK/DL) P. O. Box 5700 Bethesda, Maryland 20014	1
Larry Clampitt, Manager Spencer Laboratory Raytheon Corporation Burlington, Massachusetts	1

This contract is supervised by the Microwave Tubes Branch, Electron Tubes Division, ECD, USAEL, Fort Monmouth, New Jersey. For further technical information, contact Mr. Gunther Wurthmann, Project Engineer, Telephone 201-59-61104.

10. ABSTRACT CARD

Eitel-McCullough, Inc.
San Carlos, California

Microwave Window Multipactor
and Its Inhibition by R. Hayes

Final Report, September 1964.
DA Task No. 1G6-22001-A 055-04
Contract No. DA-36-039 SC 90818
UNCLASSIFIED REPORT

Studies on multipactor at microwave windows are presented with information on the power levels at which such discharges may occur. Methods of eliminating multipactor at windows are described and include surface coatings, and grooves cut in the window surface. Window treatments have been evaluated at alumina, beryllia and quartz windows at power levels up to 100 Mw peak equivalent transmitted power and average dissipations equivalent to over 300 kw of average power. The maximum peak power supported by multipactor-resistant windows was limited by arcing at the metal-dielectric seal. Various methods of increasing the threshold power for arcing have been tried.

1. Multipactor
2. Microwave Windows
3. Microwave Power Generation
I. R. Hayes
II. Project Defender
III. USAEL Contract No. DA-36-039 SC 90818
IV. DA Task No. 1G6-22001-A-055-04
V. In ASTIA Collection

10. ABSTRACT CARD

Eitel-McCullough, Inc.
San Carlos, California

Microwave Window Multipactor
and Its Inhibition by R. Hayes

Final Report, September 1964.
DA Task No. 1G6-22001-A-055-04
Contract No. DA-36-039 SC 90818
UNCLASSIFIED REPORT

Studies on multipactor at microwave windows are presented with information on the power levels at which such discharges may occur. Methods of eliminating multipactor at windows are described and include surface coatings, and grooves cut in the window surface. Window treatments have been evaluated at alumina, beryllia and quartz windows at power levels up to 100 Mw peak equivalent transmitted power and average dissipations equivalent to over 300 kw of average power. The maximum peak power supported by multipactor-resistant windows was limited by arcing at the metal-dielectric seal. Various methods of increasing the threshold power for arcing have been tried.

1. Multipactor
2. Microwave Windows
3. Microwave Power Generation
I. R. Hayes
II. Project Defender
III. USAEL Contract No. DA-36-039 SC 90818
IV. DA Task No. 1G6-22001-A-055-04
V. In ASTIA Collection

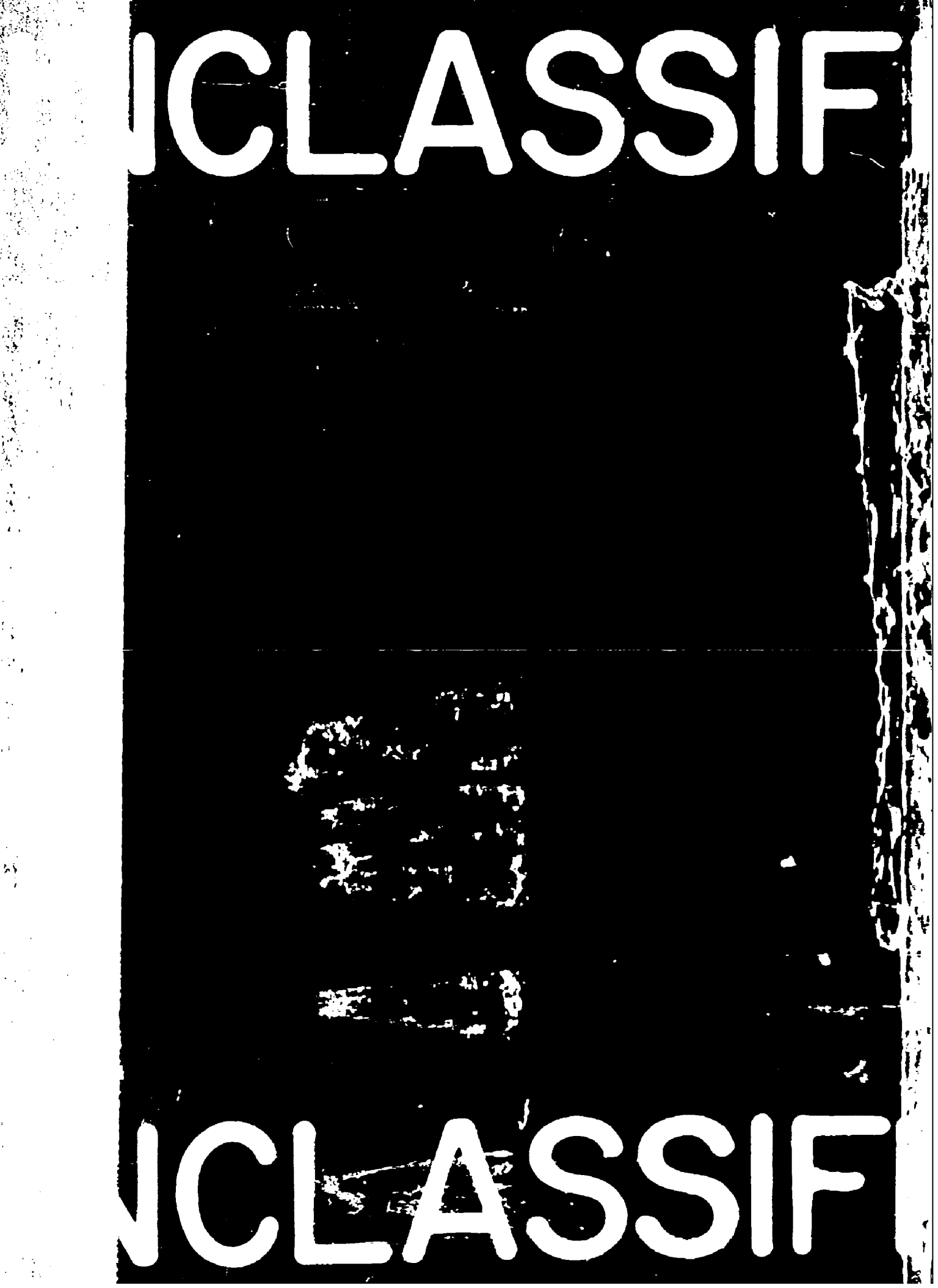
ICLASSIF
ICLASSIF